ANALYSIS AND MANAGEMENT OF INTRA- AND INTER-SYSTEM INTERFERENCE IN WIRELESS COMMUNICATIONS SYSTEMS

by

Li Li

A dissertation submitted to the Faculty of the University of Delaware in partial fulfillment of the requirements for the degree of Doctor of Philosophy in Electrical and Computer Engineering

Summer 2018

ANALYSIS AND MANAGEMENT OF INTRA- AND INTER-SYSTEM INTERFERENCE IN WIRELESS COMMUNICATIONS SYSTEMS

by

Li Li

Approved: _____

Kenneth E. Barner, Ph.D.
Chair of the Department of Electrical and Computer Engineering

Approved: _____

Babatunde Ogunnaike, Ph.D.
Dean of the College of Engineering

Approved: _____

Ann L. Ardis, Ph.D.
Senior Vice Provost for Graduate and Professional Education

I certify that I have read this dissertation and that in my opinion it meets the academic and professional standard required by the University as a dissertation for the degree of Doctor of Philosophy.

Signed: _____

Leonard J. Cimini, Jr., Ph.D.
Professor in charge of dissertation

I certify that I have read this dissertation and that in my opinion it meets the academic and professional standard required by the University as a dissertation for the degree of Doctor of Philosophy.

Signed: _____

Xiang-Gen Xia, Ph.D.
Member of dissertation committee

I certify that I have read this dissertation and that in my opinion it meets the academic and professional standard required by the University as a dissertation for the degree of Doctor of Philosophy.

Signed: _____

Chien-Chung Shen, Ph.D.
Member of dissertation committee

I certify that I have read this dissertation and that in my opinion it meets the academic and professional standard required by the University as a dissertation for the degree of Doctor of Philosophy.

Signed: _____

Aijun Song, Ph.D.
Member of dissertation committee

ACKNOWLEDGEMENTS

Pursuing a Ph.D. is a journey full of challenges, difficulties, as well as excitement, which would never end up without the support of many people. I would like to express my sincere appreciation to those who have provided continuous help during my graduate life.

First of all, I would like to express my deep gratitude to my advisor, Dr. Leonard J. Cimini, Jr., for his invaluable support, inspiring words and ceaseless encouragement in my research. Although heavily loaded with research work and family-care issues, he manages to give me timely feedback and useful comments on the weekly reports, research papers, and this thesis. His deep knowledge, research ideas, and serious attitude not only helped me develop skills during my Ph.D. studies, but will also shape my career forever.

I am thankful and honored to have Dr. Xiang-Gen Xia, Dr. Chien-Chung Shen and Dr. Aijun Song as my defense committee members. Their advice and comments made my research and this dissertation more fruitful. I am especially thankful for for Dr. Chien-Chung Shen's insightful discussions every two weeks for the Cisco project and his valuable suggestions on my papers.

I also want to thank Dr. Jim Seymour and Dr. John Graybeal for their effective collaborations and for sponsoring our research from Cisco Systems. I learned and benefited a lot from our technical discussions and their industrial suggestions.

A special thanks goes to our group in the Wireless Systems Laboratory. The experiences in this lab are some of the most valuable times in my career and life. I have to mention that, when I came to U.S.A. five years ago, the guidance and assistance from Hao Feng, Qi Wang, Yao Xiao, and Gubong Lim helped me quickly get used to living here and research to the life. Further, Guangyi Liu, Bohan Zhang, Chengming Zhou,

Jing Li, Lixing Fan, Tao Li and Yongzhao Li have provided a lot of helpful discussions when doing research together. In addition, I have enjoyed the time so much when working with Seyedmohammad Salehi and Yan-Ming Chiou on the Cisco project.

Lastly, and most importantly, I thank with love to my family. My wife, Xueqin Pang, has been extremely supportive throughout this entire process and has made countless sacrifices to help me get through this challenging period in the most positive way. My kids, Luqi Li and Iris Li, make my Ph.D. life special, provide me sweet breaks from philosophy, and motivate me to finish my degree more efficiently. My parents, Kaijun Li, Dengyu Chen, Juexin Lu (father-in-law) and Chiping Lin (mother-in-law), their selfless love and unconditional support are always presented despite the long distance between us. Without their love and support, this dissertation would not have been successful.

TABLE OF CONTENTS

LIST OF TABLES . . . . . **x**
LIST OF FIGURES . . . . . **xi**
ABSTRACT . . . . . **xvi**

Chapter

1 INTRODUCTION **1**

1.1 Background 1
1.2 Intra-System Interference in IBFD Systems 3

1.2.1 IBFD Relaying 3
1.2.2 IBFD Underwater Acoustics 5

1.3 Inter-System Interference: Coexistence of LAA and Wi-Fi 6
1.4 Dissertation Organization 8

2 COOPERATIVE IN-BAND FULL-DUPLEX (IBFD) DECODE-AND-FORWARD (DF) RELAYING **10**

2.1 Introduction 10
2.2 System Model 12
2.3 Impact of Direct Link on Outage of Cooperative IBFD Relaying . . . 15

2.3.1 Outage Analysis: Direct Link as Interference 15

2.3.1.1 Best Selection (BS) Relaying 16
2.3.1.2 Dis-STC Cooperative Relaying (Dis-STC) 18

2.3.2 Outage Analysis: Direct Link as Signal 20

2.3.2.1 Best Selection Relaying (BS) 20

2.3.2.2 Dis-STC Cooperative Relaying (Dis-STC) 21

2.3.3 Simulation Results 22

2.4 Spectral Efficiency of Cooperative IBFD Relaying with Imperfect CSI 24

2.4.1 Channel Estimation Overhead: TBBS, Dis-STC and M-group 25
2.4.2 Spectral Efficiency Analysis 28

2.4.2.1 Timer-Based Best-Select Relaying 28
2.4.2.2 Dis-STC Cooperative Relaying 30
2.4.2.3 M-group Dis-STC Cooperative Relaying 30

2.4.3 Simulation Results 31

2.5 Summary 36

3 INTERFERENCE IN IN-BAND FULL-DUPLEX (IBFD) UNDERWATER ACOUSTICS (UWA) SYSTEMS 39

3.1 Introduction 39
3.2 Interference Cancellation for IBFD UWA Transceivers 43

3.2.1 Challenges in IBFD UWA Systems 43
3.2.2 Interference Cancellation for IBFD UWA Transceivers 46
3.2.3 Residual Self-Multipath Interference from Imperfect CSI . . . 48
3.2.4 Effects of Ambient Noise and ADC Quantization Noise 50
3.2.5 Simulation Results 52

3.3 Interference Management in IBFD Cooperative UWA Communications 56

3.3.1 System Model 56
3.3.2 Impact of Residual Interference 59

3.3.2.1 Self-loop Interference Only 60
3.3.2.2 Interplay of Self-loop Interference and Reflected Self-interference 61

3.3.3 OFDM-based Delay Diversity Scheme 64

3.3.3.1 SINR Analysis for OFDM-based IBFD Relaying . . . 64
3.3.3.2 Reflected Self-interference: Delay Diversity 67

3.3.3.3 Interference from Direct Link: Delay Diversity Structure . . . 70

3.3.4 Results . . . 71

3.3.4.1 Simulation Setup . . . 71
3.3.4.2 Simulation Results and Discussion . . . 72

3.4 Summary . . . 78

4 INTER-SYSTEM INTERFERENCE IN UNLICENSED BAND . 80

4.1 Introduction . . . 80
4.2 Coexistence of Wi-Fi and LAA Networks with Adaptive Energy Detection . . . 84

4.2.1 CSMA/CA in Wi-Fi and Cat 4 LBT in LAA . . . 84

4.2.1.1 Review of CSMA/CA Adopted in Wi-Fi . . . 84
4.2.1.2 Review of Cat 4 LBT Adopted in LAA in Release 13 84

4.2.2 Coexistence Challenges: Collisions in Wi-Fi/LAA Networks . 86

4.2.2.1 Hidden Node Problem in Wi-Fi Networks . . . 87

4.2.3 Collisions in Coexistent Networks of Wi-Fi and LAA . . . 87
4.2.4 Adaptive Energy Detection Algorithm . . . 90
4.2.5 Evaluation of Coexistence Performance . . . 96

4.2.5.1 Simulation Setup . . . 96
4.2.5.2 Simulation Results and Discussion . . . 97

4.3 Multi-Carrier LBT Operation for LAA with Adaptive Energy Detection and Carrier Selection . . . 108

4.3.1 Multi-Carrier Transmissions for IEEE 802.11ac and LAA Networks . . . 108

4.3.1.1 Multi-carrier access in IEEE 802.11ac . . . 108

4.3.1.2 Multi-carrier LBT operation for LAA 109

4.3.2 Multi-carrier LBT with Adaptive Energy Detection and Carrier Selection 111

4.3.2.1 Multi-carrier Cat 4 LBT with the AED algorithm . . 111
4.3.2.2 Multi-carrier Cat 4 LBT with carrier selection 113

4.3.3 Simulation Results 114

4.4 Summary 118

5 CONTRIBUTIONS AND FUTURE WORK 120

5.1 Contributions 120
5.2 Future Research Opportunities 122

BIBLIOGRAPHY 124

Appendix

IBFD UWA RELAYING WITH RESIDUAL INTERFERENCE . 134

LIST OF TABLES

3.1 Simulation Parameters 53

4.1 Different types of MCS, the associated SINR thresholds and the absolute physical rates adopted in IEEE 802.11ac and 3GPP LTE specifications. 97

LIST OF FIGURES

1.1 Global mobile data traffic, 2016 to 2021 [1]. 2

1.2 IBFD relaying system with a possible direct link and a relaying link. The IBFD relay suffers from self-loop interference. 4

1.3 Self-multipath interference of acoustic IBFD systems in shallow water. 5

1.4 Interference in a network where LAA and Wi-Fi coexist. 7

2.1 Single-phase relaying. Among N potential relay nodes, L nodes are selected to forward messages from the source. 13

2.2 Outage probability as a function of $P_{tot}\kappa_{sd}/P_N$ for BS relaying with $N = 5$ (number of potential relays). 23

2.3 Outage probability as a function of $P_{tot}\kappa_{sd}/P_N$ for Dis-STC relaying with $N = 5$ (number of potential relays). 24

2.4 Outage probability as a function of the number of potential relay nodes for both BS and Dis-STC relaying. ($P_{tot}\kappa_{sd}/P_N = 5$ dB) . . . 25

2.5 Exact and approximate outage probability as a function of SNR margin for IBFD relaying with different K-factors, $N_t = 2$ (number of training sequences) and $N = 5$ (number of potential relays). 32

2.6 Outage probability as a function of SNR margin for IBFD and HD relaying with $N_t = 2$ (number of training sequences) and $N = 5$ (number of potential relays). 33

2.7 Spectral efficiency as a function of SNR margin for IBFD and HD relaying with $N_t = 2$ (number of training sequences) and $N = 5$ (number of potential relays). 34

2.8 Spectral efficiency as a function of the normalized power for IBFD and HD relaying with $N_t = 2$ (number of training sequences) and $N = 5$ (number of potential relays). 36

2.9 Spectral efficiency as a function of the number of potential relay nodes for IBFD and HD relaying with $N_t = 2$ (number of training sequences) and $P_s/P_{\max} = -2$ dB. 37

3.1 Self-multipath interference of acoustic IBFD systems in shallow water. 44

3.2 Path loss of the self-multipath signals in acoustic IBFD systems. . . 45

3.3 Residual interference after antenna cancellation for IBFD radios and IBFD UWA systems. Note that the range of the x-axes in the two subfigures are different. 47

3.4 Block diagram of the proposed IBFD system. 48

3.5 Receiver noise power as a function of the residual analog interference level. 52

3.6 Analog and digital cancellation performance with a normalized error of $20\log_{10}(\sigma_\epsilon) = -40$ dB. 53

3.7 Analog and digital cancellation performance with a normalized error of $20\log_{10}(\sigma_\epsilon) = -50$ dB. 54

3.8 Residual interference as a function of the variance of the normalized errors σ_ϵ^2. 55

3.9 Residual interference level for different numbers of reflections that are suppressed (M_r). 56

3.10 IBFD relaying with self-loop interference, reflected self-interference from the seafloor, and possible interference from the transmission on the direct link. 57

3.11 Delay diversity sturcture at the destination. 68

3.12 Trellis for delay diversity with three paths (desired signal mixed with the first two streams) using BPSK modulation. 69

3.13 Sound speed profile adopted in the simulations. 72

3.14 Error rate performance for different levels of residual self-loop interference. Only self-loop interference is present. 73

3.15 Error rate performance with $D = 2$ streams in the delay diversity structure, for different levels of reflected self-interference. There is both self-loop interference and reflected self-interference, and $G_{\mathrm{R}}G_{\mathrm{LI}} = -9$ dB. 74

3.16 Error rate performance with $D = 3$ streams in the delay diversity structure, for different levels of reflected self-interference. There are both self-loop interference and reflected self-interference, and $G_{\mathrm{R}}G_{\mathrm{LI}} = -9$ dB. 75

3.17 Error rate performance as a function of the power of the reflected self-interference, for different number of streams in the delay diversity structure. There is both self-loop interference and reflected self-interference, $G_{\mathrm{R}}G_{\mathrm{LI}} = -9$ dB, and SNR = 35 dB. 76

3.18 Error rate performance with $D = 3$ streams in the delay diversity structure by combining the "interference" from the direct link. We include interference from the self-loop link, the reflected link, and the direct link. ($|\beta h_{\mathrm{LI}}(m)|^2 = -9$ dB and $||\beta \mathbf{h}_f||_2^2 = -12$ dB.) 77

4.1 Cat 4 LBT procedure, which consists of LBT-iCCA and LBT-eCCA procedures [2]. 85

4.2 An example of hidden nodes in a pure Wi-Fi network, where A_1 and A_2 are two APs, and S_1 and S_2 are the associated STAs. 88

4.3 3GPP indoor topology with 4 Wi-Fi APs (circles, labeled as #1, #3, #5, and #7) and 4 LAA eNBs (diamonds, labeled as #2, #4, #6, and #8). 89

4.4 Hidden node problems in a coexistent network of Wi-Fi and LAA: the light colored blocks are Wi-Fi's downlink or uplink transmissions, and the dark colored blocks are LAA's downlink transmissions (LAA's uplink transmissions are fulfilled over the licensed band). 89

4.5 The extended Cat 4 LBT with the proposed AED algorithm, where the LAA-ED threshold is adaptively updated due to collisions. . . 94

4.6 Performance of Wi-Fi and LAA systems with $\lambda = 2.5$ as a function of the LAA-ED threshold, which is the same across all eNBs (Method III). 98

4.7 Performance of Wi-Fi and LAA with $\lambda = 2.5$ for four methods: Method III with $\eta_{\text{LAAED}} = -75$ dBm, RTS/CTS with $\eta_{\text{LAAED}} = -75$ dBm, AED with Method I using $N_r = 1$, and AED with Method II using $N_r = 1$. 100

4.8 Performance of Wi-Fi and LAA with $\lambda = 2.5$ for the four methods ($\eta_{\text{LAAED}} = -82$ dBm and $N_r = 1$). 101

4.9 Performance of Wi-Fi and LAA with $\lambda = 2.5$ for the four methods ($\eta_{\text{LAAED}} = -75$ dBm and $N_r = 1$), under two different deployments: 2 APs coexist with 2 eNBs, and 8 APs coexist with 8 eNBs. 102

4.10 Performance for individual APs and eNBs with $\lambda = 2.5$ for the four methods ($\eta_{\text{LAAED}} = -75$ dBm and $N_r = 1$). In each method, the transmitters are, from left to right, Wi-Fi #1, Wi-Fi #3, Wi-Fi #5, Wi-Fi #7, LAA #2, LAA #4, LAA #6 and LAA #8. 103

4.11 Performance for individual APs and eNBs with $\lambda = 0.5$ for the four methods ($\eta_{\text{LAAED}} = -75$ dBm and $N_r = 1$). In each method, the transmitters are, from left to right, Wi-Fi #1, Wi-Fi #3, Wi-Fi #5, Wi-Fi #7, LAA #2, LAA #4, LAA #6 and LAA #8. 104

4.12 Performance of Wi-Fi and LAA as a function of the number of retransmissions N_r for AED with Method I. ($\lambda = 2.5$). 105

4.13 The CDF of the aggregate throughput for Wi-Fi APs over 50 runs, with four different schemes: Method III with $\eta_{\text{LAAED}} = -75$ dBm, RTS/CTS with $\eta_{\text{LAAED}} = -75$ dB, AED with Method I using $N_r = 2$, and AED with Method II using $N_r = 1$. ($\lambda = 2.5$). 106

4.14 The CDF of the aggregate throughput for LAA eNBs, with four different schemes: Method III with $\eta_{\text{LAAED}} = -75$ dBm, RTS/CTS with $\eta_{\text{LAAED}} = -75$ dB, AED with Method I using $N_r = 2$, and AED with Method II using $N_r = 1$. ($\lambda = 2.5$). 107

4.15 Specific patterns for channel bonding in IEEE 802.11ac [3]. 108

4.16 Multi-carrier LBT Option 1: a single Cat 4 LBT procedure is performed on the "primary" carrier. 110

4.17 Multi-carrier LBT Option 2: Cat 4 LBT procedures are independently performed on all four carriers. 110

4.18 Overall throughput performance of Wi-Fi and LAA systems with different LAA-ED thresholds for multi-carrier LBT Option 1 and Option 2. 115

4.19 Aggregate throughput performance of Wi-Fi and LAA for four cases: pure Wi-Fi, LAA with a fixed LAA-ED threshold of -75 dBm, LAA with adaptive energy detection, and LAA with adaptive energy detection and carrier selection. 116

4.20 Effective throughput performance for individual APs and eNBs for four cases: pure Wi-Fi, LAA with a fixed LAA-ED threshold of -75 dBm, LAA with AED, and LAA with AED and carrier selection. . 117

ABSTRACT

The tremendous successes of wireless communications, including cellular systems, wireless local area networks (WLAN), satellite communications and underwater acoustics (UWA), have had a great impact on almost every aspect of human life, such as social networks, entertainment, machine-to-machine communications, smart cities and ocean resource explorations. As a result of these flourishing wireless networks, we have been confronted by an explosion of connected devices and data-hungry applications, and, future wireless systems are going to face exponentially increasing data traffic demands.

Heterogeneous networks, the integration of various technologies/standards, are a promising solution to provide ubiquitous coverage, and improve network performance (such as spectrum efficiency and energy efficiency). The third generation partnership project (3GPP) has standardised licensed-assisted access (LAA) in Release 13/14 and proposed new radio (NR) based unlicensed access in Release 15, in which cellular systems are allowed to access unlicensed spectrum. However, a major challenge to realizing the potential advantages of spectrum sharing is the inter-system interference, i.e., cellular systems have to coexist with other radio access technologies, especially WLAN, which already operate in the unlicensed medium.

In addition, instead of sharing the spectrum for transmission and reception (either in separate time slots or different frequency bands), in-band full-duplex (IBFD) has been proposed to enable wireless terminals to transmit and receive simultaneously over the same frequency band, with the advantage of doubling the spectral efficiency, in addition to the benefits obtained using other technologies. The major drawback of an IBFD system is the high level of intra-system interference created by its own transmissions while trying to receive a distant and useful signal. In general, to achieve

the two-fold spectrum efficiency gain, multiple interference cancellation schemes, includes antenna cancellation, analog cancellation, and digital cancellation, are required to suppress the severe interference.

In this dissertation, we investigate and analyze intra- and inter-system interference under three scenarios: IBFD cooperative relaying, IBFD underwater acoustic transmission, and coexistent WLAN/LAA networks.

For IBFD cooperative relaying, we evaluate three different types of interference: self-loop interference, cross-talk interference and possible direct-link interference (from the source to the destination). In particular, we first investigate the spectral efficiency of IBFD relaying when the self-loop interference and the cross-talk interference cannot be completely suppressed due to imperfect channel estimation. Then, we analyze the impact of the interference from the direct link by deriving closed-form expressions for the outage probability of half-duplex (HD) and IBFD relaying over Rayleigh fading channels. We show that the "signal" from the direct link might cause a severe error floor in the system performance, even when self-loop and cross-talk interference can be completely suppressed.

We next focus on deploying IBFD transmissions to extremely bandwidth-limited UWA systems, which is more challenging due to the much harsher UWA propagation environment. By analyzing the challenges in implementing IBFD UWA systems, we propose an acoustic-specific design that includes both analog and digital cancellation, and present its performance in the presence of imperfect channel state information (CSI), ambient noise, and quantization noise from the analog-to-digital converter. In addition, for IBFD UWA cooperative transmissions, we employ orthogonal frequency division multiplexing (OFDM) techniques to overcome the impact of the residual self-loop interference, and propose a delay-diversity scheme with a Viterbi detector to utilize the long-delay reflected interference (interference due to reflections from sea surface or seafloor).

Finally, we investigate the inter-system interference in coexistent WLAN/LAA systems. We first analyze the coexistence challenges of Wi-Fi (i.e., WLAN) and LAA

posed by frequent collisions, which are caused by the use of different sensing/detection methods. To improve the coexistence performance of Wi-Fi and LAA in downlink transmissions, a distributed adaptive algorithm is proposed to adjust LAA's Energy Detection (LAA-ED) thresholds. Further, we extend the adaptive energy detection algorithm to the multi-carrier case, and propose a simple, but efficient, carrier-selection algorithm based on LAA-ED thresholds. Via simulations, the proposed adaptive energy detection and carrier selection algorithms are shown to improve the overall system performance as well as achieve better fairness among Wi-Fi and LAA networks.

Chapter 1

INTRODUCTION

1.1 Background

Over the last thirty years, wireless communications systems, such as cellular communications, wireless local area networks (WLAN), and underwater acoustics (UWA), have experienced tremendous advances in technology and have become essential in people's daily lives. However, the exponential rise in usage of connecting devices has not shown any signs of slowing down, and the demands for high date rates, low latencies, and long battery life are still dramatically increasing due to the widespread use of wireless applications, such as 4K video streaming, e-Health, gaming, the Internet of Things (IoT), and exploration of the ocean resources [4]. As shown in Fig. 1.1, in 2016, Cisco [1] predicted that mobile data traffic demand would see a 53% compound annual growth rate from 2016 through 2021, increasing to about 49 exabytes per month by 2021.

To meet this demand and provide higher aggregate capacities for more simultaneous users, future wireless networks are expected to be a tiered mixture of networks with different sizes, transmit powers, and radio access technologies (RATs). One major limiting factor is the interference that arises due to the limited bandwidth available and the increased temporal and spectral reuse of these resources. The traditional methods for resource allocation and interference management, for example, channel allocation, power control and cell association, may not be efficient enough to deal with the interference in a dense heterogeneous environment. Other novel strategies, including cooperation [5, 6], interference alignment [7] and multi-user multiple-input multiple-output (MU-MIMO) beamforming [8], have been proposed to reduce the interference

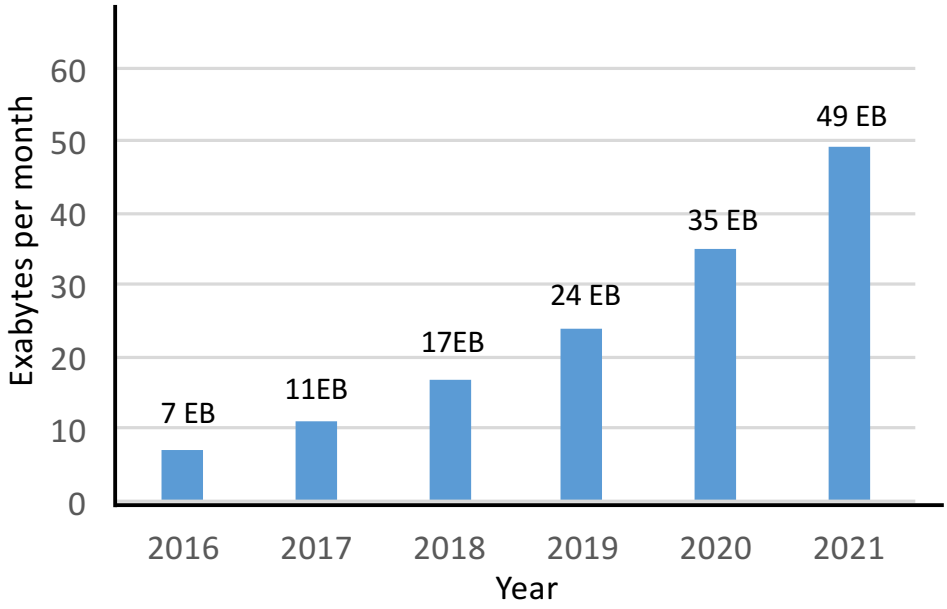

Figure 1.1: Global mobile data traffic, 2016 to 2021 [1].

and improve the system capacity in a more efficient way. For instance, MU-MIMO beamforming, which can achieve directional signal transmission or reception with linear signal processing, is standardized in current cellular and WLAN applications, e.g. the 3rd Generation Partnership Project Long Term Evolution (3GPP LTE) [9] and IEEE 802.11ac specifications [3].

To potentially double the spectral efficiency, the use of in-band full-duplex (IBFD) transmission (for example, see [10–14]) has been proposed to enable wireless terminals to transmit and receive simultaneously over the same frequency band. In addition, to keep up with the emerging traffic demands in cellular systems, 3GPP Release 14 has standardized licensed-assisted access (LAA) and Release 15 has proposed "new radio (NR) based unlicensed access" and "enhancements to LTE operation in unlicensed spectrum," where the evolution of LAA will allow 5G to access the unlicensed spectrum [15–18]. Unfortunately, without a careful system design, new types of interference will be introduced using these techniques. Even though IBFD transceivers can

ideally double the spectral efficiency independently of any other technique employed, the self-loop (intra-system) interference, which arises from the leakage of transmitted signals in the receiver, may cause significant degradation in performance. Using LTE in the unlicensed spectrum can clearly provide a benefit to cellular subscribers through spectrum sharing, as they can get access to more spectrum resources. However, this can cause inter-system interference to others using these bands, especially to Wi-Fi networks. Therefore, a closer investigation of the interference management problem in these scenarios is required.

In this dissertation, we will first evaluate and analyze these new types of intra- and inter-system interference under three sample scenarios: IBFD cooperative relaying, IBFD underwater acoustics, and mixed LAA/WLAN networks. Then, new strategies will be presented that address the interference management problem for these scenarios.

1.2 Intra-System Interference in IBFD Systems

1.2.1 IBFD Relaying

Cooperative relaying, typically, half-duplex (HD) relaying, has been presented as a promising solution to combat fading in wireless channels due to the benefits of spatial diversity [5,6]. However, HD relays transmit and receive either in different time slots or over different frequency bands. For example, two orthogonal time slots are employed to facilitate communication: in the first slot, the source broadcasts its message and all cooperating nodes listen; in the second slot, some relays are selected to forward the source information to the destination. In contrast, IBFD relays transmit and receive simultaneously on the same frequency, which can ideally double the capacity achieved with HD.

The reason why IBFD relaying has not been widely employed in the past is quite simple: the system performance might decrease rapidly due to strong interference from its own transmission, which is difficult to be completely suppressed with a practical implementation. This type of interference is called self-loop interference. As illustrated in Fig. 1.2, there is one IBFD relay node (R) between the source (S) and the destination

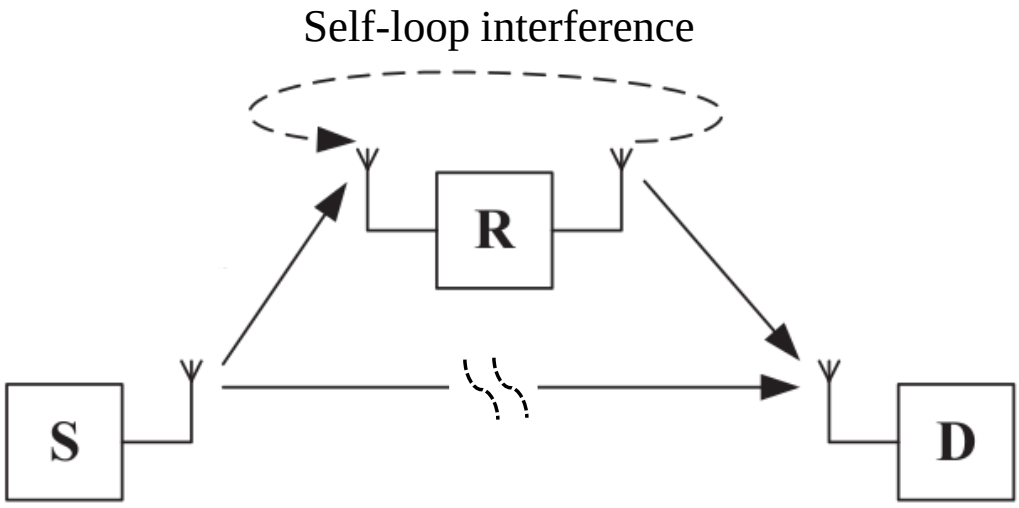

Figure 1.2: IBFD relaying system with a possible direct link and a relaying link. The IBFD relay suffers from self-loop interference.

node (D). The source node communicates with the destination via the IBFD relay node and (possibly) a direct link. The IBFD relay node receives and transmits signals simultaneously using the same frequency; so, there will be a self-loop link (dashed line in Fig. 1.2) between the transmitter and the receiver of the relay node. Since the distance between the receive and transmit antennas is usually small, this self-loop interference could be several orders of magnitude stronger than the signal received from the source. In recent years, advanced cancellation schemes have been proposed to significantly suppress/cancel the self-loop interference [11,13], making IBFD feasible in some practical applications. Unfortunately, in cooperative communications, multiple nodes may be selected to forward source messages. In this case, each IBFD relay would suffer from not only the self-loop interference from its own transmitter, but also from the cross-talk interference from the transmitters of other relays [19, 20]. Worse still, the signals directly transmitted from the source may also interfere with the received signals at the destination.

In the presence of intra-system interference, it is not clear whether IBFD still outperforms HD relaying. The effect of this interference needs to be evaluated, and

new schemes for interference management need to be devised and studied.

1.2.2 IBFD Underwater Acoustics

The fundamental difficulty in achieving high data rates for UWA communication networks lies in the narrow bandwidth available, with a maximum of only tens of kilohertz. Thus, it is reasonable and desirable to investigate the employment of IBFD in UWA systems. However, even though radio frequency (RF) IBFD wireless communications has been successfully demonstrated [13, 14], direct application to the UWA channel is not possible due to the much harsher UWA propagation environment [21–25].

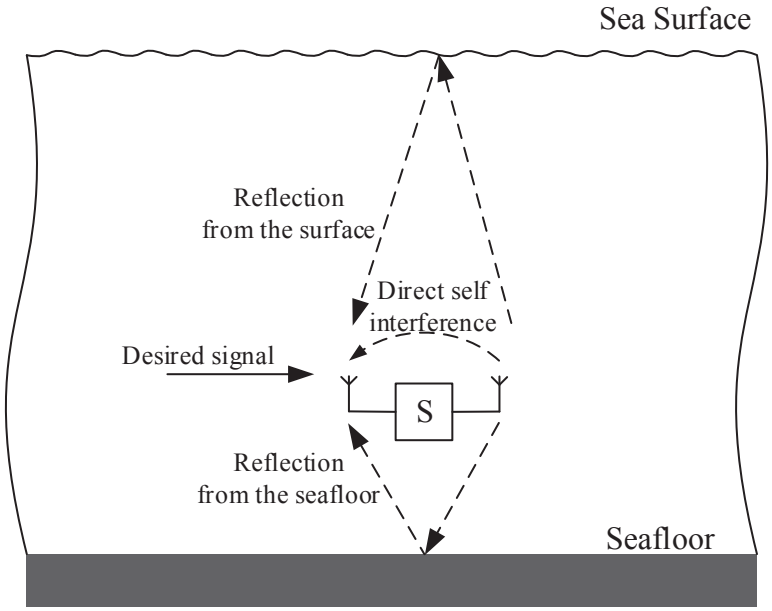

Figure 1.3: Self-multipath interference of acoustic IBFD systems in shallow water.

As shown in Fig. 1.3, an IBFD UWA transceiver is equipped with a transmitter (transducer) as well as a receiver (hydrophone). In shallow water, the hydrophone hears the desired signal from a remote transducer, self-loop interference from its own transducer, and reflections from the sea surface and seafloor. Therefore, there are two types of interference for an IBFD UWA transceiver: 1) self-loop interference from its

own transmission; and 2) interference due to reflections, called self-multipath interference, which makes the interference cancellation more challenging. Even in the deep ocean, where the multipath interference can be neglected, additional challenges exist. First, the self-loop interference in the underwater acoustic channel has a delay several orders of magnitude larger than that in the RF environment (due to the slow speed of sound[1]), which makes it difficult to generate an artificial copy that adds destructively to cancel out the strong interference. Second, the acoustic path loss offered by the antenna separation is limited for short ranges (within meters); thus, higher suppression gain is needed. Third, some existing cancellation schemes used for the RF channel, for example, the antenna cancellation scheme in [10], cannot be adopted due to the strong frequency-dependence of acoustic propagation.

In light of these difficulties, acoustic-specific methods are necessary to suppress and/or utilize the strong self-loop interference as well as the long-delayed interference caused by reflections.

1.3 Inter-System Interference: Coexistence of LAA and Wi-Fi

Cellular communication systems were originally designed to operate in a licensed frequency band with periodic channel access to maximize spectral efficiency, minimize interference, and optimize user experience. On the other hand, Wi-Fi data transmissions operate in unlicensed bands employing random access with contention-based algorithms used to mitigate interference from other radios. To keep up with the emerging traffic demands expected in 4G and 5G systems, the 3GPP standardization group has investigated and standardized LAA to expand LTE operation to the unlicensed band [26]. In one typical scenario of the current specifications, the unlicensed band, specifically the 5-GHz band, is used as a secondary cell (SCell), which is always

[1] The speed of sound is variable and depends on the properties of the medium through which the waves are travelling. In sea water, a typical value for the speed of sound is 1500 m/s, while the speed of electromagnetic waves in free space is 3×10^8 m/s.

anchored by a licensed primary cell (PCell) within the LTE carrier aggregation framework. The PCell is used to exchange critical control signals and guarantee quality of service, whereas, the SCell can be employed to boost the downlink data rate [27, 28].

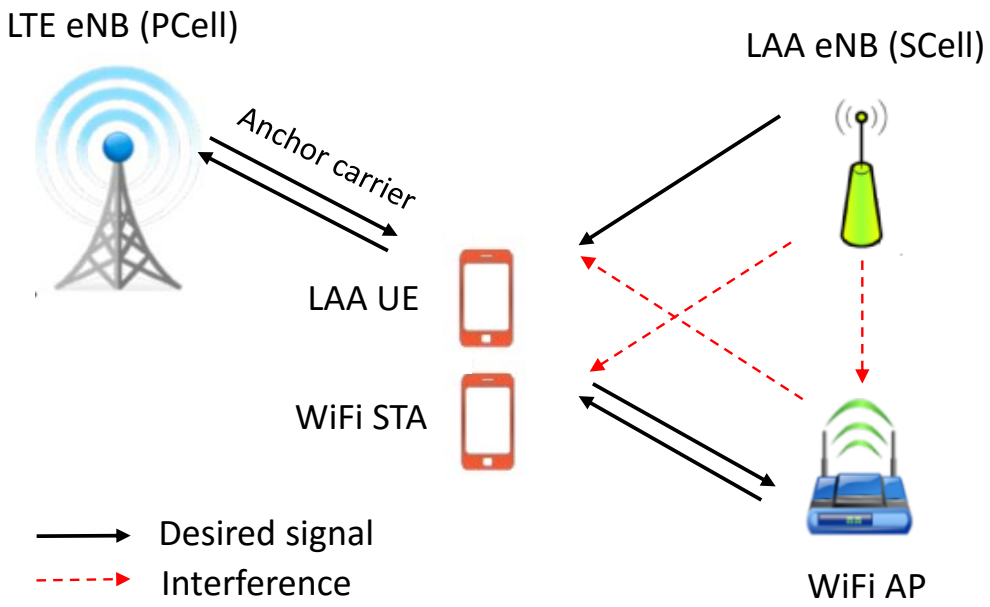

Figure 1.4: Interference in a network where LAA and Wi-Fi coexist.

In Fig. 1.4, a simple example is shown for a network where LAA and Wi-Fi coexist, with one LTE Evolved Node B (eNB) (PCell), one LAA eNB (SCell), one LAA User Equipment (UE), one Wi-Fi Access Point (AP), and one Wi-Fi station (STA). Here, LAA and Wi-Fi both operate in the unlicensed band, and LTE uses the licensed band. When the LAA eNB and Wi-Fi AP both have data to transmit and happen to choose the same carrier (frequency band), they will interfere with each other: the downlink LAA transmission might cause interference to both the downlink and uplink of the Wi-FI system, and the Wi-Fi AP's transmission might interfere with reception at the LAA UE. In IEEE 802.11 networks, carrier sense multiple access with collision avoidance (CSMA/CA) works well for managing access to provide different nodes with equal transmitting opportunity. Considering that the main incumbent system in the

5-GHz band is the widely deployed WLAN technology, including IEEE 802.11 a/n/ac devices [3], the basic criterion for LAA operation is that it should not impact Wi-Fi transmissions more than an additional Wi-Fi network on the same carrier. Hence, similar to CSMA/CA, a listen-before-talk (LBT) procedure is recommended for LAA [26] in order to sense if the channel is idle or not before any data transmission. This requires scheduling and optimization between the two wireless networks to ensure fair coexistence between LAA and Wi-Fi, and also effective coexistence between different LAA operator nodes.

As a first step, the coexistence feasibility of these two wireless access technologies has to be evaluated under different scenarios. Then, strategies must be devised to minimize the inter-system interference in LAA and Wi-Fi networks to ensure that fair access and effective coexistence are achieved from the perspective of both throughput and latency.

1.4 Dissertation Organization

In this dissertation, we investigate the impact of intra- and inter-system interference on the performance of different wireless communication systems. We start with a cooperative IBFD relaying scenario, and we analyze the spectral efficiency and outage of different cooperative schemes with imperfect channel estimation. Then, we extend the RF interference cancellation approaches to acoustic-specific cancellation techniques for IBFD UWA transceivers, and design delay diversity schemes to effectively exploit the residual interference in IBFD transceivers. Finally, we evaluate the coexistence challenges for LAA and Wi-Fi systems, and propose adaptive energy detection and carrier selection algorithms to achieve fair and effective coexistence.

In Chapter 2, we first explicitly model the residual self-loop interference and cross-talk interference caused by imperfect channel estimation. Also, we analyze the impact of overhead on the outage probability and spectral efficiency of three typical cooperative schemes when the relays operate in FD mode. Then, to better understand

the impact of direct-link signals, we derive closed-form expressions for the outage probabilities of HD and IBFD relaying over Rayleigh fading channels when the direct-link signals can or cannot be combined with the relay-to-destination transmission.

In Chapter 3, we develop IBFD modems for the UWA channel. First, we discuss three challenges in implementing IBFD UWA systems: 1) strong interference with significant delay due to reflections from the sea surface and seafloor; 2) limitations of analog cancellation in acoustics; and 3) effectiveness of some existing cancellation methods adopted from IBFD radios for UWA systems. Also, we design an acoustic-specific cancellation scheme for IBFD UWA systems with different types of residual interference. Then, to deal with the residual interference from the self-loop link and reflections, we employ delay-diversity codes and orthogonal frequency division multiplexing (OFDM) [29–31] techniques to utilize the residual interference so that we can achieve diversity gain with imperfect cancellation.

In Chapter 4, we first study the coexistence of Wi-Fi (IEEE 802.11ac) and LAA in the 5-GHz band with a single shared carrier (20 MHz). Extensive computer simulations are carried out to obtain insights on the coexistence of Wi-Fi and LTE under several different realistic implementation scenarios. Because Wi-Fi adopts preamble decoding to detect Wi-Fi signals and energy detection to sense non-Wi-Fi signals while LAA only employs energy detection, we develop adaptive energy detection algorithms for LAA to ensure the fair coexistence of these two different wireless access techniques. Then, these analyses and the adaptive energy detection algorithms are extended to the case of multiple carriers. Channel bonding is employed for IEEE 802.11ac to aggregate certain carriers to support higher throughput [3],while LAA can transmit on *any* idle carriers using carrier aggregation techniques. Based on the adaptive energy detection algorithms, an efficient carrier selection is proposed to further improve the performance of coexistent Wi-Fi and LAA networks.

Finally, we summarize our contributions and describe interesting open problems for future research in Chapter 5.

Chapter 2

COOPERATIVE IN-BAND FULL-DUPLEX (IBFD) DECODE-AND-FORWARD (DF) RELAYING

2.1 Introduction

IBFD relaying [14] can potentially double the spectral efficiency of HD relaying by allowing simultaneous transmission and reception, but it may also suffer from significant performance loss due to the severe intra-system interference, including self-loop interference, cross-talk interference and possible interference from the direct link. Thus, two questions must be answered in designing cooperative IBFD relaying schemes: (i) How to suppress or utilize these different types of interference in IBFD relaying? (ii) Does IBFD relaying really outperform HD relaying without ideal interference cancellation, if so, how much cancellation do we need?

In [14], taking the residual self-loop interference into account, the authors investigate a coverage extension scenario with one relay node, and introduce hybrid IBFD/HD relaying schemes that switch opportunistically between IBFD and HD modes. In [19], a distributed linear convolutional distributed space-time-coded relaying (DLC-STC) scheme is proposed to utilize both residual self-loop and the signals from the direct link instead of removing them for IBFD amplifier-and-forward (AF) cooperative networks. In some works [32, 33], the messages from the direct link are viewed as interference at the destination for IBFD decode-and forward (DF) relaying, and in [32], the system outage probability was derived with the residual self-loop interference and direct-link interference. Some authors have tried to utilize the direct-link messages using block Markov encoding [34, 35] or space-time coding [36]. In these works [32–35], there is only one relay in the system, but multiple relays may exist in real cooperative networks.

For a cooperative network with multiple relays, timer-based best-select relaying (TBBS) [37], Dis-STC [38] and M-group Dis-STC relaying (M-group) are three attractive schemes for practical applications since central control or full inter-relay communications is not required[1]:

- TBBS [37] is a popular selective cooperative relaying approach, where only the best node is selected to forward the source information. In particular, every eligible cooperating node sets up an individual timer based on certain performance metrics, and the node whose timer expires first is considered as the best node. Once the best node begins transmitting, all other node back off.
- In the Dis-STC scheme [38], all eligible cooperating nodes coordinate simultaneous transmissions from the multiple relays using a STC. Notice that both TBBS and Dis-STC can achieve the full diversity order [40].
- M-group Dis-STC relaying (M-group) [41] is a special case of randomized Dis-STC [42], which can significantly reduce the amount of control information in Dis-STC. In M-group, all the eligible cooperating nodes are employed, but each relay randomly chooses one column of an underlying M-column STC matrix to transmit. The diversity order is upper-bounded by M.

In this chapter, we analyze the outage probability and spectral efficiency of IBFD relaying for the three cooperative schemes described above, and determine whether IBFD relaying really outperforms HD relaying.

First, to understand the impact of the direct link, we assume the self-loop and cross-talk interference can be completely suppressed, and closed-form expressions for the outage probability for HD and IBFD relaying over Rayleigh fading channels are derived for two cases: (i) no scheme is adopted to deal with the direct-link messages, i.e., the direct-link messages are viewed as interference; and (ii) the direct-link messages are assumed to be combined with the relay-to-destination transmission. We show that the direct link plays a critical role in the performance of IBFD relaying.

Then, we analyze the spectral efficiency of cooperative IBFD systems without considering the signal or interference from the direct link. In particular, the residual

[1] The spectral efficiency of these three cooperative schemes under HD operation is analyzed in [39].

self-loop interference and cross-talk interference caused by imperfect channel estimation are explicitly modeled, and the overhead, outage probability and spectral efficiency are analyzed for IBFD relaying systems. We show that (i) the residual interference can significantly degrade the outage probability, especially for Dis-STC; (ii) IBFD can achieve a much higher spectral efficiency than HD, especially for high signal-to-noise ratio (SNR) margins; and (iii) M-group with $M \geq 3$ cannot be applied in IBFD cooperative communications.

2.2 System Model

We consider a DF cooperative network with one source-destination pair and N IBFD relay nodes, illustrated in Fig. 2.1, where the source and the destination are single-antenna nodes and the relays are equipped with separate receive and transmit antennas. For all nodes, we assume that the data transmission stage follows the channel estimation or relay selection stage, and that there is perfect time and frequency synchronization among the nodes. Different from HD relaying, IBFD relays can receive messages from the source and forward the messages to the destination at the same time. However, as shown in Fig. 2.1, due to the simultaneous transmission and reception, there exist three types of interference: 1) self-loop interference: the receive antenna of relay R_i hears its own transmission; 2) cross-talk interference: the relay R_i also receives the transmissions coming from other relays; and 3) possible interference from the direct link: the messages directly transmitted from the source to the destination may interfere with the messages forwarded by the relays. Recent cancellation schemes mainly consider the cancellation of self-loop interference [11,13,14], and they can be extended to suppress the cross-talk interference since each relay can also have information about the transmissions of the other relays. Note that the cancellation performance of cross-talk interference may decrease with time due to the accumulation of noise in the transmitted signal when amplify-and-forward relays are employed [19,20]. In contrast, in DF relaying, there will be no accumulation of noise with successful decoding at the relays.

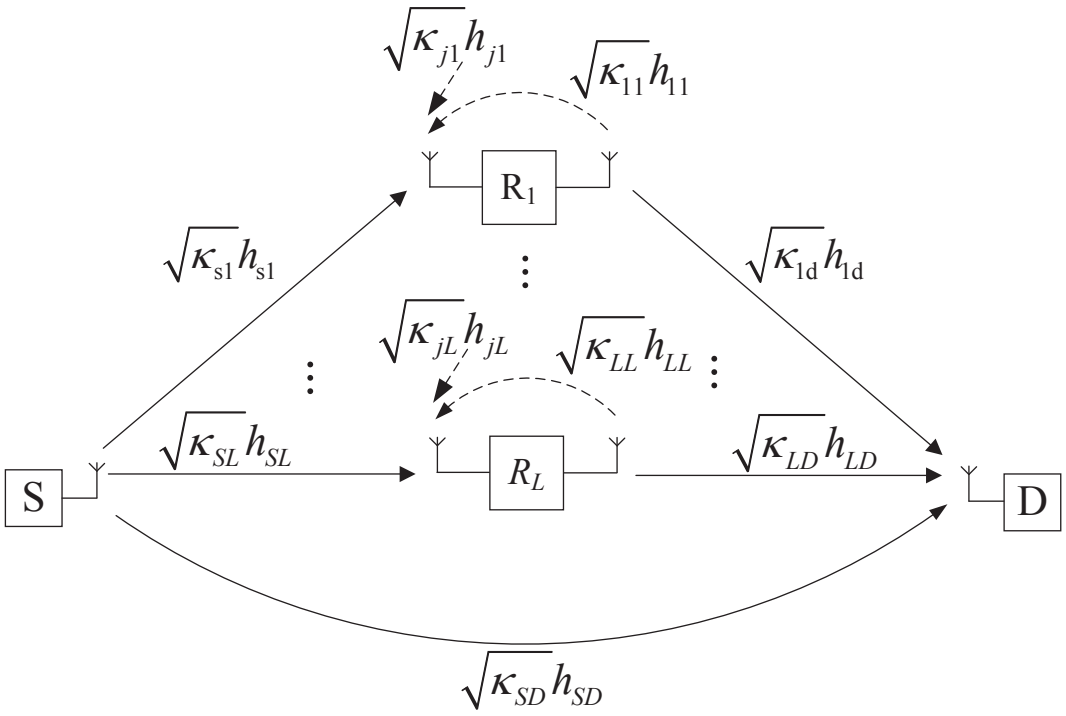

Figure 2.1: Single-phase relaying. Among N potential relay nodes, L nodes are selected to forward messages from the source.

Let γ_i denote the received signal-to-interference-plus-noise ratio (SINR) at relay R_i. We call R_i a decodable node if γ_i is larger than a pre-specified threshold γ_{th}. Let $\mathcal{D} = \{R_1, R_2, \cdots, R_L\}$ $(0 \leq L \leq N)$ denote the set of decodable nodes, where N is the total number of potential relay nodes. Note that $L = 0$ means that $\mathcal{D}$ is an empty set; in this case, we assume an outage occurs. The channel coefficient of the link from the source to relay R_i is denoted as $\sqrt{\kappa_{si}}h_{si}$ $(1 \leq i \leq L)$, where κ_{si} and h_{si} capture the path loss and multipath fading effects of the link from the source to R_i, respectively. Similarly, let $\sqrt{\kappa_{ii}}h_{ii}$, $\sqrt{\kappa_{ji}}h_{ji}$, $\sqrt{\kappa_{id}}h_{id}$ and $\sqrt{\kappa_{sd}}h_{sd}$ denote the channel coefficients of the self-loop link at R_i, the cross-talk link from R_j to R_i, the link from R_i to the destination, and the link from the source to the destination, respectively, where κ_{ii}, κ_{ji}, κ_{id} and κ_{sd} denote the path loss, and h_{ii}, h_{ji}, h_{id} and h_{sd} denote the fading effects.

We employ the classical path-loss model $\kappa(d) = G_0(\frac{d}{d_0})^{-\mu}$, where d is the distance between two nodes, d_0 is the reference distance, G_0 is the path loss at the

reference distance from the transmitter, and μ is the path loss exponent. The fading channel on the self-loop links are modeled as Rician with large K-factor [11], and the channel coefficients are assumed to be i.i.d. complex Gaussian random variables, i.e., $h_{ii} \sim \mathcal{CN}(m, \sigma^2)$ with $m^2 + \sigma^2 = 1$ [2] and $K = \frac{m^2}{\sigma^2}$, where $\mathcal{CN}(\cdot)$ denotes a complex Gaussian distribution. Rayleigh fading is assumed for all other links. Without loss of generality, the channel coefficients are assumed to be i.i.d. complex Gaussian random variables, i.e., $h_{si} \sim \mathcal{CN}(0,1), h_{id} \sim \mathcal{CN}(0,1)$ and $h_{ji} \sim \mathcal{CN}(0,1)$ for $j \neq i$. Then, at time n, the received signal at relay R_i is

$$\begin{aligned} r_i(n) = &\sqrt{P_s \kappa_{si}} h_{si} x(n) + \sqrt{P_i \kappa_{ii}} h_{ii} x_D^i(n - \tau_i) \\ &+ \sum_{j=1, j\neq i}^{L} \sqrt{P_j \kappa_{ji}} h_{ji} x_D^j(n - \tau_j) + z_i(n) \end{aligned} \tag{2.1}$$

where P_s and P_i represent the transmitted power at the source and R_i, respectively, $x(n)$ denotes the transmitted signal, τ_i denotes the processing delay at relay R_i, $x_D^i(n-\tau_i)$ is the transmitted signal at relay R_i (note that, $x_D^i(n-\tau_i)$ may be different from $x(n-\tau_i)$ if a STC matrix is applied to the transmitted signals), and $z_i(n)$ is the additive white Gaussian noise (AWGN) at relay R_i, $1 \leq i \leq L$. In summary, the first term is the desired signal, the second term is the self-loop interference, and the third term is the cross-talk interference. To avoid severe interference, the relays have to apply cancellation to eliminate the second and third terms.

Without loss of generality, we make the following assumptions: 1) all relays transmit with the same power $P_r = P_R/L$, where P_R denotes the total transmitted power at relays that forward messages; 2) the processing delay times τ_i are the same at all relays and are set as $\tau_i = 1$ $(1 \leq i \leq L)$; and 3) each relay knows the columns of the STC matrix employed by other selected relays. With these assumptions, we can

[2] Here, for simplicity, $m^2 + \sigma^2$ is normalized to 1 so that the self-loop links have the same power gain as other links. In real IBFD systems, the residual self-loop interference might still be strong; in this case, we can assume a larger $m^2 + \sigma^2$.

let $x_D^i(n) = x(n)$, and the signal at relay R_i after cancellation is

$$r_i(n) = \sqrt{P_s \kappa_{si}} h_{si} x(n) + \sqrt{P_r \kappa_{ii}} (h_{ii} - \hat{h}_{ii}) x(n-1) + \sum_{j=1, j\neq i}^{L} \sqrt{P_r \kappa_{ji}} (h_{ji} - \hat{h}_{ji}) x(n-1) + z_i(n) \tag{2.2}$$

where $\hat{h}_{ii}$ and $\hat{h}_{ji}$ denote the estimated values of h_{ii} and h_{ji}, respectively.

Similarly, the received signal at the destination is

$$r_d(n) = \sum_{i=1}^{L} \sqrt{P_i \kappa_{id}} h_{id} x_D^i(n-1) + \sqrt{P_s \kappa_{sd}} h_{sd} x(n) + z_d(n) \tag{2.3}$$

where $z_d(n)$ is AWGN at the destination, and the second term on the right side represents the messages from the direct link.

2.3 Impact of Direct Link on Outage of Cooperative IBFD Relaying

In this section, to study the impact of the direct link on the performance of an IBFD DF cooperative network, we assume perfect channel estimation can be achieved, i.e., $h_{ji} = \hat{h}_{ji}$ for $1 \leq j \leq L$ in (2.2). In other words, there will be no residual self-loop interference and cross-talk interference; the impact of these two types of interference will be analyzed in Section 2.4. In addition, to isolate our discussion from stochastic geometry [43], we assume that all the relay nodes are located close to one point between the source and the destination, i.e., the distances from the source (or destination) to different relays are approximately the same, but all relays still experience independent fading.

2.3.1 Outage Analysis: Direct Link as Interference

For IBFD relaying, since the destination receives the messages from the source and the relays simultaneously, the direct link will interfere with the relays' transmissions if one does not carefully deal with the direct link. In contrast, due to the orthogonality of the source and the relays' transmissions in HD relaying, the messages from the direct link can be ignored or easily combined at the destination.

Here, we analyze the outage of IBFD relaying when the direct link is not utilized, i.e., the messages directly received from the source are viewed as interference at the destination. For comparison purposes, we also derive the outage of HD relaying, in which we assume the direct link is simply ignored.

The SNR at relay R_i for IBFD relaying is the same as that for HD relaying,

$$\gamma_{si} = \frac{P_s \kappa_{si} |h_{si}|^2}{P_N} \tag{2.4}$$

Since the h_{si}'s are i.i.d., and $h_{si} \sim \mathcal{CN}(0,1)$, we have $|h_{si}|^2 \sim Exp(1)$ (exponentially distributed with mean 1), and the outage of the source-to-relay link is the same for all $i \in [1, L]$, i.e.,

$$p_{sr}^{HD} = \Pr(\gamma_{si} < \gamma_{th}^{HD}) = 1 - \exp\left(-\frac{\gamma_{th}^{HD}}{\overline{\gamma}_r}\right) \tag{2.5}$$

$$p_{sr}^{FD} = \Pr(\gamma_{si} < \gamma_{th}^{FD}) = 1 - \exp\left(-\frac{\gamma_{th}^{FD}}{\overline{\gamma}_r}\right) \tag{2.6}$$

where $\overline{\gamma}_r$ denotes the average SNR at each relay, $\overline{\gamma}_r = P_s \kappa_{si} / P_N$, $\gamma_{\text{th}}^{HD} = g \times (2^{2r/B} - 1)$ [44], and $\gamma_{\text{th}}^{FD} = g \times (2^{r/B} - 1)$ with the coding gain g and the target spectral efficiency r/B. Note that, in this proposal, we let HD and IBFD relaying have the same target spectral efficiency r/B; thus, the thresholds for HD (γ_{th}^{HD}) and IBFD (γ_{th}^{FD}) are different.

The SNRs at the destination for HD and IBFD will be different, and can easily be derived as

$$\gamma_{id}^{HD} = \frac{P_r \kappa_{id} |h_{id}|^2}{P_N} \tag{2.7}$$

$$\gamma_{id}^{FD} = \frac{P_r \kappa_{id} |h_{id}|^2}{P_s \kappa_{sd} |h_{sd}|^2 + P_N} \tag{2.8}$$

In (2.8), the messages from the direct link are considered as interference.

2.3.1.1 Best Selection (BS) Relaying

In the TBBS scheme, if multiple relays have the same or similar channel gains, more than one relay might be selected and a collision could happen. For simplicity, we ignore this unsuccessful relay selection and consider a general best selection

(BS) scheme here; the outage and overhead caused by relay selection in TBBS will be analyzed in Section 2.4. In the BS scheme, only one relay in $\mathcal{D}$, the one with the highest channel gain to the destination, is selected to forward the source message; then, $P_r = P_R$. For HD relaying, the relay-to-destination links are independent of each other, so the outage at the destination is

$$\begin{aligned} p_{rd}^{HB} &= \Pr\{\gamma_{1d}^{HD} < \gamma_{th}^{HD}, \gamma_{2d}^{HD} < \gamma_{th}^{HD}, ..., \gamma_{Ld}^{HD} < \gamma_{th}^{HD}\} \\ &= \prod_{i=1}^{L} Pr\{\gamma_{id}^{HD} < \gamma_{th}^{HD}\} = \left(1 - \exp(\frac{\gamma_{th}^{HD}}{\overline{\gamma}_d})\right)^L \end{aligned} \tag{2.9}$$

where $\overline{\gamma}_d$ denotes the average SNR at the destination, and $\overline{\gamma}_d = P_R\kappa_{id}/P_N$.

For IBFD relaying, the SNR for the link from R_i to the destination is given in (2.8). We define $\alpha = P_R/P_s$, and $\beta = \kappa_{id}/\kappa_{sd}$; then, the SINR γ_{id}^{FD} can be written as

$$\gamma_{id}^{FD} = \frac{\alpha\beta\overline{\gamma}_d|h_{id}|^2}{\overline{\gamma}_d|h_{sd}|^2 + \alpha\beta} \tag{2.10}$$

Thus, the outage at the destination for a given decoded set is

$$\begin{aligned} p_{rd}^{FB} &= \Pr\{\gamma_{1d}^{FD} < \gamma_{th}^{FD}, \gamma_{2d}^{FD} < \gamma_{th}^{FD}, \cdots, \gamma_{Ld}^{FD} < \gamma_{th}^{FD}\} \\ &= \int_0^\infty \prod_{i=1}^{L} Pr\{\gamma_{id}^{FD} < \gamma_{th}^{FD} | |h_{sd}|^2\} f_{|h_{sd}|^2}(x)dx \\ &= \int_0^\infty \left(1 - \exp(-\frac{\gamma_{th}^{FD}x}{\alpha\beta} - \frac{\gamma_{th}^{FD}}{\overline{\gamma}_d})\right)^L \exp(-x)dx \\ &= \sum_{i=0}^{L} \binom{L}{i} \prod_{j=1}^{i} \frac{j\gamma_{th}^{FD}}{j\gamma_{th}^{FD} + \alpha\beta} \left(1 - \exp(-\frac{\gamma_{th}^{FD}}{\overline{\gamma}_d})\right)^{L-i} \exp(-\frac{i\gamma_{th}^{FD}}{\overline{\gamma}_d}) \end{aligned} \tag{2.11}$$

The above outage at the destination for IBFD looks too complicated to give an intuitive explanation of the impact of the direct link interference. To show this impact, we consider the simplest case of $L = 1$ (in this case, there will be no relay selection process and this relay is considered as the "best" one). Then, the outages at the destination for HD and IBFD are

$$p_{rd}^{HB} = 1 - \exp\left(-\frac{\gamma_{th}^{HD}}{\overline{\gamma}_d}\right) \tag{2.12}$$

$$p_{rd}^{FB} = 1 - \frac{\alpha\beta}{\gamma_{th}^{FD} + \alpha\beta} \exp\left(-\frac{\gamma_{th}^{FD}}{\overline{\gamma}_d}\right) \tag{2.13}$$

We can conjecture that IBFD will outperform HD at low SNR since $\gamma_{th}^{HD} > \gamma_{th}^{FD}$, but IBFD will suffer from an error floor due to the existence of the factor $\alpha\beta/(\gamma_{th}^{FD} + \alpha\beta)$; this will be verified by simulation results in Section 2.3.3.

If we consider both the source-to-relay link and the relay-to-destination link, the overall outage for IBFD relaying is

$$p_{FB} = 1 - \sum_{L=1}^{N} \binom{N}{L} p_{sr}^{FD\,N-L} (1 - p_{sr}^{FD})^{L} (1 - p_{rd}^{FB}) \tag{2.14}$$

The overall outage for HD (p_{HB}) can be similarly obtained by replacing p_{sr}^{FD} and p_{rd}^{FB} with p_{sr}^{HD} and p_{rd}^{HB}.

2.3.1.2 Dis-STC Cooperative Relaying (Dis-STC)

In Dis-STC, instead of selecting the best relay, all the nodes in $\mathcal{D}$ will forward the source signal simultaneously to the destination, and each node in $\mathcal{D}$ is assigned one unique column of an L-column STC matrix to transmit, where L is the cardinality of $\mathcal{D}$. Then, to have a fair comparison with the BS scheme, we set $P_r = P_R/L$ for the Dis-STC scheme. Thus, the $|h_{id}|^2$'s are i.i.d. exponentially distributed with mean $1/L$, that is, $|h_{id}|^2 \sim Exp(L)$. Assuming orthogonal STC [45] and coherent detection are employed, the SNR at the destination is the summation of the SNRs of all the links. Let $h_\sigma = \sum_{i \in D} |h_{id}|^2$, and we have $h_\sigma \sim Erlang(L, 1)$. The associated probability density function is

$$f_{h_\sigma}(x) = \frac{x^{L-1} e^{-x}}{(L-1)!}, x \geq 0 \tag{2.15}$$

Thus, the outage at the destination for HD is

$$\begin{aligned} p_{rd}^{HS} &= \Pr\left\{\sum_{i\in D}\gamma_{id}^{HD} < \gamma_{th}^{HD}\right\} \\ &= \Pr\left\{\sum_{i=0}^{L-1}\frac{\overline{\gamma}_d|h_{id}|^2}{L} < \gamma_{th}^{HD}\right\} \\ &= 1-\exp(-\frac{L\gamma_{th}^{HD}}{\overline{\gamma}_d})\sum_{j=0}^{L-1}\frac{1}{j!}(\frac{L\gamma_{th}^{HD}}{\overline{\gamma}_d})^j \end{aligned} \tag{2.16}$$

where $\overline{\gamma}_d = P_R\kappa_{id}/P_N$.

For IBFD relaying, similar to (2.10), the SINR γ_{id}^{FD} is

$$\gamma_{id}^{FD} = \frac{\alpha\beta\overline{\gamma}_d|h_{id}|^2}{L\overline{\gamma}_d|h_{sd}|^2 + L\alpha\beta} \tag{2.17}$$

Then, we have

$$\begin{aligned} &\Pr(\sum_{i\in D}\gamma_{id}^{FD} < \gamma_{th}^{FD}\,|h_\sigma\,) \\ &= \Pr\left\{\alpha\beta(\frac{h_\sigma}{L\gamma_{th}^{FD}} - \frac{1}{\overline{\gamma}_d}) < |h_{sd}|^2\,|h_\sigma\right\} \\ &= \begin{cases} \exp\left(-\alpha\beta(\frac{h_\sigma}{L\gamma_{th}^{FD}} - \frac{1}{\overline{\gamma}_d})\right), & h_\sigma > \frac{L\gamma_{th}^{FD}}{\overline{\gamma}_d} \\ 1, & \text{otherwise} \end{cases} \end{aligned} \tag{2.18}$$

and the outage at the destination for IBFD is

$$\begin{aligned} p_{rd}^{FS} &= \Pr(\sum_{i\in D}\gamma_{id}^{FD} < \gamma_{th}^{FD}) = \int_0^\infty \Pr(\sum_{i\in D}\gamma_{id}^{FD} < \gamma_{th}^{FD}\,|h_\sigma\,)f_{h_\sigma}(x)dx \\ &= \int_0^{\frac{L\gamma_{th}^{FD}}{\overline{\gamma}_d}} \frac{x^{L-1}e^{-x}}{(L-1)!}dx + \int_{\frac{L\gamma_{th}^{FD}}{\overline{\gamma}_d}}^\infty \exp\left(-\alpha\beta(\frac{x}{L\gamma_{th}^{FD}} - \frac{1}{\overline{\gamma}_d})\right)\frac{x^{L-1}e^{-x}}{(L-1)!}dx \\ &= 1-\exp(-\frac{L\gamma_{th}^{FD}}{\overline{\gamma}_d})\left(\sum_{j=0}^{L-1}\frac{1}{j!}(\frac{L\gamma_{th}^{FD}}{\overline{\gamma}_d})^j - \sum_{j=0}^{L-1}\frac{1}{j!}(\frac{L\gamma_{th}^{FD}}{\overline{\gamma}_d})^j(\frac{L\gamma_{th}^{FD}}{\alpha\beta + L\gamma_{th}^{FD}})^{L-j}\right) \end{aligned} \tag{2.19}$$

It is easy to verify that, when $L = 1$, the outages with HD and IBFD relaying for Dis-STC are the same as for the BS scheme, which is given in (2.12) and (2.13).

By comparing the SINR (2.10) and (2.17) for the two schemes, we can see that the SINR of Dis-STC is worse than that of BS for each relay-to-destination link. Thus, we can conjecture that Dis-STC using IBFD relaying will suffer from a higher error floor than that of TBBS; this will be verified by simulation results in Section 2.3.3.

The overall outage for Dis-STC p_{FS} and p_{HS} can be similarly obtained.

2.3.2 Outage Analysis: Direct Link as Signal

Though the direct link can be easily combined at the destination for HD relaying, it is not convenient to utilize the direct link in IBFD relaying. Here, no matter what method is used, we assume the messages from the direct link can be combined with the signals from the relays for both HD and IBFD relaying. Then, the derivation of the outage for HD and IBFD will be similar, except with different decoding thresholds. Note that, $\gamma_{\text{th}}^{HD} = g \times (2^{2r/B} - 1)$, and $\gamma_{\text{th}}^{FD} = g \times (2^{r/B} - 1)$.

For simplicity, we use similar notation as in Section 2.3.1. For each relay-to-destination link, we have

$$\gamma_{id}^{HD} = \gamma_{id}^{FD} = \frac{P_r \kappa_{id} |h_{id}|^2}{P_N} \tag{2.20}$$

2.3.2.1 Best Selection Relaying (BS)

After combining the signals from the source and the best relay, the SNR at the destination is

$$\gamma_d = max\{\gamma_{1d}^{FD}, \gamma_{2d}^{FD} ..., \gamma_{Ld}^{FD}\} + \gamma_{sd} \tag{2.21}$$

and the outage for a given decoded set is

$$\begin{aligned}
p_{rd}^{FB} &= \Pr\{max\{\gamma_{1d}^{FD}, \gamma_{2d}^{FD}..., \gamma_{Ld}^{FD}\} + \gamma_{sd} < \gamma_{th}^{FD}\} \\
&= \int_0^{\infty} \prod_{i=1}^{L} Pr\{\gamma_{id}^{FD} + \gamma_{sd} < \gamma_{th}^{FD} || h_{sd}|^2\} f_{|h_{sd}|^2}(x) dx \\
&= \int_0^{\alpha\beta\gamma_{th}^{FD}/\overline{\gamma}_d} \left(1 - \exp(-\frac{\gamma_{th}^{FD}}{\overline{\gamma}_d} + \frac{x}{\alpha\beta})\right)^L \exp(-x) dx \\
&= \sum_{i=0}^{L} \binom{L}{i} \frac{1}{\prod_{j=1}^{i} (j - \alpha\beta)} \left(1 - \exp(-\frac{\gamma_{th}^{FD}}{\overline{\gamma}_d})\right)^{L-i} \\
&\times \exp(-\frac{i\gamma_{th}^{FD}}{\overline{\gamma}_d}) - \frac{L!}{\prod_{i=1}^{L} (i - \alpha\beta)} \exp(-\frac{\alpha\beta\gamma_{th}^{FD}}{\overline{\gamma}_d})
\end{aligned} \tag{2.22}$$

Note that, we should have $0 < max\{\gamma_{1d}^{FD}, \gamma_{2d}^{FD}..., \gamma_{Ld}^{FD}\} < \gamma_{th}^{FD}$ and $0 < \gamma_{sd} < \gamma_{th}^{FD}$. Thus, $0 < |h_{sd}|^2 < \frac{\alpha\beta\gamma_{th}^{FD}}{\overline{\gamma}_d}$; this is different from the case when the direct link is considered as interference.

For HD relaying, similar results can be obtained when γ_{th}^{FD} is replaced with γ_{th}^{HD}, and the overall outage p_{FB} and p_{HB} can be obtained as in deriving (2.14).

2.3.2.2 Dis-STC Cooperative Relaying (Dis-STC)

For Dis-STC, the SNR at the destination for IBFD relaying is

$$\gamma_d = \sum_{i \in D} \gamma_{id}^{FD} + \gamma_{sd} \tag{2.23}$$

Then,

$$\begin{aligned}
\Pr(\sum_{i \in D} \gamma_{id}^{FD} + \gamma_{sd} < \gamma_{th}^{FD} \,|h_\sigma) &= \Pr\left\{|h_{sd}|^2 < \alpha\beta(\frac{\gamma_{th}^{FD}}{\overline{\gamma}_d} - \frac{h_\sigma}{L}) \,|h_\sigma\right\} \\
&= 1 - \exp\left(-\frac{\alpha\beta\gamma_{th}^{FD}}{\overline{\gamma}_d} + \frac{\alpha\beta h_\sigma}{L}\right)
\end{aligned} \tag{2.24}$$

and the outage at the destination for IBFD is

$$
\begin{aligned}
p_{rd}^{FS} &= \Pr(\sum_{i\in D}\gamma_{id}^{FD}+\gamma_{sd}<\gamma_{th}^{FD}) = \int_0^{\infty}\Pr(\sum_{i\in D}\gamma_{id}^{FD}+\gamma_{sd}<\gamma_{th}^{FD}\,|h_\sigma)f_{h_\sigma}(x)dx \\
&= \int_0^{\frac{L\gamma_{th}^{FD}}{\overline{\gamma}_d}}\left(1-\exp(-\frac{\alpha\beta\gamma_{th}^{FD}}{\overline{\gamma}_d}+\frac{\alpha\beta x}{L})\right)\frac{x^{L-1}e^{-x}}{(L-1)!}dx \\
&= 1-\exp(-\frac{L\gamma_{th}^{FD}}{\overline{\gamma}_d})\left\{\sum_{i=1}^{L}\frac{1}{(L-i)!}\left(1-(\frac{L}{L-\alpha\beta})^{i}\right)(\frac{L\gamma_{th}^{FD}}{\overline{\gamma}_d})^{L-i}\right\} \\
&- (\frac{L}{L-\alpha\beta})^{L}\exp(-\frac{\alpha\beta\gamma_{th}^{FD}}{\overline{\gamma}_d})
\end{aligned}
\tag{2.25}
$$

Note that, since $0<\sum_{i\in D}\gamma_{id}^{FD}+\gamma_{sd}<\gamma_{th}^{FD}$, we should have $0<|h_{sd}|^2<\frac{\alpha\beta\gamma_{th}^{FD}}{\overline{\gamma}_d}$ and $0<\sum_{i\in D}\gamma_{id}^{FD}<\frac{L\gamma_{th}^{FD}}{\overline{\gamma}_d}$. Similarly, the overall outage can be derived as in (2.14).

2.3.3 Simulation Results

We evaluate the impact of the direct link for different cooperative relaying schemes under HD and IBFD relaying using simulations. Both HD and IBFD relaying have the same target spectral efficiency $r/B = 2$ bps/Hz, and we choose the degree of coding $g = 1$. In the path-loss model, we set $d_0 = 1$ m, $10 * \log_{10}G_0 = -38$ dB, and $\mu = 4$.

To verify the correctness of the derivations in Sections 2.3.1 and 2.3.2, we plot the outage probability as a function of $P_{tot}\kappa_{sd}/P_N$ from the formulas (solid line) and using Monte Carlo simulation (dashed line) in Fig. 2.2 and Fig. 2.3 for BS and Dis-STC, respectively. As shown in Fig. 2.2, we use "UDL" to denote the case when the direct link is combined with the signals from the relays (the analysis in Section 2.3.2), and "NDL" to denote the other case (the analysis in Section 2.3.1). First, the outage curves match very well for both cases under HD and IBFD relaying. Also, we can see that, in the "NDL" case, IBFD outperforms HD at low SNR since $\gamma_{th}^{FD}<\gamma_{th}^{HD}$, but IBFD relaying will suffer from a high error floor due to the existence of interference from the direct link. Further, in the "UDL" case, the performance of IBFD relaying

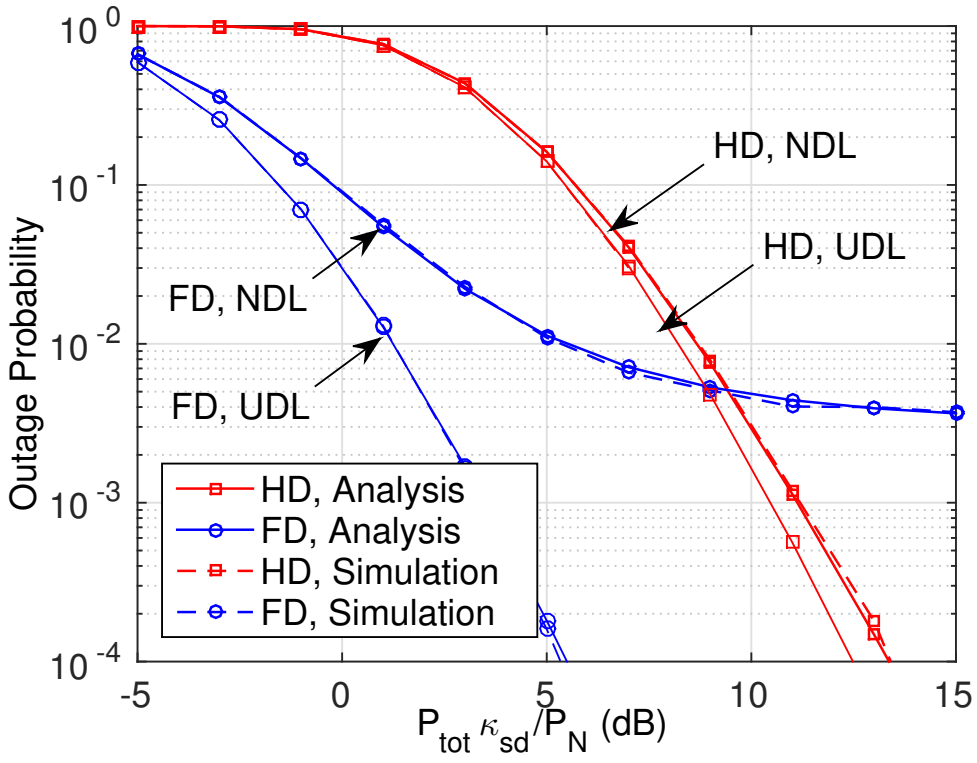

Figure 2.2: Outage probability as a function of $P_{tot}\kappa_{sd}/P_N$ for BS relaying with $N = 5$ (number of potential relays).

is greatly improved compared with that of the "NDL" case, and the performance gain for HD relaying is limited; this means that the direct link cannot offer much diversity gain due to relatively weak signal strength, but may severely degrade the performance of IBFD relaying when it is viewed as interference.

For Dis-STC relaying, similar conclusions can be obtained from Fig. 2.3, and STC suffers from a higher error floor than that of BS relaying. These results are consistent with the conjectures in Section 2.3.1.

In Fig. 2.4, the outage is plotted as a function of the number of potential relay nodes for BS (solid line) and Dis-STC relaying (dashed line). First, as the number of potential relay nodes increases, the outage will decrease because of the diversity gain. Also, the utilization of the direct link can significantly improve the performance for IBFD relaying. From all of the results, we can conclude that the direct link plays a

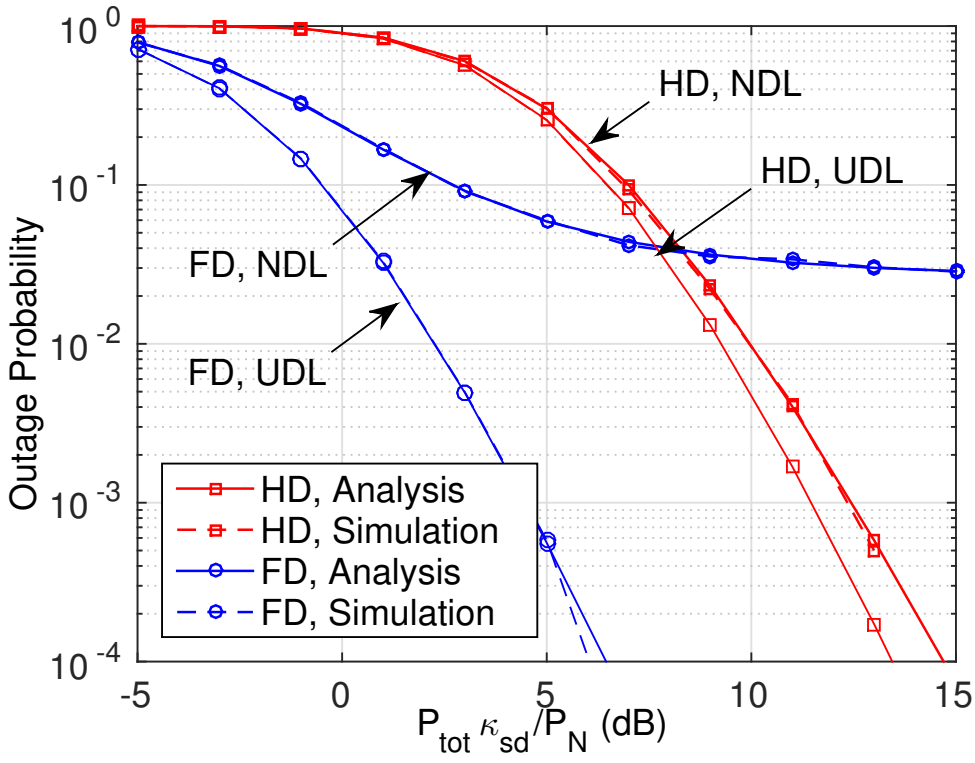

Figure 2.3: Outage probability as a function of $P_{tot}\kappa_{sd}/P_N$ for Dis-STC relaying with $N = 5$ (number of potential relays).

critical role in the performance of IBFD relaying, and certain techniques are necessary to utilize the direct link to avoid severe performance loss.

2.4 Spectral Efficiency of Cooperative IBFD Relaying with Imperfect CSI

In Section 2.3, we investigated the impact of the direct link on performance of an IBFD DF cooperative network by assuming ideal cancellation of the self-loop and cross-talk interference. However, ideal cancellation is difficult to achieve due to imperfect channel estimation and non-ideal signal processing. In this section, we analyze the spectral efficiency of IBFD relaying with residual self-loop and cross-talk interference caused by imperfect channel estimation. The direct link from the source to destination is assumed to be very weak due to the presence of deep fading or shadowing, i.e., the

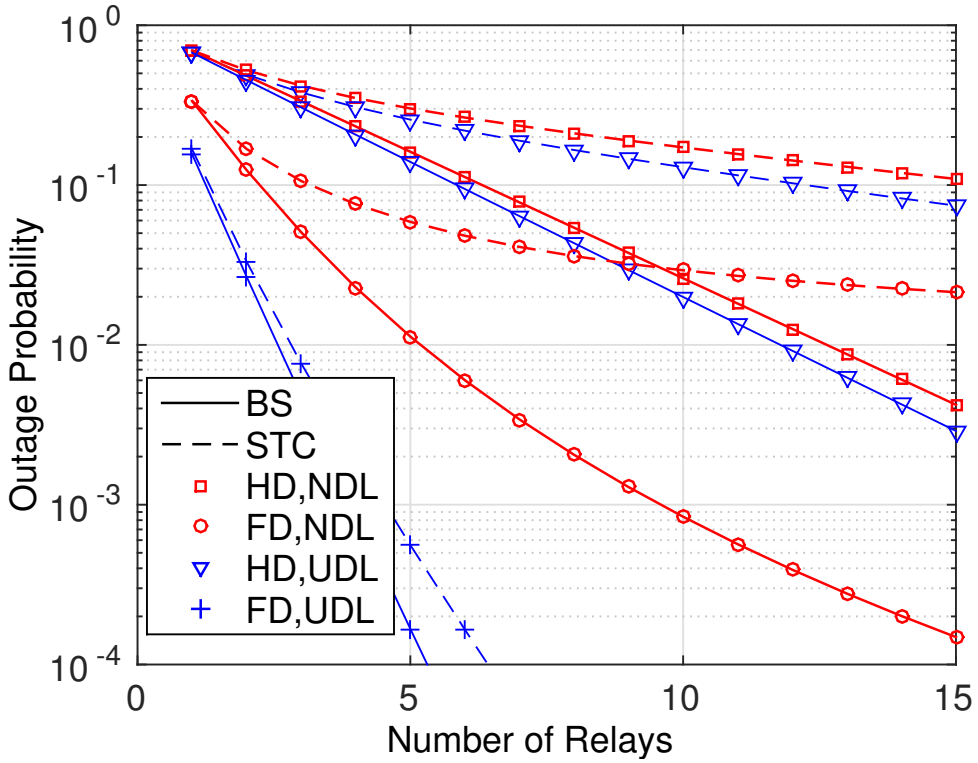

Figure 2.4: Outage probability as a function of the number of potential relay nodes for both BS and Dis-STC relaying. ($P_{tot}\kappa_{sd}/P_N = 5$ dB)

received signal at the destination, (2.3), becomes

$$r_d(n) = \sum_{i=1}^{L} \sqrt{P_i \kappa_{id}} h_{id} x_D^i(n-1) + z_d(n) \tag{2.26}$$

2.4.1 Channel Estimation Overhead: TBBS, Dis-STC and M-group

Generally, a training sequence is used to estimate the channel response. Let h and $\hat{h}$ denote the actual channel and the estimated channel, respectively. However, due to the existence of residual interference, the overhead incurred by the channel estimation of IBFD relaying is different from that of HD relaying. Assuming h and $\hat{h}$ are jointly ergodic and stationary Gaussian processes, we can write

$$h = \hat{h} + \epsilon \tag{2.27}$$

where $h \sim \mathcal{CN}(m_h, \sigma_h^2)$ with $m_h^2 + \sigma_h^2 = 1$, so that the gain is normalized, and where ϵ is the estimation error. Assuming a linear minimum-mean-square-error estimator, ϵ is uncorrelated with $\hat{h}$ and is distributed as $\epsilon \sim \mathcal{CN}(0, \sigma_\epsilon^2)$ [46], where

$$\sigma_\epsilon^2 = \frac{\sigma_h^2}{1 + \overline{\gamma}\sigma_h^2 N_t} \tag{2.28}$$

where $\overline{\gamma}$ is the average SNR for the training sequence and N_t is the number of training sequences. The received signal at relay R_i is given in (2.2); then, using a maximum likelihood receiver, the output of the detector is

$$\hat{x}(n) = \sqrt{P_s \kappa_{si}} \hat{h}_{si}^* r_i(n) \tag{2.29}$$

where $[\cdot]^*$ denotes conjugation. Then, the SINR at relay R_i, including the estimation error and residual interference, is

$$\gamma_i = \frac{P_s \kappa_{si} \left|\hat{h}_{si}\right|^2}{P_s \kappa_{si} \sigma_{\epsilon_{si}}^2 + P_r \kappa_{ii} \sigma_{\epsilon_{ii}}^2 + \sum_{j=1, j\neq i}^{L} P_r \kappa_{ji} \sigma_{\epsilon_{ji}}^2 + P_N} \tag{2.30}$$

where P_N is the power of the noise, and $\sigma_{\epsilon_{si}}^2$, $\sigma_{\epsilon_{ii}}^2$, and $\sigma_{\epsilon_{ji}}^2$ are the variances of the estimation errors of h_{si}, h_{ii} and h_{ji}, respectively. According to (2.28), we have

$$\sigma_{\epsilon_{si}}^2 = \frac{1}{1 + \frac{P_s \kappa_{si}}{P_N} N_t} \approx \frac{1}{\frac{P_s \kappa_{si}}{P_N} N_t} \tag{2.31}$$

$$\sigma_{\epsilon_{ii}}^2 = \frac{\sigma^2}{1 + \frac{P_r \kappa_{ii}}{P_N} \sigma^2 N_t} \approx \frac{1}{\frac{P_r \kappa_{ii}}{P_N} N_t} \tag{2.32}$$

$$\sigma_{\epsilon_{ji}}^2 = \frac{1}{1 + \frac{P_r \kappa_{ji}}{P_N} N_t} \approx \frac{1}{\frac{P_r \kappa_{ji}}{P_N} N_t} \tag{2.33}$$

where the approximation is very accurate in the high SNR region, i.e., $\frac{P_s \kappa_{si}}{P_N} \gg 1$, $\frac{P_r \kappa_{ii}}{P_N} \sigma^2 \gg 1$ and $\frac{P_r \kappa_{ji}}{P_N} \gg 1$. Considering that high SNR is often the case of interest, we use the above approximations in the following analyses. Then, (2.30) can be simplified as

$$\gamma_i \approx \frac{\frac{P_s}{P_N} \kappa_{si} \left|\hat{h}_{si}\right|^2}{\frac{L+1}{N_t} + 1} \tag{2.34}$$

Note that, although the interference is much stronger than the desired signals, the channel estimation of the self-loop link and the cross-talk link are more accurate due to a higher SNR. Thus, the impact of imperfect channel estimation on the SINR for different signals is similar, as can be seen from (2.34). Also, the SINR decreases as the number of selected nodes increases.

In selective relaying, like TBBS [37], since only one relay is selected for transmission, there will be no cross-talk interference, and the SINR at R_i is

$$\gamma_i^{\mathrm{BS}} \approx \frac{\frac{P_s}{P_N}\kappa_{si}\left|\hat{h}_{si}\right|^2}{\frac{2}{N_t}+1} \tag{2.35}$$

If γ_i^{BS} is higher than the specified threshold γ_{th}, relay R_i is selected as a potential relay, and all the potential relays comprise the decoded set $\mathcal{D}_{\mathrm{BS}}$.

If Dis-STC [38] is used, the number of potential relays depends on the SINR, which is related to the size of the decoded set. Thus, we cannot determine the decoded set in this case. One simple approach is to define $\widetilde{\gamma} = (\frac{P_s}{P_N}\kappa_{si}\left|\hat{h}_{si}\right|^2)/(\frac{N+1}{N_t}+1)$, where N is the total number of potential relay nodes. If $\widetilde{\gamma}$ is higher than the specified threshold γ_{th}, relay R_i is included in the decoded set $\mathcal{D}_{\mathrm{ST}}$. Let L denote the cardinality of $\mathcal{D}_{\mathrm{ST}}$, then, each node in $\mathcal{D}_{\mathrm{ST}}$ is assigned one unique column of an L-column STC matrix to transmit. Then, the SINR of Dis-STC (γ_i^{STC}) reduces to (2.34).

In M-group [41], an underlying M-column STC matrix is utilized, and every potential relay randomly chooses one column to transmit. Thus, the decoded set is equivalently divided into M groups, $\mathcal{G}_1, \mathcal{G}_2, \cdots, \mathcal{G}_M$ (note that M does not change with the decoded set and empty groups might exist). As stated in [39], since the relays in one group transmit the same message, the composite channel link from the relays in one group to the destination can be viewed as a Rayleigh channel. Here, we can also obtain similar equivalent channels for the channel links among relays nodes. For example, for a group $\mathcal{G}_m$ that includes R_i ($1 \le m \le M, 1 \le i \le N$), the self-loop link of R_i together with the cross-talk links from other relays in $\mathcal{G}_m$ to R_i can be modeled as a Rician channel. In addition, the links from relays in other groups $\mathcal{G}_{\overline{m}}$ ($\overline{m} \neq m$ and $1 \le \overline{m} \le M$) to R_i can be modeled as a Rayleigh channel. Note that, although

the variances of the equivalent Rician and Rayleigh channels are the summation of the variances of the individual channels, the approximations in (2.31)-(2.33) are still accurate when the number of nodes in each group is not large. Therefore, we can view the potential relays as M virtual nodes both during the channel estimation stage and the data transmission stage. Thus, the SINR at R_i is approximated as

$$\gamma_i^M \approx \frac{\frac{P_s}{P_N}\kappa_{si}\left|\hat{h}_{si}\right|^2}{\frac{M+1}{N_t}+1} \tag{2.36}$$

Relay R_i is selected as a potential relay if $\gamma_i^M > \gamma_{\text{th}}$, and all the potential relays comprise the decoded set $\mathcal{D}_{\text{M}}$. In Section 2.4.2, we will show that only $M = 2$ can be used for IBFD relays.

2.4.2 Spectral Efficiency Analysis

In this section, to analyze the performance-overhead trade-off for different cooperative techniques with IBFD relaying, we follow the work of [39]; the efficiency is defined as

$$\eta = \frac{r}{B}\frac{T_e}{T}p_{\text{suc}} \tag{2.37}$$

where r is the bit rate of the data transmission, T_e is the effective data transmission time, B is the bandwidth, T is the total transmission time, and p_{suc} is the successful decoding probability at the destination. Note that there is an additional factor of $1/2$ for HD relaying [39]. In the following analysis, to isolate our discussion from the issues of stochastic geometry [43], we assume that the distance from the source to relay R_i and that from R_i $(1 \leq i \leq N)$ to the destination are all approximately the same; in this case, the path loss (κ_{si} and κ_{id}) can be normalized to one. The impact of randomly distributed relays will be discussed in Section 2.4.3.

2.4.2.1 Timer-Based Best-Select Relaying

In the channel estimation stage, the relays do not transmit training sequences when the source or destination is broadcasting its training signals; this guarantees that the channel estimation is not severely degraded. Thus, in TBBS, three training

sequences are required to estimate CSI: the first one is broadcast from the source to all relays to obtain $\hat{h}_{si}$, the second one is broadcast from the destination to all relays to obtain $\hat{h}_{id}$ (the channels are assumed to be reciprocal), and the last one is transmitted from the selected relay R_i so that R_i can obtain $\hat{h}_{ii}$ and the destination can acquire $\hat{h}_{id}$. In addition, in the selection stage, each node in the decoded set $\mathcal{D}_{\text{BS}}$ sets up an individual timer, which is configured as $t_i = \lambda/|\hat{h}_{id}|^2$ [37], where λ is a scaling factor associated with the average SNR and $\hat{h}_{id}$ is the estimated channel coefficient. If one timer expires, the associated node immediately forwards the source message to the destination, and, at the same time, all other relays back off when they overhear this transmission. We use T_s to denote the selection time, and T_t to represent the time period of one training sequence. Thus, the effective time for data transmission is $T_e = T - 3T_t - T_s$.

For the link from the source to R_i, we have $\hat{h}_{si} = h_{si} - \epsilon_{si} \sim \mathcal{CN}(0, \sigma_{si}^2)$, and $\sigma_{si}^2 = 1 - \sigma_{\epsilon_{si}}^2 = \frac{\overline{\gamma}_i N_t}{\overline{\gamma}_i N_t + 1}$, where $\overline{\gamma}_i$ is the average SNR at R_i, i.e., $\overline{\gamma}_i = P_s/P_N$. Then, $|\hat{h}_{si}|^2 \sim Exp(\frac{1}{\sigma_{si}^2})$. Since the h_{si}'s are i.i.d., the outage of the source-to-relay link is the same for all i, giving

$$\begin{aligned} p_{\text{BS}} &= Pr\{\gamma_i^{\text{BS}} < \gamma_{\text{th}}\} \approx Pr\{|\hat{h}_{si}|^2 < \frac{\gamma_{\text{th}}}{\overline{\gamma}_i}\frac{N_t+2}{N_t}\} \\ &= 1 - \exp\left[-\frac{\gamma_{\text{th}}}{\overline{\gamma}_i}\frac{N_t+2}{N_t}\frac{\overline{\gamma}_i N_t + 1}{\overline{\gamma}_i N_t}\right] \end{aligned} \tag{2.38}$$

Since DF relaying is assumed, there will be no difference for the link from the relay to the destination whether HD or IBFD is used. Let $p_{\text{BS,II}}$ denote the outage of the relay-to-destination link; this is given in Eq. (12) of [39]. Therefore, the spectral efficiency of TBBS is

$$\begin{aligned} \eta_{\text{BS}} = \frac{r}{B}\sum_{L=1}^{N}\binom{N}{L}(1-p_{\text{BS}})^L(p_{\text{BS}})^{N-L}(1-p_{\text{BS,II}}^L) \\ \times \frac{T-3T_t-T_s}{T}[1-p_{\text{coll}}(L)] \end{aligned} \tag{2.39}$$

where p_{coll} is the collision probability in the selection stage, which is given in Eq. (6) of [39]. Here, a collision means that more than one node is selected for transmission,

which can occur if the difference between the two timers is small [37].

2.4.2.2 Dis-STC Cooperative Relaying

In the Dis-STC scheme, each selected relay R_i is required to transmit one training sequence. Then, R_i can obtain the estimated self-loop channel gain $\hat{h}_{ii}$, other relays R_j ($j \in \mathcal{D}_{\mathrm{ST}}$ and $j \neq i$) obtain $\hat{h}_{ij}$, and the destination also acquires $\hat{h}_{id}$. In this case, assuming the size of $\mathcal{D}_{\mathrm{ST}}$ is L, then, LT_t is required in Dis-STC to obtain the associated CSI. In addition, as discussed in Section 2.4.1, each relay needs to know the columns of the STC matrix employed by other selected relays to suppress cross-talk interference, and the destination needs to assign a unique column of an L-column STC matrix to each relay in $\mathcal{D}_{\mathrm{ST}}$; the latter can be done by broadcasting the assignment from the destination (the time consumption is assumed to be T_t). Thus, including the T_t consumed to obtain $\hat{h}_{si}$, the effective data transmission time is $T_e = T - (L+2)T_t$.

Similar to the derivation of (2.38), the outage probability of the link from the source to any relay is

$$p_{\mathrm{ST}} \approx 1 - \exp\left[-\frac{\gamma_{\mathrm{th}}}{\overline{\gamma}_i}\frac{N_t + L + 1}{N_t}\frac{\overline{\gamma}_i N_t + 1}{\overline{\gamma}_i N_t}\right] \tag{2.40}$$

Therefore, the spectral efficiency of Dis-STC becomes

$$\begin{aligned}\eta_{\mathrm{ST}} = \frac{r}{B}\sum_{L=1}^{N}\binom{N}{L}(1-p_{\mathrm{ST}})^{L}(p_{\mathrm{ST}})^{N-L}\frac{\lceil L/2\rceil + 1}{2\lceil L/2\rceil} \\ \times \frac{T-(L+2)T_t}{T}[1 - p_{\mathrm{ST,II}}(L)]\end{aligned} \tag{2.41}$$

where $\lceil x\rceil$ denotes the least integer not less than x, the factor $\frac{\lceil L/2\rceil+1}{2\lceil L/2\rceil}$ is the maximum code rate for orthogonal STC [45], and $p_{\mathrm{ST,II}}$ is the outage probability at the destination, which is given in Eq. (17) of [39].

2.4.2.3 M-group Dis-STC Cooperative Relaying

As discussed in Section 2.4.1, in the M-group scheme, the relay nodes in each group can be viewed as a virtual node, which means that the relays in one group can transmit a training sequence simultaneously. Thus, a time consumption of MT_t

is required to estimate the virtual links from each group to the destination, and the virtual links from one group to itself and other groups. In addition, to suppress the cross-talk interference, each relay, when using IBFD, needs to know the columns of the STC matrix employed by other groups. In other words, each group has to broadcast the information about its chosen column to other relays. However, M-group has been proposed to reduce the overhead incurred in Dis-STC [41], i.e., to avoid inter-node communication. Therefore, M-group is not appropriate in IBFD cooperative communications if $M \geq 3$. For 2-group, one group automatically obtains the information about the chosen column of the other group. The total time consumed for 2-group is thus $3T_t$, which includes the T_t consumed to obtain $\hat{h}_{si}$. Similar to the derivation of (2.38), the outage of the link from the source to any relay is

$$p_{\mathrm{M}} \approx 1 - \exp\left[-\frac{\gamma_{\mathrm{th}}}{\overline{\gamma}_i}\frac{N_t+3}{N_t}\frac{\overline{\gamma}_i N_t+1}{\overline{\gamma}_i N_t}\right] \tag{2.42}$$

Therefore, the spectral efficiency of M-group is

$$\begin{aligned}\eta_{\mathrm{M}} = {} & \frac{r}{B}\sum_{L=1}^{N}\binom{N}{L}(1-p_M)^L(p_M)^{N-L} \\ & \times \frac{T-3T_t}{T}[1-p_{\mathrm{M,II}}(L)]\end{aligned} \tag{2.43}$$

where $p_{\mathrm{M,II}}$ is the outage at the destination, which is given in Eq. (21) of [39].

2.4.3 Simulation Results

In this section, we first evaluate the impact of overhead on the spectral efficiency for different cooperative relaying schemes without considering the effect of path loss. The end-to-end transmission duration is set as $T = 1$ msec, and one symbol length is assumed to be 0.01 msec, which means that $T_t/T = N_t/100$. The SNR threshold γ_{th} for the relays and the destination are both determined from $g \times (2^{2r/B} - 1)$ [44], where r/B is the maximum possible spectral efficiency and g depends on the degree of coding; we choose $r/B = 1$ bps/Hz and $g = 1$. For a fair comparison, a total transmit

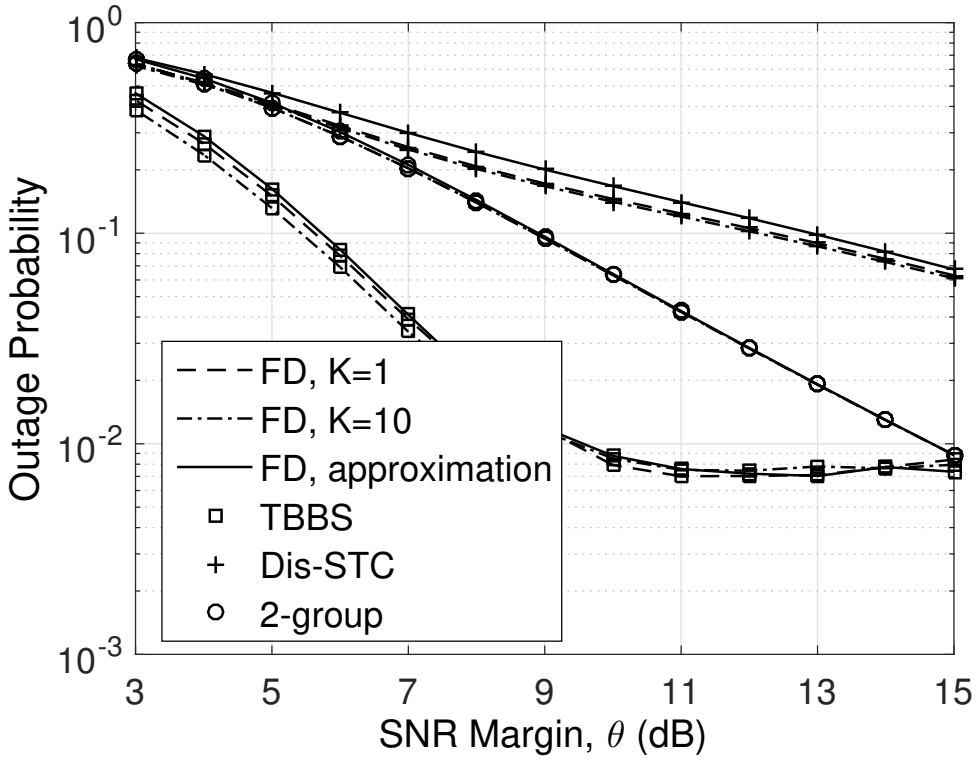

Figure 2.5: Exact and approximate outage probability as a function of SNR margin for IBFD relaying with different K-factors, $N_t = 2$ (number of training sequences) and $N = 5$ (number of potential relays).

power constraint is applied, and uniform power allocation is assumed for the selected relays[3], i.e., $LP_r = P_s$.

To verify the accuracy of the approximations for SINR in Section 2.4.1, in Fig. 2.5, we present the exact and approximate outage probabilities of different cooperative schemes for IBFD relaying with different K-factors. The outage probability is plotted as a function of the SNR margin θ, which is defined as the ratio of the average SNR (P_s/P_N) to the SNR threshold (γ_{th}), $\theta = P_s/(\gamma_{\text{th}}P_N)$. Two training sequences $(N_t = 2)$ and five potential relays $(N = 5)$ are assumed. We can see from the results that the

[3] Compared to HD relaying, IBFD relaying may consume more energy due to the interference cancellation required; this has not been considered here. Thus, we refer to transmit power for simplicity, and the transmit power budget is set to be the same for both HD and IBFD relaying.

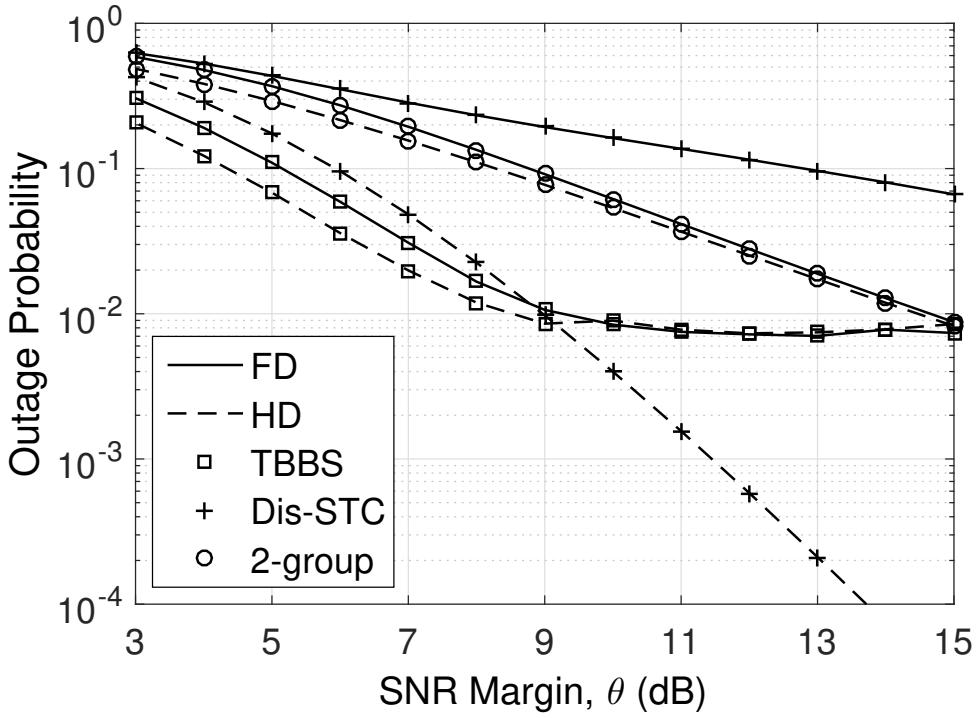

Figure 2.6: Outage probability as a function of SNR margin for IBFD and HD relaying with $N_t = 2$ (number of training sequences) and $N = 5$ (number of potential relays).

approximations are quite accurate for all three cooperative schemes. Therefore, in what follows, we only present results using the approximate SINRs.

In Fig. 2.6, we compare the outage probability for IBFD and HD relaying. It can be seen that the outage probability in IBFD relaying is worse than that for HD relaying for all three cooperative schemes, especially at low SNR, due to the existence of residual interference. In particular, for HD relaying, TBBS and Dis-STC outperform 2-group at low SNR due to the high diversity order. Also, for a large SNR margin, the advantage of TBBS disappears; the outage for TBBS increases slowly as the SNR increases because of a large decoded set and small timer differences [37] resulting in a high collision probability. For IBFD relaying, Dis-STC suffers severe performance loss, which agrees with the analysis in Section 2.4.1, i.e., the SINR decreases inversely with the number of selected relays for Dis-STC, resulting in a small decoded set and high

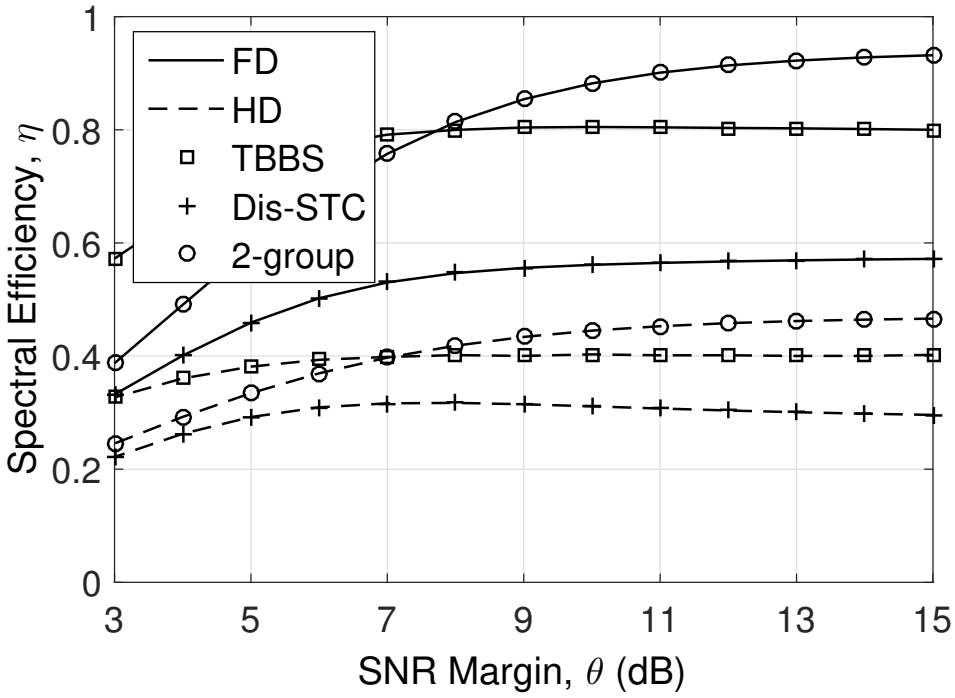

Figure 2.7: Spectral efficiency as a function of SNR margin for IBFD and HD relaying with $N_t = 2$ (number of training sequences) and $N = 5$ (number of potential relays).

outage.

In Fig. 2.7, we show the spectral efficiency of different cooperative schemes as a function of the SNR margin θ. First, we see that the spectral efficiency of IBFD relaying is much higher than that of HD relaying due to simultaneous transmissions at the same frequency. At low SNR margin, the gain is less than a factor of 2 due to the existence of residual interference. In contrast, the spectral efficiency is almost double that of HD at high SNR margin. In this case, the channel estimation is very accurate, and the impact of the interference is negligible. Moreover, we notice that 2-group requires a higher SNR margin to outperform TBBS for IBFD relaying compared to HD relaying; this is caused by the fact that the residual interference of 2-group is larger than that of TBBS for IBFD relaying, which is even worse for Dis-STC.

Next, we evaluate the spectral efficiencies of TBBS and 2-group in the presence of path loss. The N potential relays are uniformly distributed in a square area of size 100 m $\times$ 100 m, and the source and destination nodes are placed at opposite corners. The path-loss model $\kappa(d) = G_0(\frac{d}{d_0})^{-\mu}$ is employed, where G_0 is the path loss at the reference distance, d_0, from the transmitter, and we consider $d_0 = 1$ m, $10 * \log_{10} G_0 = -38$ dB, and $\mu = 4$. In the following simulations, the locations of all the other potential relays are randomly generated and 100 realizations are considered. For any given geographic distribution, a large number of realizations of instantaneous channel gains are generated to evaluate the outage probability. Finally, the spectral efficiency is averaged over all the realizations of the geographic distributions of the nodes. Moreover, since Dis-STC suffers a great performance loss due to the high overhead, in what follows, we focus on TBBS and 2-group.

To normalize our results, we plot the spectral efficiency as a function of $P_s/P_{\max}$, where $P_{\max}$ is the transmit power required for the direct link (the link between the source and destination) to achieve the maximum possible spectral efficiency r/B without Rayleigh fading [44]. As shown in Fig. 2.8, IBFD relaying can almost double the spectral efficiency of HD, especially when $P_s/P_{\max}$ is large. Fig. 2.9 illustrates the spectral efficiencies of TBBS and 2-group with different numbers of potential relays and $N_t = 2$; it shows that 2-group outperforms TBBS as the number of nodes increases even for a small value of $P_s/P_{\max}$ (-2 dB). Therefore, we can conclude that the gain of 2-group over TBBS becomes even larger when $P_s/P_{\max}$ or N increases for both HD and IBFD relaying; this is because TBBS suffers from increased relay selection overhead while 2-group has a constant amount of overhead. Also, due to the impact of residual interference, 2-group requires more cooperative nodes to outperform TBBS in the IBFD relaying case compared to HD relaying. In addition, Figs. 2.8 and 2.9 show that the path loss and randomness of the relay locations have little effect on the performance gap between HD and IBFD relaying.

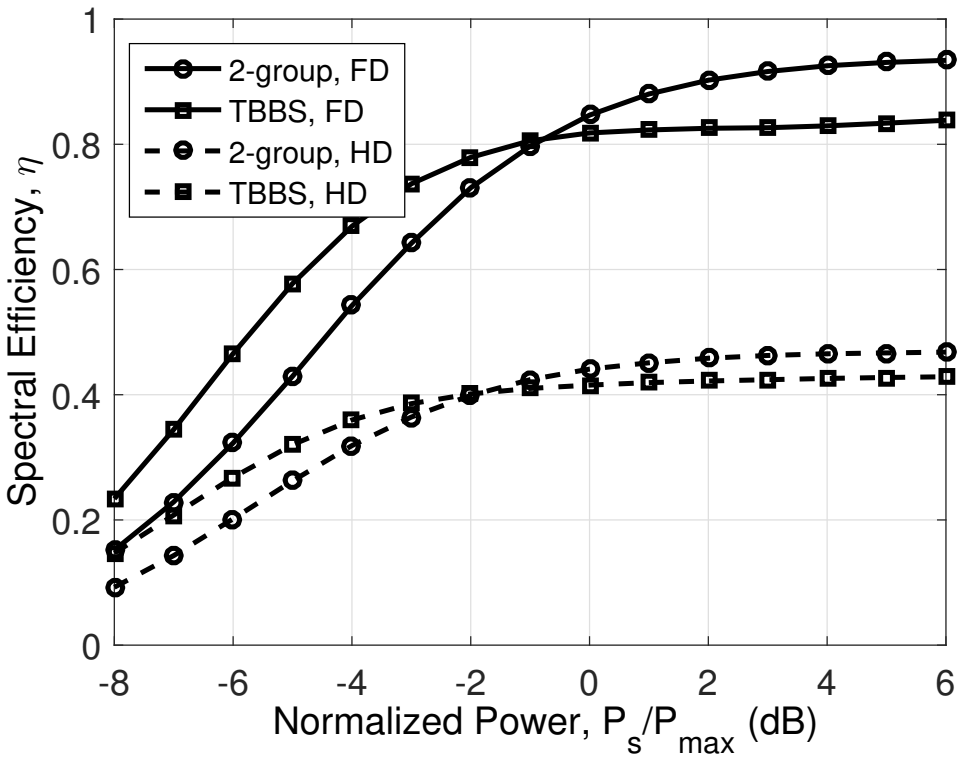

Figure 2.8: Spectral efficiency as a function of the normalized power for IBFD and HD relaying with $N_t = 2$ (number of training sequences) and $N = 5$ (number of potential relays).

2.5 Summary

In this chapter, we first analyzed the impact of the direct link for IBFD cooperative communications under two conditions: 1) the signals from the direct link are considered as interference at the destination, and 2) the signals from the direct link are combined with the relays' transmissions at the destination. Both analytical and simulation results showed that the direct link may cause a severe error floor and significantly degrade the performance of IBFD relaying for both BS and STC relaying.

Then, we studied the spectral efficiency of IBFD relaying, in which self-loop interference and cross-talk interference cannot be completely suppressed due to imperfect channel estimation. Particularly, the residual interference is viewed as extra overhead for IBFD relaying and the spectral efficiencies of three typical cooperative

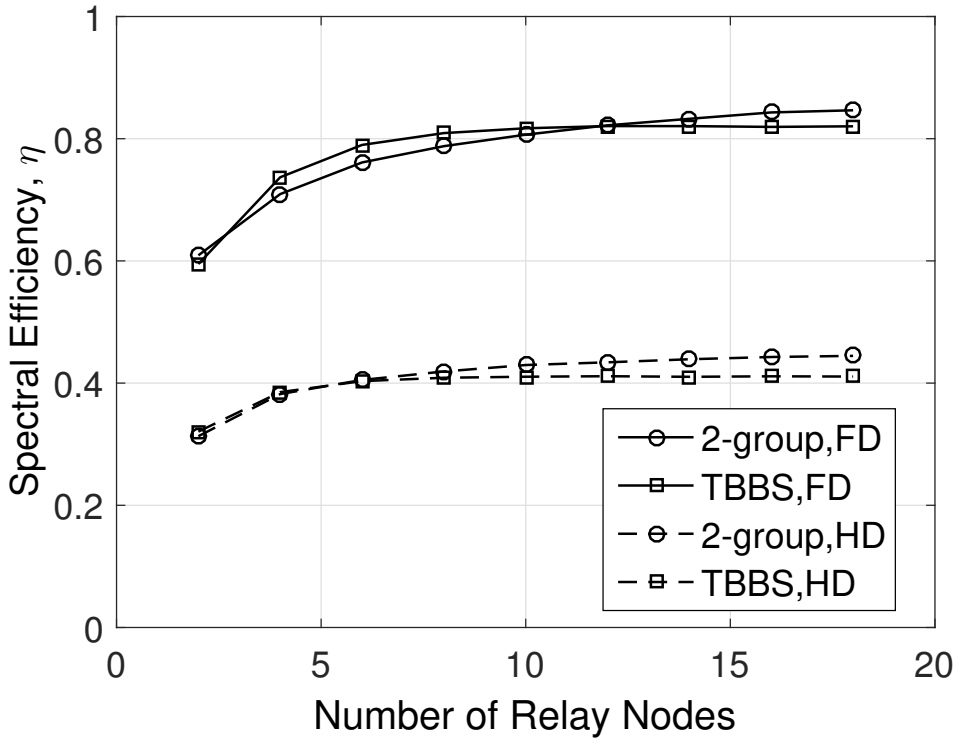

Figure 2.9: Spectral efficiency as a function of the number of potential relay nodes for IBFD and HD relaying with $N_t = 2$ (number of training sequences) and $P_s/P_{\max} = -2$ dB.

relaying schemes are derived. In summary, the results exhibit three main differences between HD and FD: (i) the SINR will decrease for IBFD relaying, which will degrade the outage probability of cooperative communications, especially for Dis-STC; (ii) although the overhead incurred in IBFD relaying is higher than that of HD, IBFD can still achieve a much higher spectral efficiency due to the simultaneous transmissions at the same frequency; and (iii) only 2-group is applicable for IBFD cooperative communications since inter-node communication is prohibited in M -group.

In the future, the following three aspects can be investigated: 1) analyze the spectral efficiency of IBFD relaying with three different types of interference, i.e., the interference from a relay's own transmission, from other relays' transmissions, and also from the source's transmission; 2) design STC schemes to utilize the residual

interference so that IBFD relaying will not suffer from error floor problems; and 3) study the relay selection problem in IBFD-like cooperative transmission schemes as proposed in [47–51], which adopt multiple HD relays to mimic IBFD relays so that the factor of 1/2 in HD relaying and the strong self-loop interference in IBFD relaying can both be avoided.

Chapter 3

INTERFERENCE IN IN-BAND FULL-DUPLEX (IBFD) UNDERWATER ACOUSTICS (UWA) SYSTEMS

3.1 Introduction

Underwater acoustic (UWA) communications has been widely discussed for monitoring marine environments, exploring ocean resources, and responding to man-made disasters. However, due to the extremely limited bandwidth of UWA channels, with a maximum of only tens of kilohertz, and the harsh ocean environment, UWA communications generally provides only low data rates [52–54], especially over long communication distances. Significant progress has been made over the past two decades in supporting high data rates with acceptable reliability in UWA communications. For example, channel modeling and equalization [53], multicarrier modulation, especially in the form of orthogonal frequency-division multiplexing (OFDM) [55–57], and multiple-input-multiple-output (MIMO) techniques [58–60] have resulted in improved throughput and enhanced robustness of UWA communication systems.

As mentioned in Chapter 1, the fundamental difficulty for UWA communication networks lies in the narrow bandwidth available, with a maximum of only tens of kilohertz [21, 23, 24]. Recently, radio-frequency (RF) testbed implementations [10, 12, 13] have proven that in-band full-duplex (IBFD) is feasible and can outperform half-duplex (HD) systems. This approach enables two transceivers to communicate over a bidirectional channel using the same temporal and spectral resources. Therefore, IBFD ideally renders up to double the spectral efficiency with respect to conventional HD systems. Considering that the bandwidth available for UWA communications is extremely limited [23], it is reasonable and desirable to investigate the employment of IBFD techniques in UWA systems. As described in [10, 12, 13], the suppression or cancellation of

the strong self-loop interference caused by its own transmission plays the most critical role in the performance of an IBFD RF transceiver. In [10], an extra transmit chain is used to generate an RF reference signal for cancellation. Implementations in [12] employ multiple antennas or fixed phase shifters to create a null point at the receive antennas. In [13], samples of the RF self-loop interference are interpolated to generate the reference signal for cancellation. Among the limited work on IBFD UWA systems, the UWA modems in [22] perform FD communications through a frequency division scheme. A FD underwater network, through separate frequency bands, is proposed in [61] to solve the hidden/exposed terminal problems. In [62], FD communications through code division multiple access (CDMA) is used to support simultaneous data transmission and reception in the acoustic channel. FD communications via frequency division schemes or CDMA does not increase the spectral efficiency; however, IBFD communications does.

In addition, cooperative transmission has been investigated in the UWA community [63–65]. Cooperative UWA communications, where one or more relays transmit replicas of the source signals, can reduce transmission power, extend the communication range, and provide spatial diversity. In [66], a time-reversal distributed space-time block coding scheme with amplify-and-forward (AF) relaying is proposed and analyzed for distributed UWA cooperative communications. Different from the traditional cooperative schemes designed for radio networks, a new cooperative transmission scheme is proposed in [67], which takes advantage of the low speed of sound. In [68], a delay-independent cyclic-prefix (CP) insertion scheme and an associated symbol detection algorithm are developed. In [69], a pilot-assisted cascade channel estimation and equalization algorithm is proposed for OFDM-based AF relaying in the UWA channel. In [70] and [71], the capacity of cooperative UWA communications is analyzed for both AF and decode-and-forward (DF) relaying. Originally developed in [72], delay diversity is a special case of space-time coding that exploits the transmitter spatial diversity [72–74]. In [52], by adding an appropriate CP, an efficient OFDM-based scheme is developed to

combat the asynchronism issues among geographically separated relays, and a delay diversity gain is obtained at the destination. In most of the current acoustic cooperative efforts, relays operate only in half-duplex (HD) mode, i.e., a relay is restricted to receive and transmit on orthogonal channels, either in a frequency-division or a time-division fashion. The HD mode either introduces delay or reduces spectral efficiency.

In-band full-duplex (IBFD) relays can receive messages from the source and forward the messages to the destination using the same temporal and spectral resources, which can ideally double the spectral efficiency achieved with respect to conventional HD relaying [75]. However, the performance of IBFD systems might decrease due to the existence of strong self-loop interference when the transceiver can hear its own transmission. Full suppression of this self-interference may be difficult.

In radio-frequency (RF) communications, testbeds [76–78] have been developed and advanced cancellation schemes have been implemented that demonstrate the feasibility of radio IBFD systems. These IBFD systems significantly outperform HD systems. IBFD cooperative communications has been investigated in the RF wireless environment [19, 20, 79, 80]. The impact of self-interference is analyzed in [79] and two distributed linear convolutional space-time coding coding schemes [19, 20] are employed to suppress/utilize the residual interference, and the high spectral efficiency of IBFD relaying is maintained without significant performance loss. In [80], a delay diversity OFDM scheme is proposed to provide spatial diversity by including the direct source-to-destination link, the relay forwarding link and the residual self-loop interference. However, different from IBFD RF relaying, there might exist additional reflected interference in IBFD UWA relaying system due to the existence of sea surface and seafloor.

Considering the limited bandwidth available for UWA communications, it is desirable to consider IBFD relaying in UWA systems. There is relatively little literature on acoustic IBFD. The challenges in implementing IBFD UWA systems are discussed in [81], where an acoustic-specific cancellation scheme is proposed. In [82], a time-reversal scheme is investigated for a bidirectional OFDM-based UWA cooperative system. In

this effort, one user transmits (receives) messages to (from) the other user via the help of a relay. The relay transmits and receives at the same time using frequency division, but each user transmits and receives simultaneously in the same frequency band. Then, interference cancellation is applied to both users to suppress the self-loop interference.

In IBFD UWA, as stated in [81], ideal cancellation of self-interference is difficult to achieve. The self-loop interference has a delay several orders of magnitude larger than that in the RF environment. Further, acoustic IBFD may suffer from strong interference with extended delays due to reflections from the sea surface and seafloor. Some existing cancellation schemes used for RF communications, like antenna cancellation [76], cannot be adopted because of the strong frequency-dependency of acoustic propagation and the limited path loss offered by antenna separation.

In this chapter, we describe interference cancellation schemes for IBFD UWA transceivers as well as STC schemes for cooperative IBFD UWA relays. First, we discuss three challenges in implementing IBFD UWA systems: 1) strong interference with significant delay due to reflections from the sea surface and sea floor; 2) limitations of analog cancellation in acoustics; and 3) effectiveness of some existing cancellation methods adopted from IBFD radios for UWA systems. For IBFD UWA transceivers, we propose an acoustic-specific cancellation scheme to deal with the different types of interference: self-loop interference and multipath interference due to reflections. Simulation results show that the proposed scheme performs well when the reflected acoustic returns do not have fast fluctuations. Then, for IBFD UWA relaying, we investigate the impact of self-interference in a UWA system through a SINR analysis for two cases: 1) when there is only self-loop interference; and 2) when there are mixed self-loop and reflected interferences. OFDM with a CP is employed to deal with the self-loop interference. Further, we adopt delay diversity codes to *utilize* the reflected interference and interference from the direct link as useful signals.

3.2 Interference Cancellation for IBFD UWA Transceivers

3.2.1 Challenges in IBFD UWA Systems

As illustrated in Fig. 3.1, there are two types of interference for an IBFD transceiver: 1) self-loop interference from its own transmission; and 2) interference due to reflections from the sea surface and sea floor, called self-multipath interference. In the presence of self-multipath interference, the received signal is

$$r(t) = \sum_{i=0}^{\infty} x(t-\tau_i) * h_i(t) + s(t) + z(t), \tag{3.1}$$

where $x(t)$ is the transmitted signal from the self transducer, τ_i denotes the propagation delay of the i-th self-multipath link, $h_i(t)$ is the overall channel responses (including the amplifier and transducer responses, and the medium effects of the i-th interference link), $s(t)$ is the desired signal from a remote transmitter, and $z(t)$ is the ambient noise in the ocean. Therefore, the first term in (3.1) is the summation of all interference from the self-loop $x(t-\tau_0) * h_0(t)$ and the later multipath $x(t-\tau_i) * h_i(t)$, $i \geq 1$. Note that $s(t)$ may contain distortion from multipath effects between the transceiver and the remote transmitter.

Different from the self-loop interference in IBFD radios, the reflected interference in the underwater acoustic channel could be strong, and the interference arrives at the transceiver after a significant delay. These characteristics make the interference suppression much more difficult. Here, we provide an example to calculate the path loss associated with reflected interference for the scenario shown in Fig. 3.1. We use the acoustic model from [23]

$$A(d, f) = (d/d_0)^{\mu} a(f)^{d-d_0}, \tag{3.2}$$

where f is the signal frequency, d is the transmission distance, d_0 is the reference distance, μ is the path loss exponent (2 is adopted here), and the absorption coefficient

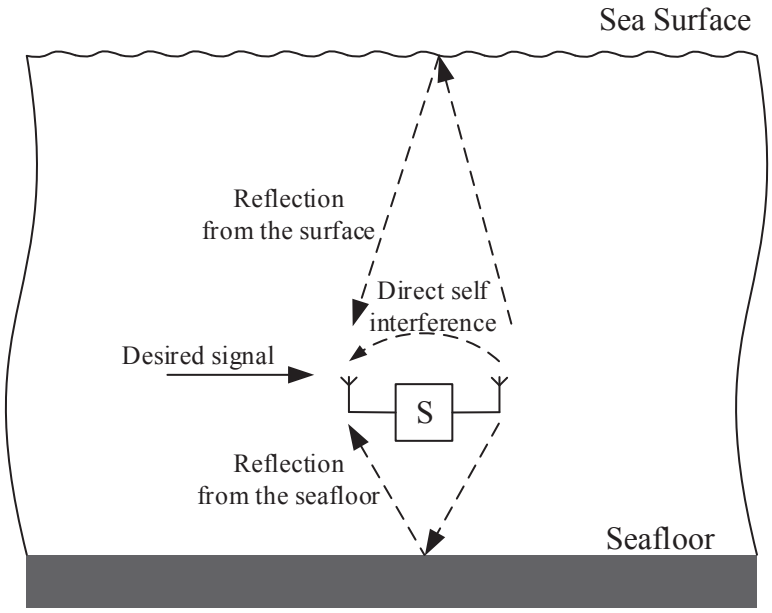

Figure 3.1: Self-multipath interference of acoustic IBFD systems in shallow water.

$a(f)$ can be expressed empirically (for frequencies above a few hundred Hz) using Thorp's formula [23], which gives $a(f)$ in dB/km for f in kHz

$$10\log a(f) = 0.11\frac{f^2}{1+f^2} + 44\frac{f^2}{4100+f^2} + 2.75 * 10^{-4} f^2 + 0.003 \tag{3.3}$$

We assume the speed of sound is 1500 m/s, the acoustic carrier frequency is 25 kHz, and the distances from the transceiver to sea surface and to sea floor are $d_{\text{ts}} = 60$ m and $d_{\text{tf}} = 40$ m, respectively. The calculated path loss and propagation delay of the self-multipath interference are shown in Fig. 3.2 [1]. Twenty reflected returns from the surface and sea floor are shown. We can see that some of these reflections with long delays (on the order of a tenth of a second) are still strong, creating significant interference to the desired signal in this example.

[1] Note that acoustic propagation at short ranges, within meters, is very complex to model. Often it requires measurements in field tests. This shares some similarities with RF electromagnetic wave propagation, where the near field effects are also difficult to delineate.

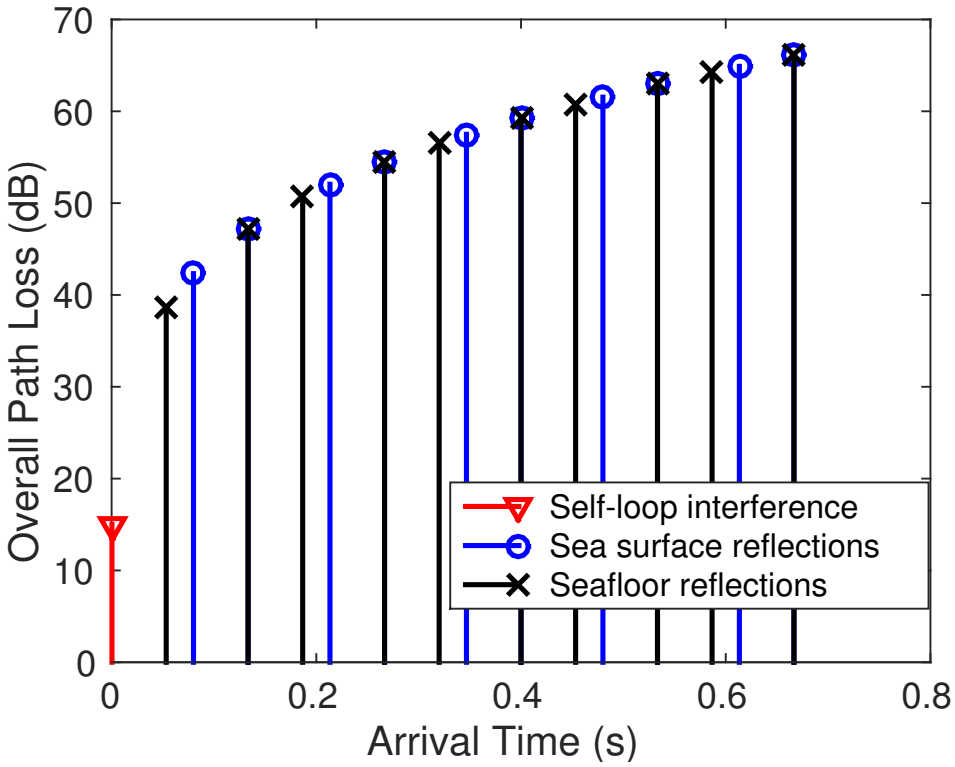

Figure 3.2: Path loss of the self-multipath signals in acoustic IBFD systems.

As discussed in Chapter 1, even in the deep ocean where the multipath interference can be neglected, additional challenges exist. First, the self-loop interference in the underwater acoustic channel still has a delay several orders of magnitude larger than that in the RF environment, due to the slow speed of sound. In analog cancellation schemes in IBFD radios, the channel response of the self-loop link is estimated, and then an artificial signal is generated to approximate the self-loop interference by properly delaying and attenuating the original "known" transmitted signal. Then, the artificial signal is subtracted from the received signal. In IBFD radios, the self-loop delay is small enough so that it can be generated by printed circuit board lines [13]. In the acoustic channel, the self-loop delay can easily reach tens of milliseconds, which cannot realistically be generated by circuit delay lines.

Second, the acoustic path loss offered by the antenna separation is limited for short ranges (within meters); thus, higher suppression gain is needed. In addition, the ambient noise may be non-white, which means that effective cancellation methods should provide enough suppression for the worst case in the communication band.

Third, some existing cancellation schemes from the RF channel, for example the antenna cancellation scheme in [10], cannot be adopted due to the strong frequency-dependency of acoustic propagation. Following the scheme from [10], we can cancel the interference by adding two acoustic signals destructively at the hydrophone. For example, two transducers are placed at distances d and $d + \lambda/2$ away from the hydrophone (as in [10]). Equivalently, two transducers are placed at the same distance from the hydrophone but a fixed π phase shifter exists between the two transmitted signals (as in [12]). However, these methods can only create a null at the center frequency. The cancellation performance decreases quickly with an increase in the bandwidth.

In Fig. 3.3, we compare the cancellation performance between an RF and an acoustic system. The center frequency and bandwidth for the IBFD radio are 2 GHz and 10 MHz, respectively; and those for the acoustic system are set as 10 kHz and 1 kHz, respectively. As shown, the antenna cancellation for the radio can provide about 35 dB suppression at 1.995 GHz (or 2.005 GHz). But less than 10 dB suppression can be obtained at the frequency of 9.5 kHz (or 10.5 kHz) for the acoustic system. The result indicates that acoustic antenna cancellation only works with a narrow bandwidth, less than 1 kHz.

In light of these difficulties, we conclude that acoustic-specific methods are necessary to suppress the strong and long-delayed multipath interference.

3.2.2 Interference Cancellation for IBFD UWA Transceivers

In this section, we describe the proposed IBFD UWA system and analyze its interference performance in the presence of several imperfections. These imperfections include imperfect channel state information (CSI), analog-to-digital converter (ADC) quantization noise, and ambient noise.

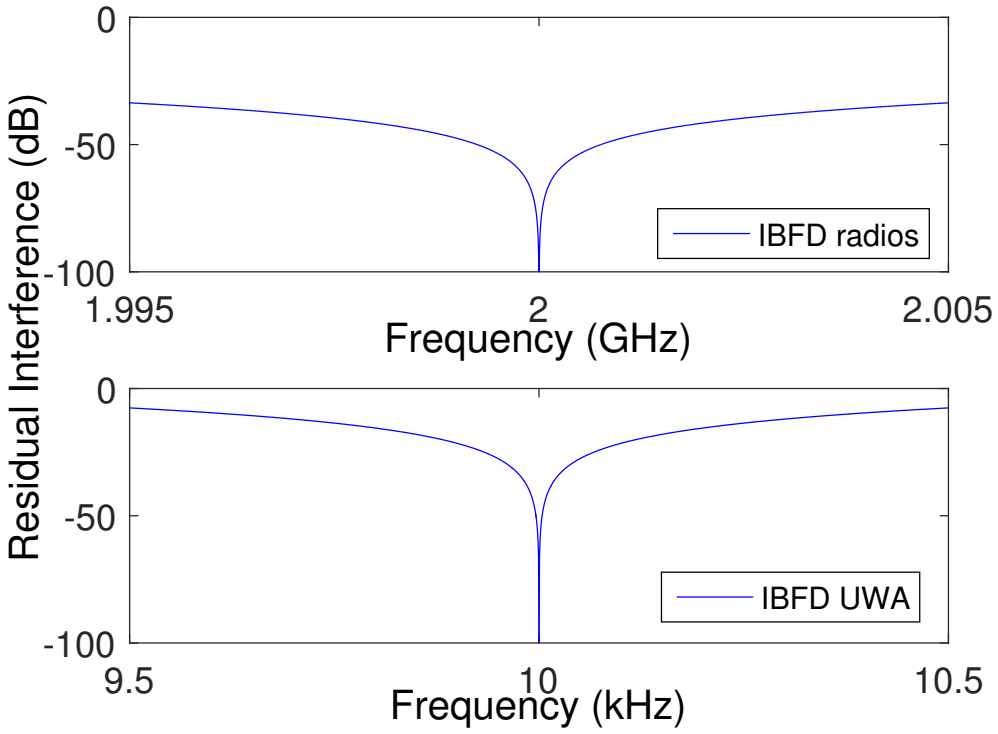

Figure 3.3: Residual interference after antenna cancellation for IBFD radios and IBFD UWA systems. Note that the range of the x-axes in the two sub-figures are different.

To deal with strong self-multipath interference and the large delay, we use a hybrid solution that contains both analog and digital interference suppression schemes, as shown in Fig. 3.4. The acoustic IBFD transceiver adds one auxiliary transmit chain for interference cancellation, in addition to the common transmit and receive chains in HD systems. We employ multiple buffers in the digital domain to match the large delay of the self-multipath interference. We also adopt a directional transmit antenna to provide about 25-dB of suppression [83].

At the transmitter side, we use orthogonal frequency division multiplexing (OFDM) as the modulation scheme. The information symbol sequence, $x[k]$, is modulated, amplified, and converted into acoustic energy through the use of a directional

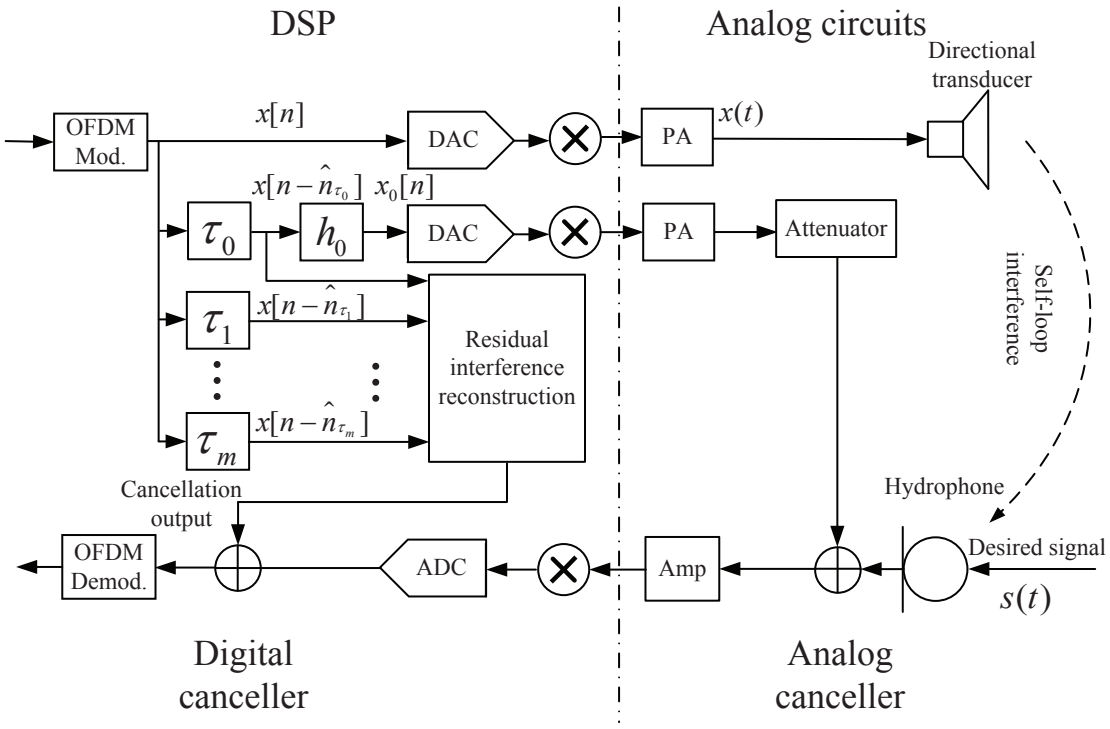

Figure 3.4: Block diagram of the proposed IBFD system.

transducer. At the receiver side, the received signal is converted to an electrical signal by a hydrophone. We assume that there is no hydrophone saturation[2]. Then, after analog and digital cancellation, the desired signal is demodulated via an OFDM demodulator.

3.2.3 Residual Self-Multipath Interference from Imperfect CSI

In the auxiliary transmit chain, we treat the self-loop interference and the self-multipath interference differently. The reason is that the self-loop interference is much stronger while the self-multipath interference has much longer delays. To deal with the

[2] The most significant phenomenon associated with saturation is the presence of nonlinear distortion. A hydrophone usually has a wide dynamic range so that the output voltage increases/decreases linearly as the acoustic pressure increases/decreases.

strong self-loop interference, the signal $x[n]$ is first delayed by a buffer and then passed through an artificial channel. The output is

$$\hat{x}_0[n] = x[n - \hat{n}_{\tau_0}] * \hat{h}_0[n], \tag{3.4}$$

where $*$ is the linear convolution operator, $\hat{n}_{\tau_0}$ denotes the integer part of the estimated delay, τ_0, and $\hat{h}_0[n]$ is the estimate of $h_0(t)$ in the digital domain. After passing through the digital-to-analog converter (DAC) and mixer, the output $\hat{x}_0(t)$ is fine-tuned with attenuation and delay. Then, it is combined destructively with the received signal. The residual self-loop interference is

$$y_0^{\mathrm{a}}(t) = x(t - \tau_0) * h_0(t) - G \cdot \hat{x}_0(t - \tau_a), \tag{3.5}$$

where G is the attenuator gain and τ_a is the delay generated in the analog domain. Here, we implement $\hat{h}_0[n]$ in the digital domain rather than the analog domain because this simplifies the design of the analog canceller; only an attenuator and delay module are required in the analog cancellation.

We define

$$r_{\epsilon_h}(t) = (h_0(t) - G \cdot \hat{h}_0(t))/h_0(t), \tag{3.6}$$

and

$$r_{\epsilon_\tau}(t) = (\tau_0 - \hat{\tau}_0 - \tau_a)/\tau_0, \tag{3.7}$$

as the normalized errors of the channel estimation and the delay mismatch, respectively. We assume $r_{\epsilon_h}(t)$ and $r_{\epsilon_\tau}(t) \sim \mathcal{CN}(0, \sigma_\epsilon^2)$. In the ideal case, $\sigma_\epsilon^2 = 0$, which means that we can obtain ideal CSI with perfect analog circuits; there is no residual interference. Due to imperfect channel estimation and circuitry, however, digital cancellation is necessary after the analog circuitry to further suppress the interference. To facilitate digital cancellation, we view all prior processing modules collectively as a "channel". The "channel" response ($h_{\mathrm{res}}[n]$) is estimated to reconstruct the residual self-loop interference. The estimated residual digital interference is

$$y_0^{\mathrm{d}}[n] = x[n - n_{\hat{\tau}_0}] * \hat{h}_{\mathrm{res}}[n] - y_0^{\mathrm{a}}[n], \tag{3.8}$$

where $\hat{h}_{\text{res}}[n]$ is the estimate of $h_{\text{res}}[n]$, and $y_0^{\text{a}}[n]$ is the discrete version of $y_0^{\text{a}}(t)$.

To cancel the reflected interference, we use buffers to match the large delays from the reflections. Due to the path loss at longer distances, the reflected interference is weaker than the self-loop interference; in the example of Section 3.2.1, the strongest reflected interference is about 25 dB below the self-loop interference. Thus, we can directly apply digital cancellation for the reflected interference. Let $h_i[n]$ and n_{τ_i} denote the digitized version of $h_i(t)$ and τ_i, respectively. Then, the residual interference for the i-th reflection is

$$y_i^{\text{d}}[n] = x[n - n_{\hat{\tau}_i}] * \hat{h}_i[n] - x[n - n_{\tau_i}][n] * h_i[n], \tag{3.9}$$

where $n_{\hat{\tau}_i}$ and $\hat{h}_i[n]$ are the estimates of τ_i and $h_i[n]$, respectively. We also assume that the normalized channel estimation error for the reflections obeys a complex Gaussian distribution. Note that, if some reflected interference is strong, as when the transceiver is deployed close to the ocean boundaries (i.e., surface or floor), we need to use additional analog cancellation, as we used for the self-loop interference cancellation. Here, we make the assumption that the channels for the reflected interference do not vary during the training for the the interference cancellation.

3.2.4 Effects of Ambient Noise and ADC Quantization Noise

We adopt the empirical formulations in [21] to model the ambient non-white noise in the ocean, which consists of four noise components (turbulence, shipping,

waves and thermal noise) in dB re μPa[3] per Hz as a function of frequency in kHz,

$$\begin{aligned}
10\log N_t(f) &= 17 - 30\log f \\
10\log N_s(f) &= 40 + 20(s-0.5) + 26\log f - 60\log(f+0.03) \\
10\log N_w(f) &= 50 + 7.5w^{1/2} + 20\log f - 40\log(f+0.4) \\
10\log N_{th}(f) &= -15 + 20\log f
\end{aligned} \tag{3.10}$$

where s is the shipping activity, whose value ranges between 0 and 1, and w is the wind speed in meters/second. We assume there is no shipping activity in our simulations in Section 3.2.5.

The ADC noise is a uniformly distributed noise introduced by the signal quantization. For an m-bit ADC, the quantization noise power can be calculated as [84]

$$P_q = \frac{1}{\beta_{\text{LNA}}^2}\frac{1}{12\cdot 2^{2m-2}} = \frac{\sigma_q^2}{\beta_{\text{LNA}}^2}, \tag{3.11}$$

where $\sigma_q^2 = \frac{1}{12\cdot 2^{2m-2}}$ is the quantization noise variance, and β_{LNA} is the gain of the low-noise amplifier in the receiver front-end. If the residual interference at the input of the ADC is strong, the gain β_{LNA} should be small to avoid saturation; however, a smaller gain increases the quantization noise power (which can be seen from (3.11)). For a $m = 12$-bit ADC, the average noise power over a frequency band of 20-30 kHz is plotted in Fig. 3.5; the noise power increases as the residual analog interference increases. Thus, strong analog cancellation is required; otherwise, the transceiver will experience high noise levels, which are difficult to suppress in later stages of the receiver.

[3] For sounds in water, the reference level is expressed as "dB re 1 μPa": the amplitude of a sound wave's intensity with a pressure of 1 microPascal (μPa). The relationship between dB re 1 μPa and dBW is $10\log\frac{P}{1\text{W}} = 20\log\frac{p_{rms}}{1\mu\text{Pa}} - 170.8$, where P is the transmit power in Watts and p_{rms} denotes the root-mean-square (RMS) amplitude of pressure changes in Pa. RMS means that the instantaneous sound pressures (which can be positive or negative) are squared and averaged, and then, the square root of the average is taken.

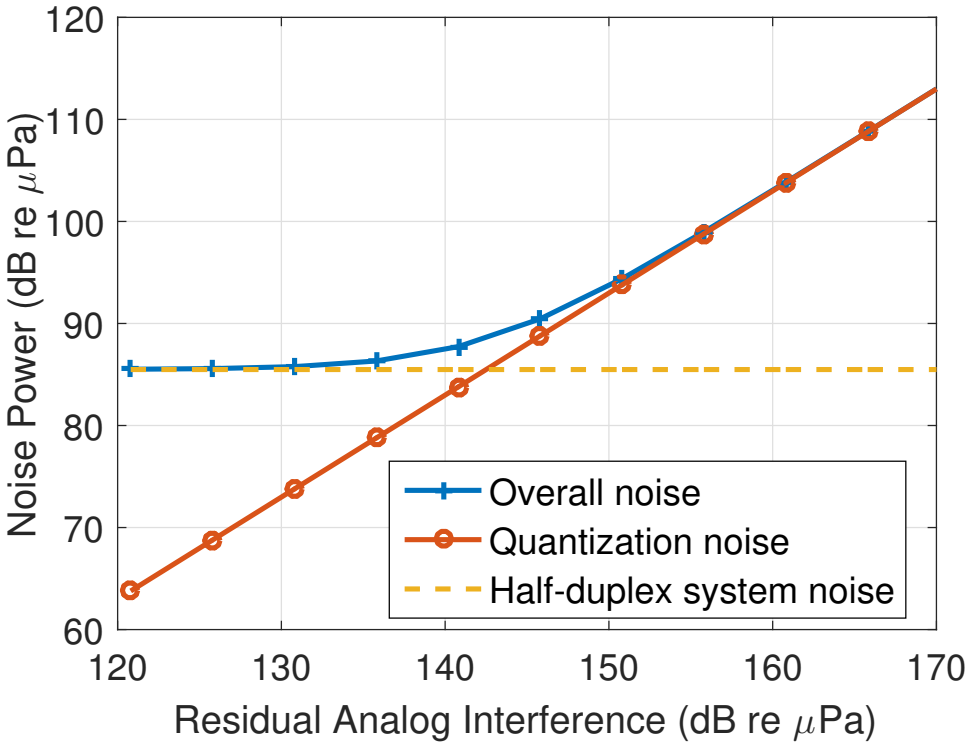

Figure 3.5: Receiver noise power as a function of the residual analog interference level.

3.2.5 Simulation Results

In this section, we demonstrate the effectiveness of the proposed interference cancellation scheme. The acoustic IBFD system has a center frequency of 25 kHz and a bandwidth of 10 kHz. We assume there is no shipping activity ($s = 0$), and the wind speed is $w = 10$ meters/second. With the empirical formulations shown in (3.10), the noise variance is about 86 dB re 1 μPa. We employ OFDM modulation at the transmitter side. The ITC-3001 is used as as the transducer, which has a directional gain of 25 dB [83], and the average transmit power level is 180 dB re 1 μPa. A 12-bit ADC is used in the receiver. Other parameters are shown in Table 4.1.

We first consider the case of the deep ocean, where there is only self-loop interference. The cancellation performance of the proposed scheme with different σ_ϵ is shown in Fig. 3.6 and Fig. 3.7. Due to the use of directional transmissions and the

Table 3.1: Simulation Parameters

Center frequency	$f_c = 25$ kHz
Bandwidth	$B = 10$ kHz
Speed of sound in the ocean	$v = 1500$ m/s
Separation of the transmit and receive antennas	$d_{tr} = 0.5$ m
Modulation	BPSK
Number of OFDM subcarriers	$N = 512$
Length of cyclic prefix	$N_{\mathrm{CP}} = 128$

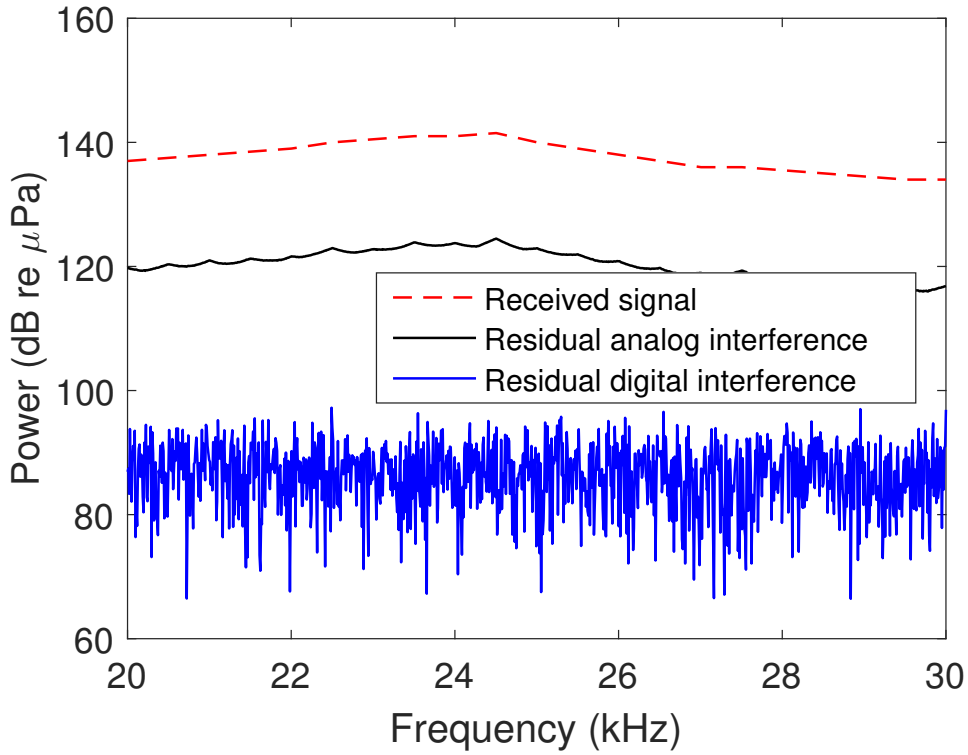

Figure 3.6: Analog and digital cancellation performance with a normalized error of $20\log_{10}(\sigma_\epsilon) = -40$ dB.

existence of path loss, the average received power is about 40 dB lower than the average transmit power. The analog cancellation can offer about 40 dB (or 20 dB) suppression gain when $20\log_{10}(\sigma_\epsilon)$ is -50 dB (or -40 dB). In Fig. 3.8, the average residual analog

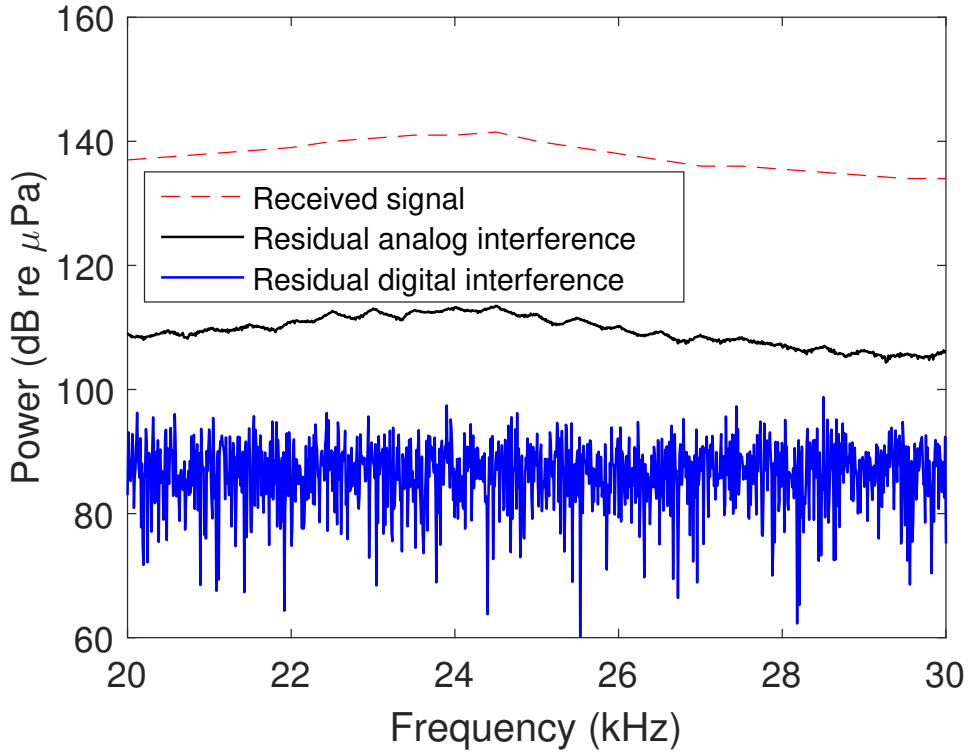

Figure 3.7: Analog and digital cancellation performance with a normalized error of $20\log_{10}(\sigma_\epsilon) = -50$ dB.

and digital interference levels are shown as a function of the variance of the normalized errors σ_ϵ^2; the receiver noise floor is also shown. We can see that the performance of analog cancellation strongly depends both on the accuracy of the channel estimation and on the ability to closely match the propagation delay. However, the interference can be further suppressed to the noise level by using digital cancellation, regardless of the residual interference level after the analog cancellation. Notice that the receiver noise floor and residual digital interference increase as σ_ϵ becomes large. This is because the analog cancellation cannot provide enough suppression, which leads to large quantization noise.

In shallow water, the strength of the reflected interference depends on the distance between the ocean boundaries and the receive antenna. Here, we assume $d_{st} = 60$ m and $d_{sf} = 40$ m. In Fig. 3.9, we show the residual interference level as a function

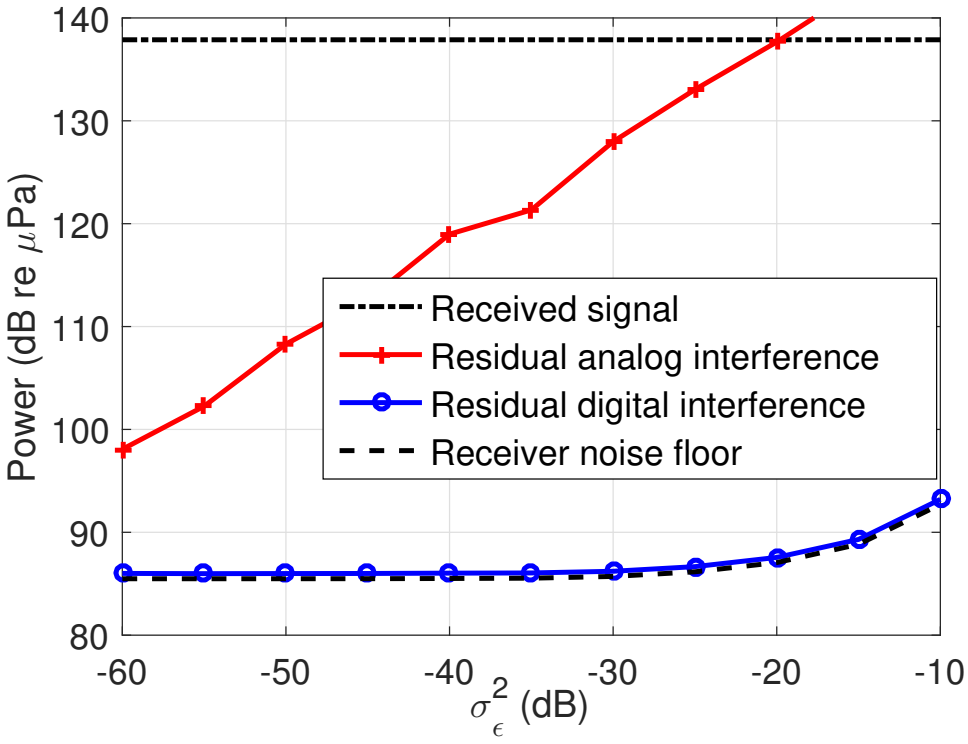

Figure 3.8: Residual interference as a function of the variance of the normalized errors σ^2_ϵ.

of M_r, the number of reflections that are suppressed. Particularly, $M_r = 0$ means that we only reconstruct and suppress the self-loop interference in the digital canceller. If $M_r = 5$, we reconstruct and suppress the first five reflections (in Fig. 3.3). As shown in Fig. 3.9, the digital cancellation experiences enhanced performance as M_r increases. The residual digital interference is about 90 dB re 1 μPa when the first ten reflections are cancelled. It is still about 5 dB higher than the receiver noise floor, this is because the residual digital interference accumulates when we cancel the self-loop interference and the reflections.

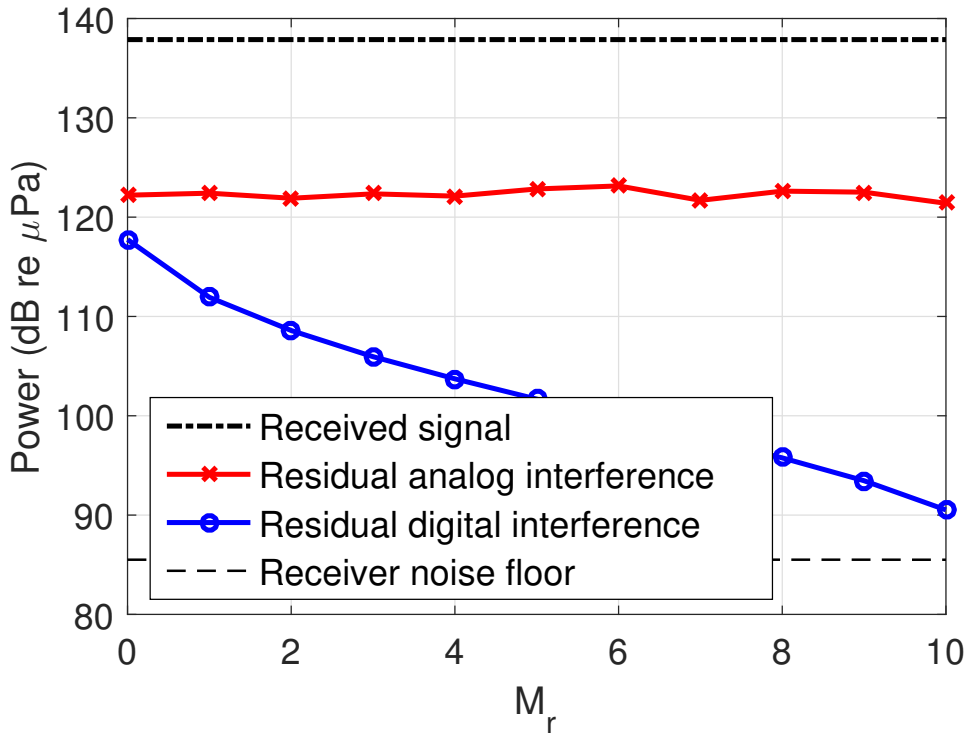

Figure 3.9: Residual interference level for different numbers of reflections that are suppressed (M_r).

3.3 Interference Management in IBFD Cooperative UWA Communications

3.3.1 System Model

In this section, we consider an IBFD cooperative UWA system, shown in Fig. 3.10, in which there is one source (S) and one destination (D), and one IBFD relay (R). The IBFD relay helps the source forward its messages to the destination using AF relaying. For simplicity, we assume the relay is located close to the seafloor, but far from the sea surface. Therefore, at the IBFD relay, there is self-loop interference and one reflected interfering signal (called the reflected self-interference) from the seafloor. Due to the slow speed of sound, the delay of the reflected self-interference can be relatively large. At the destination node, without a careful design, the reception of messages forwarded by the IBFD relay could also experience interference from the transmission

on the direct link.

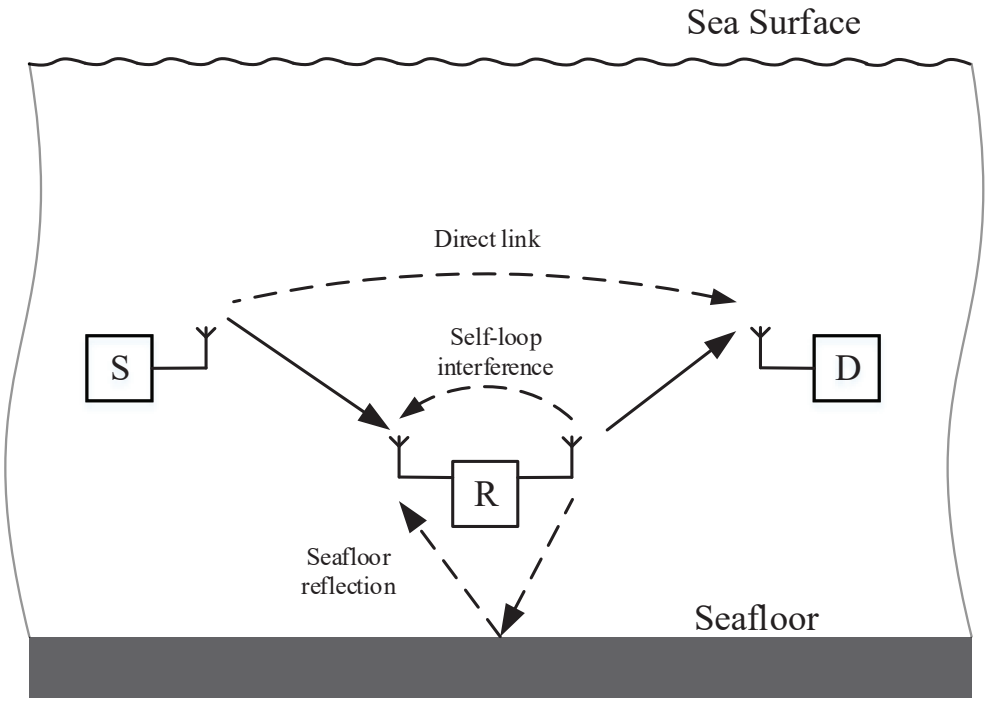

Figure 3.10: IBFD relaying with self-loop interference, reflected self-interference from the seafloor, and possible interference from the transmission on the direct link.

At the source, we employ a conventional OFDM transmission technique with N subcarriers. Using a discrete baseband representation, after channel coding and mapping, the m-th ($m \in 1, 2, \cdots$) data block in the frequency domain is denoted by $\mathbf{X}^m = [X(m,0), X(m,1), \cdots, X(m,N-1)]^T$, where $(\cdot)^T$ is the transpose operation. Then, the time samples of the m-th transmitted OFDM block are represented by $\mathbf{x}^m = \mathcal{F}^{-1}(\mathbf{X}^m) = [x(m,0), x(m,1), \cdots, x(m,N-1)]^T$, where $\mathcal{F}^{-1}(\cdot)$ denotes the inverse discrete Fourier transform (IDFT), i.e., $x(m,n) = \frac{1}{N}\sum_{k=0}^{N-1} X(m,k)e^{j2\pi kn/N}$. After adding a CP of length N_{CP} to $\mathbf{x}^m$, the generated data blocks $\mathbf{x}_{\mathrm{S}}^m$ ($m \in 1, 2, \cdots, M$) are transmitted from the source (where the subscript S denotes the source transmission).

If the self-interference (including the self-loop interference and the reflected self-interference) at the IBFD relay can be completely suppressed, and let $\mathbf{x}_{\mathrm{R}}^m =$

$[x_{\mathrm{R}}(m,0), x_{\mathrm{R}}(m,1), \cdots, x_{\mathrm{R}}(m, N+N_{\mathrm{CP}}-1)]$ denote the m-th data block received at the IBFD relay (designated by subscript R), the received time samples at the relay are

$$x_{\mathrm{R}}(m,n) = \sum_{l=0}^{L_{\mathrm{SR}}} h_{\mathrm{SR}}(m,l) x_{\mathrm{S}}(m,n-l) + z_R(m,n) \tag{3.12}$$

where $h_{\mathrm{SR}}(m,l)$ is the channel impulse response of the source-to-relay link (for data block m and time l), L_{SR} is the number of associated resolvable paths, and $z_R(m,n)$ is the ambient noise at the receiver of the relay. Then, the transmitted signal from the relay is

$$y_{\mathrm{R}}(m,n) = \beta x_{\mathrm{R}}(m, n-n_\tau) \tag{3.13}$$

where β is the amplifying factor at the IBFD relay and does not change with time, and we assume there exists a potential processing delay of n_τ samples at the relay. The role of this processing delay will be discussed in Section 3.3.2.

For the system shown in Fig. 3.10, without perfect interference cancellation, there are two types of residual interference at the IBFD relay: self-loop interference and reflected self-interference from the seafloor. The received signal at the IBFD relay is

$$\tilde{x}_{\mathrm{R}}(m,n) = x_{\mathrm{R}}(m,n) + \Delta x(m,n) \tag{3.14}$$

where $\Delta x(m,n)$ denotes the residual self-interference, which could come from previous symbols in the same OFDM block or even from previous OFDM blocks. Similarly, the transmitted signal from the IBFD relay in this case is

$$y_{\mathrm{R}}(m,n) = \beta \tilde{x}_{\mathrm{R}}(m, n-n_\tau). \tag{3.15}$$

Let $\mathbf{x}_{\mathrm{D}}^m = [x_{\mathrm{D}}(m,1), x_{\mathrm{D}}(m,2), \cdots, x_{\mathrm{D}}(m, N+N_{\mathrm{CP}}-1)]$ denote the m-th received data block at the destination (designated by subscript D), and

$$x_{\mathrm{D}}(m,n) = \sum_{l=0}^{L_{\mathrm{RD}}} h_{\mathrm{RD}}(m,l) y_{\mathrm{R}}(m,n-l) + \sum_{l=0}^{L_{\mathrm{SD}}} h_{\mathrm{SD}}(m,l) x_{\mathrm{S}}(m,n-l) + z_{\mathrm{D}}(m,n) \tag{3.16}$$

where $h_{\mathrm{RD}}(m-1,l)$ and L_{RD} are the channel impulse response and the number of resolvable paths for the relay-to-destination link, respectively, $h_{\mathrm{SD}}(m,l)$ and L_{SD} are

the channel impulse response and the number of resolvable paths for the source-to-destination link, respectively, and $z_{\mathrm{D}}(m,n)$ is the ambient noise at the destination. After CP removal, OFDM demodulation, channel equalization, demapping, and decoding, the source information can be recovered at the destination. Note that, at the destination, the difference in delays among the signals received from the source and the relay can be quite large due to the slow speed of sound, and the signals on the direct link might interfere with the reception of the forwarded signals from the IBFD relay.

3.3.2 Impact of Residual Interference

In an IBFD cooperative UWA system, the system suffers from three types of interferences: self-loop interference at the relay, reflected self-interference at the relay, and possible interference from the direct link transmission.

In this section, we focus on analyzing the impact of residual self-loop interference and reflected self-interference at the relay. In the UWA system shown in Fig. 3.10, with a typical system setting, the delay of the self-loop interference can be on the order of a symbol in one OFDM block, and the delay of the reflection can be on the order of an OFDM block. For example, if the distance between the IBFD transducer and hydrophone is 0.15 m, the distance from the seafloor to the relay is 35 m, the total bandwidth is 10 kHz, and the number of subcarriers is $N = 512$. Then, the duration of one symbol (i.e., the duration of $x(m,n)$) is 0.1 ms, and the duration of one OFDM block (i.e., the duration of $\mathbf{x}^m$) is about 50 ms. Using the speed of sound at sea as $v = 1500$ m/s, the delay for the self-loop link is 0.1 ms, and the delay for the reflection is about 50 ms.

In this chapter, we assume that we have a rough estimate of the delay for the reflected link at the IBFD relay. Then, by adjusting the processing delay (n_τ samples) at the relay, we can have the delay of the reflected interference (the addition of the propagation and processing delays) to be roughly an integer multiple of the duration of one OFDM block. With the help of the CP, and at the expense of reduced spectral efficiency, the system can deal with the intersymbol interference (ISI) when the delay

of the reflected interference is not an exact integer multiple of an OFDM block. Note that n_τ is necessary to guarantee the spectral efficiency of IBFD relaying. For example, without the processing delay of n_τ samples, if the propagation delay of the reflected link happens to be half of an OFDM block, a long CP has to be added to align the received signals from the source and the reflected self-interference. For the self-loop delay, it is always an integer multiple of the duration of one symbol in the discrete baseband representation. In this work, we assume that the delay of the self-loop interference is roughly the duration of one symbol, and the delay of the reflected interference is roughly the duration of one OFDM block.

3.3.2.1 Self-loop Interference Only

First, we consider the case where there is only self-loop interference, for example, when the IBFD relay is far away from both the sea surface and seafloor. The residual interference is

$$\Delta x(m,n) = h_{\mathrm{LI}}(m,n) y_{\mathrm{R}}(m,n-1) \tag{3.17}$$

where $y_{\mathrm{R}}(m,n-1)$ denotes the delayed self-loop interference, and $h_{\mathrm{LI}}(m,n)$ is the self-loop channel impulse response (designated with subscript LI), after interference cancellation (using a directional transducer, analog cancellation, and digital cancellation), associated with the m-th block. Note that we assume a single-tap self-loop channel here, which is practical due to the small distance between the transducer and hydrophone. Then, (3.14) becomes

$$\tilde{x}_{\mathrm{R}}(m,n) = x_{\mathrm{R}}(m,n) + h_{\mathrm{LI}}(m,n) y_{\mathrm{R}}(m,n-1) \tag{3.18}$$

By iteratively substituting (3.18) into (3.15), we obtain the transmitted signal at the IBFD relay

$$y_{\mathrm{R}}(m,n) = \beta \tilde{x}_{\mathrm{R}}(m,n) = \beta x_{\mathrm{R}}(m,n) + \beta \sum_{l=1}^{\infty} \left\{ x_{\mathrm{R}}(m,n-l) \prod_{i=0}^{l-1} (\beta h_{\mathrm{LI}}(m,n-i)) \right\} \tag{3.19}$$

where the first term is the desired signal, and the second term is the interference caused by the self-loop link. Here, the self-loop channel impulse response is infinite, i.e., it corresponds to an infinite impulse response (IIR) channel. We assume the self-loop channel impulse response varies slowly, remaining stationary over one OFDM block, i.e., $h_{\mathrm{LI}}(m, n-i) \approx h_{\mathrm{LI}}(m)$ for $i = 0, 1, \cdots, N-1$. Also, to avoid amplifying the residual interference, it is required that $|\beta h_{\mathrm{LI}}(m)| < 1$; and, we also assume $|\beta h_{\mathrm{LI}}(m)|^{L+1} \approx 0$, where L is the number of symbols that are actually affected by the self-loop interference (typically $L \ll N$). Thus, (3.19) can be simplified to

$$y_{\mathrm{R}}(m,n) \approx \beta x_{\mathrm{R}}(m,n) + \beta \sum_{l=1}^{L} (\beta h_{\mathrm{LI}}(m))^l x_{\mathrm{R}}(m, n-l) = \beta \sum_{l=0}^{L} (\beta h_{\mathrm{LI}}(m))^l x_{\mathrm{R}}(m, n-l) \tag{3.20}$$

Define vectors $\mathbf{y}_{\mathrm{R}}^m = [y_{\mathrm{R}}(m,0), y_{\mathrm{R}}(m,1), \cdots, y_{\mathrm{R}}(m, N+N_{\mathrm{CP}}-1)]^T$ and $\mathbf{x}_{\mathrm{R}}^m = [x_{\mathrm{R}}(m,0), x_{\mathrm{R}}(m,1), \cdots, x_{\mathrm{R}}(m, N+N_{\mathrm{CP}}-1)]^T$, which denote the m-th OFDM blocks transmitted and received at the relay, respectively. Also, define a vector $\mathbf{h}_0^m$, the equivalent channel impulse response of the self-loop link, as

$$\mathbf{h}_0^m = [\beta, \beta^2 h_{\mathrm{LI}}(m), \beta^3 h_{\mathrm{LI}}^2(m), \cdots, \beta(\beta h_{\mathrm{LI}}(m))^L] \tag{3.21}$$

Then, we can write (3.20) in a linear convolutional form as

$$\mathbf{y}_{\mathrm{R}}^m = \mathbf{h}_0^m * \mathbf{x}_{\mathrm{R}}^m \tag{3.22}$$

where $*$ denotes the convolution operation.

3.3.2.2 Interplay of Self-loop Interference and Reflected Self-interference

In this subsection, we consider a UWA system with both self-loop interference and reflected self-interference (as shown in Fig. 3.10). The received signal, with the residual interference, is

$$\begin{aligned} \tilde{x}_{\mathrm{R}}(m,n) &= x_{\mathrm{R}}(m,n) + \Delta x(m,n) \\ &= x_{\mathrm{R}}(m,n) + h_{\mathrm{LI}}(m) y_{\mathrm{R}}(m, n-1) \\ &\quad + \sum_{l=0}^{L_{\mathrm{RI}}} h_{\mathrm{RI}}(m-1, l) y_{\mathrm{R}}(m-1, n-l) \end{aligned} \tag{3.23}$$

where $h_{\mathrm{LI}}(m)$ is the self-loop channel impulse response associated with the m-th block, $y_{\mathrm{R}}(m, n-1)$ denotes the previous OFDM block transmitted at the relay, $h_{\mathrm{RI}}(m-1, l)$ is the channel impulse response of the reflected channel (designated with subscript RI) associated with the $(m-1)$-th block, and L_{RI} is the number of resolvable paths. For simplicity, in the following analyses, we assume the reflected channel is a single-tap channel (i.e., $L_{\mathrm{RI}} = 0$); this can be easily extended to consider a multi-tap reflected channel. With this assumption, (3.23) simplifies to

$$\begin{aligned}\tilde{x}_{\mathrm{R}}(m, n) = x_{\mathrm{R}}(m, n) + h_{\mathrm{LI}}(m) y_{\mathrm{R}}(m, n-1) \\ + h_{\mathrm{RI}}(m-1) y_{\mathrm{R}}(m-1, n)\end{aligned} \tag{3.24}$$

where $h_{\mathrm{RI}}(m-1)$ is the one-tap reflected channel impulse response and $y_{\mathrm{R}}(m-1, n)$ is the reflected self-interference from the last OFDM block.

By substituting (3.24) into (3.15), we can obtain the transmitted signal at the relay

$$y_{\mathrm{R}}(m, n) = \bar{y}(m, n) + \bar{y}(m-1, n) + \cdots + \bar{y}(1, n) \tag{3.25}$$

where $\bar{y}(m, n)$ is the signal created by the self-loop channel at the m-th OFDM block, which is given in (3.20), i.e.,

$$\bar{y}(m, n) = \beta \sum_{l=0}^{L} (\beta h_{\mathrm{LI}}(m))^l x_{\mathrm{R}}(m, n-l), \tag{3.26}$$

and $\bar{y}(m-k, n)$ $(k \in \{1, 2, \cdots, m-1\})$, the interference caused by the interaction of the reflected and self-loop channels on the m-th OFDM block from the $(m-k)$-th OFDM block is given by (for $k = 1, 2, \cdots, m-1$)

$$\bar{y}(m-k, n) = \beta \prod_{i=1}^{k} \beta h_{\mathrm{RI}}(m-i) \left\{ \sum_{l=0}^{L} \left[\sum_{\substack{r_0+\cdots+r_k=l \\ 0 \le r_0, \cdots, r_k \le l}} \prod_{j=0}^{k} (\beta h_{\mathrm{LI}}(m-j))^{r_j} \right] x_{\mathrm{R}}(m-k, n-l) \right\} \tag{3.27}$$

In (3.28), we expand the terms in (3.26) and (3.27) to illustrate the impact of the residual interference. It can be seen that the current transmitting OFDM block

suffers from interference from all previous transmitted OFDM blocks (i.e., ISI) due to the interplay of the self-loop and reflected self-interference.

$$
\begin{aligned}
\bar{y}(m,n) &= \beta x_{\mathrm{R}}(m,n) + G_{\mathrm{R}} h_{\mathrm{LI}}(m) x_{\mathrm{R}}(m,n-1) + \beta^3 h_{\mathrm{LI}}(m)^2 x_{\mathrm{R}}(m,n-2) + \cdots \\
\bar{y}(m-1,n) &= G_{\mathrm{R}} h_{\mathrm{RI}}(m-1) x_{\mathrm{R}}(m-1,n) \\
&\quad + \beta^3 h_{\mathrm{RI}}(m-1) \left[h_{\mathrm{LI}}(m) + h_{\mathrm{LI}}(m-1) \right] x_{\mathrm{R}}(m-1,n-1) \\
&\quad + \beta^4 h_{\mathrm{RI}}(m-1) \left[{h_{\mathrm{LI}}}^2(m) + h_{\mathrm{LI}}(m) h_{\mathrm{LI}}(m-1) + {h_{\mathrm{LI}}}^2(m-1) \right] x_{\mathrm{R}}(m-1,n-2) \\
&\quad + \cdots \\
\bar{y}(m-2,n) &= \beta^3 h_{\mathrm{RI}}(m-1) h_{\mathrm{RI}}(m-2) x_{\mathrm{R}}(m-1,n) \\
&\quad + \beta^4 h_{\mathrm{RI}}(m-1) h_{\mathrm{RI}}(m-2) \left[h_{\mathrm{LI}}(m) + h_{\mathrm{LI}}(m-1) + h_{\mathrm{LI}}(m-2) \right] x_{\mathrm{R}}(m-2,n-1) \\
&\quad + \beta^5 h_{\mathrm{RI}}(m-1) h_{\mathrm{RI}}(m-2) \left[{h_{\mathrm{LI}}}^2(m) + \cdots + {h_{\mathrm{LI}}}^2(m-2) \right] x_{\mathrm{R}}(m-2,n-2) \\
&\quad + \cdots \\
&\quad \vdots
\end{aligned}
\tag{3.28}
$$

We define $\bar{\mathbf{y}}^m = [\bar{y}(m,0), \bar{y}(m,1), \cdots, \bar{y}(m, N+N_{\mathrm{CP}}-1)]^T$, then (3.28) can be re-written in a linear convolutional form as

$$
\begin{aligned}
\bar{\mathbf{y}}^m &= \mathbf{h}^m * \mathbf{x}_{\mathrm{R}}^m \\
\bar{\mathbf{y}}^{m-1} &= \mathbf{h}^{m-1} * \mathbf{x}_{\mathrm{R}}^{m-1} \\
\bar{\mathbf{y}}^{m-2} &= \mathbf{h}^{m-2} * \mathbf{x}_{\mathrm{R}}^{m-2} \\
&\quad \vdots
\end{aligned}
\tag{3.29}
$$

where $*$ denotes the linear convolution operation, and the corresponding channel responses are

$$
\begin{aligned}
\mathbf{h}^m &= [\beta, \beta^2 h_{\mathrm{LI}}(m), \beta^3 {h_{\mathrm{LI}}}^2(m), \cdots] \\
\mathbf{h}^{m-1} &= \beta h_{\mathrm{RI}}(m-1) \cdot [\beta, \beta^2 \left[h_{\mathrm{LI}}(m) + h_{\mathrm{LI}}(m-1) \right], \cdots] \\
\mathbf{h}^{m-2} &= \beta^2 h_{\mathrm{RI}}(m-1) h_{\mathrm{RI}}(m-2) \cdot [\beta, \beta^2 \left[h_{\mathrm{LI}}(m) + h_{\mathrm{LI}}(m-1) + h_{\mathrm{LI}}(m-2) \right], \cdots] \\
&\quad \vdots
\end{aligned}
\tag{3.30}
$$

and the m-th OFDM block transmitted at the relay is

$$
\mathbf{y}_{\mathrm{R}}^m = \bar{\mathbf{y}}^m + \bar{\mathbf{y}}^{m-1} + \cdots + \bar{\mathbf{y}}^1 \tag{3.31}
$$

In (3.30), $\mathbf{h}^m$ denotes the equivalent channel created by the residual self-loop interference for the m-th OFDM block; due to the existence of the reflected self-interference, there are multiple "channels" $(\mathbf{h}^m, \mathbf{h}^{m-1}, \mathbf{h}^{m-2}, \cdots)$. Note that, usually, we have $|\beta h_{\mathrm{LI}}| << 1$ and $|\beta h_{\mathrm{RI}}| << 1$. Thus, the high-order terms in (3.30) can be ignored.

3.3.3 OFDM-based Delay Diversity Scheme

In this section, we employ OFDM to overcome the impact of the self-loop interference. Then, the "interferences" from the reflected link and the direct link are *utilized* as useful signals at the destination.

3.3.3.1 SINR Analysis for OFDM-based IBFD Relaying

According to Section 3.3.2, the self-loop channel is equivalent to a multipath channel. Then, OFDM can be used to deal with the self-loop interference. Here, to focus on the impacts of the self-loop gain and the CP length, we ignore the interference from the reflected link and the direct link, and also assume there is no multipath for the source-to-relay and relay-to-destination links. Then, the received signal at the relay is simply

$$x_{\mathrm{R}}(m,n) = x_{\mathrm{S}}(m,n) + z_R(m,n) \tag{3.32}$$

and the transmitted signals at the relay are given in (3.26). At the destination, we have $y_{\mathrm{D}}(m,n) = y_{\mathrm{R}}(m,n) + z_D(m,n)$. The received SINR determines the quality of the source signal recovery.

Here, we derive SINR expressions for OFDM-based IBFD relaying by extending the analyses presented in [85–87]. Let $G_{\mathrm{LI}} = \mathcal{E}\{|h_{\mathrm{LI}}(m)|^2\}$ and $G_{\mathrm{R}} = \beta^2$ denote the channel gain of the residual self-loop interference and the amplifying gain of the IBFD relay, respectively. For the channel response of the self-loop link in (3.21), we have

$$\mathcal{E}\{\| \mathbf{h}_0^m \|^2\} = \sum_{i=1}^{L} G_{\mathrm{R}} \mathcal{E}\{|(\beta h_{\mathrm{LI}}(m))^{i-1}|^2\} \approx \frac{G_{\mathrm{R}}}{1 - \mathcal{E}\{|\beta h_{\mathrm{LI}}(m)|^2\}} = \frac{G_{\mathrm{R}}}{1 - G_{\mathrm{R}} G_{\mathrm{LI}}} \tag{3.33}$$

where $\mathcal{E}\{\cdot\}$ denotes the expectation operator. Note that $G_{\mathrm{R}} G_{\mathrm{LI}} < 1$ is required to guarantee a finite transmit power, and we assume $(G_{\mathrm{R}} G_{\mathrm{LI}})^{L+1} \approx 0$.

Let $\mathcal{S}_{\mathrm{D}}(m,n)$, $\mathcal{I}_{\mathrm{D}}(m,n)$, and $\mathcal{Z}_{\mathrm{D}}(m,n)$ denote the desired signal, interference, and noise, respectively. Let P_{S} denote the transmit power at the source ($\mathcal{E}\{|x_{\mathrm{S}}(m,n)|^2\}$). Then, we define the SINR at the destination γ_D as

$$\gamma_D = \frac{\mathcal{E}\{|\mathcal{S}_{\mathrm{D}}(m,n)|^2\}}{\mathcal{E}\{|\mathcal{I}_{\mathrm{D}}(m,n)|^2\} + \mathcal{E}\{|\mathcal{Z}_{\mathrm{D}}(m,n)|^2\}} \tag{3.34}$$

where the power of the desired signal is

$$\mathcal{E}\{|\mathcal{S}_{\mathrm{D}}(m,n)|^2\} = P_{\mathrm{S}} \sum_{i=1}^{\infty} c^2(i)(G_{\mathrm{R}}G_{\mathrm{LI}})^{i-1} \tag{3.35}$$

and the interference power is

$$\mathcal{E}\{|\mathcal{I}_{\mathrm{D}}(m,n)|^2\} = P_{\mathrm{S}} \sum_{i=1}^{\infty} (1 - c^2(i))(G_{\mathrm{R}}G_{\mathrm{LI}})^{i-1} \tag{3.36}$$

where $c(i)$ is the bias function derived in [85] and employed in [86, 87] to analyze the system SINR for fading channels, which is given as

$$c(i) = \begin{cases} 0, & i < -N \\ (N+i)/N, & -N \le i < 0 \\ 1, & 0 \le i < N_{\mathrm{CP}} \\ (N-(i-N_{\mathrm{CP}}))/N, & N_{\mathrm{CP}} \le i \le N + N_{\mathrm{CP}} \\ 0, & i \ge N + N_{\mathrm{CP}} \end{cases} \tag{3.37}$$

Note that, the same as in [85], we assume that the signal variations arriving at different delays are uncorrelated and that the correlation properties of all channels are stationary.

A closed-form expression for (3.35) can be derived (see Appendix), but it is fairly complicated and provides little insight. Thus, we consider two extreme cases: (i) when the CP is sufficient (i.e., ${G_{\mathrm{LI}}}^{N_{\mathrm{CP}}} \approx 0$); and (ii) when there is no CP added to the OFDM block (i.e., $N_{\mathrm{CP}} = 0$).

As shown in the Appendix, for Case (i), the power of the desired signal can be approximated as

$$\mathcal{E}\{|\mathcal{S}_{\mathrm{D}}(m,n)|^2\} \approx \frac{G_{\mathrm{R}}P_{\mathrm{S}}}{1 - G_{\mathrm{R}}G_{\mathrm{LI}}} \tag{3.38}$$

and the interference power as

$$\mathcal{E}\{|\mathcal{I}_{\mathrm{D}}(m,n)|^2\} \approx 0 \tag{3.39}$$

For Case (ii), the power of the desired signal can be approximated as

$$\mathcal{E}\{|\mathcal{S}_{\mathrm{D}}(m,n)|^2\} \approx \frac{G_{\mathrm{R}}P_{\mathrm{S}}}{1-G_{\mathrm{R}}G_{\mathrm{LI}}} - \frac{2G_{\mathrm{R}}P_{\mathrm{S}}}{N(1-G_{\mathrm{R}}G_{\mathrm{LI}})^2} \tag{3.40}$$

and the interference power as

$$\mathcal{E}\{|\mathcal{I}_{\mathrm{D}}(m,n)|^2\} \approx \frac{2G_{\mathrm{R}}P_{\mathrm{S}}}{N(1-G_{\mathrm{R}}G_{\mathrm{LI}})^2} \tag{3.41}$$

Let P_{R} denote the transmit power at the relay, and we have

$$P_{\mathrm{R}} = \mathcal{E}\{|\mathcal{S}_{\mathrm{D}}(m,n)|^2\} + \mathcal{E}\{|\mathcal{I}_{\mathrm{D}}(m,n)|^2\} = \frac{G_{\mathrm{R}}P_{\mathrm{S}}}{1-G_{\mathrm{R}}G_{\mathrm{LI}}}. \tag{3.42}$$

At the destination, the noise power includes two components: the noise forwarded by the relay and the noise at the destination receiver. Due to the existence of the self-loop link, we have

$$\mathcal{Z}_{\mathrm{D}}(m,n) = \sum_{i=0}^{L} h_0(m,i)z_{\mathrm{R}}(m,n-i) + z_{\mathrm{D}}(m,n) \tag{3.43}$$

We assume the noise at the relay and the destination have the same average power P_{N}, and the noises are independent of each other. Then, we have

$$\begin{aligned}
\mathcal{E}\left\{|\mathcal{Z}_{\mathrm{D}}(m,n)|^2\right\} &= \mathcal{E}\left\{|\mathbf{h}_0^m * \mathbf{z}_{\mathrm{R}}^m + z_{\mathrm{D}}(m,n)|^2\right\} \\
&= \mathcal{E}\left\{\| \mathbf{h}_0^m \|^2\right\} P_{\mathrm{N}} + P_{\mathrm{N}} \\
&= \frac{G_{\mathrm{R}}}{1-G_{\mathrm{R}}G_{\mathrm{LI}}} P_{\mathrm{N}} + P_{\mathrm{N}} = \frac{P_{\mathrm{R}}}{P_{\mathrm{S}}} P_{\mathrm{N}} + P_{\mathrm{N}}
\end{aligned} \tag{3.44}$$

where the first term is the forwarded noise from the IBFD relay, and the second term is the ambient noise at the destination. By substituting (3.38)-(3.44) into (3.34), we can obtain the SINR for the two extreme cases.

For Case (i), we simply have

$$\gamma_D = \frac{P_{\mathrm{R}}}{\frac{P_{\mathrm{R}}}{P_{\mathrm{S}}}P_{\mathrm{N}} + P_{\mathrm{N}}} \tag{3.45}$$

since the impact of the residual self-loop interference is negligible.

For Case (ii), the SINR is

$$\gamma_D = \frac{\frac{G_{\mathrm{R}}P_{\mathrm{S}}}{1-G_{\mathrm{R}}G_{\mathrm{LI}}} - \frac{2G_{\mathrm{R}}P_{\mathrm{S}}}{N(1-G_{\mathrm{R}}G_{\mathrm{LI}})^2}}{\frac{2G_{\mathrm{R}}P_{\mathrm{S}}}{N(1-G_{\mathrm{R}}G_{\mathrm{LI}})^2} + \frac{P_{\mathrm{R}}}{P_{\mathrm{S}}}P_{\mathrm{N}} + P_{\mathrm{N}}} \tag{3.46}$$

and without sufficient CP, the system suffers a degradation in performance. For UWA systems, considering that the number of OFDM subcarriers is usually quite large, with an appropriate CP, the impact of self-loop interference could be relatively small.

3.3.3.2 Reflected Self-interference: Delay Diversity

1) SINR analysis

At the destination, without the interference from the direct link (the direct link should be relatively weak in a coverage extension scenario), after CP removal and FFT operation, the frequency-domain received signals can be denoted as

$$\mathbf{X}_{\mathrm{D}}^{m} = \sum_{k=0}^{m-1} \mathbf{X}^{m-k} \cdot \mathbf{H}_{\mathrm{SR}}^{m-k} \cdot \mathbf{H}_{\mathrm{RD}}^{m-k} \cdot \mathbf{H}^{m-k} + \mathbf{Z}^{m} \tag{3.47}$$

where $\mathbf{H}_{\mathrm{SR}}^{m-k}$ and $\mathbf{H}_{\mathrm{RD}}^{m-k}$ $(0 \leq k \leq m-1)$ are, respectively, the frequency responses of the source-to-relay link and the relay-to-destination link for the $(m-k)$-th OFDM block. In (3.47), $\mathbf{H}^{m-k}$ is the frequency response corresponding to the "channel" $\mathbf{h}^{m-k}$ in (3.30), and $\mathbf{Z}^{m}$ is the noise component in the frequency domain. From (3.47), we see that the received signals at the destination are the superposition of the previous transmitted OFDM blocks.

To show the impact of the reflected self-interference, we assume the CP is sufficient to deal with the self-loop interference. Then, according to (3.31), we can obtain the power of the desired signal as given in (3.38), and the power of the interference as

$$\begin{aligned}
\mathcal{E}\{|\mathcal{I}_{\mathrm{D}}(m,n)|^2\} &= \mathcal{E}\{\| \bar{\mathbf{y}}^{m-1} \|^2\} + \mathcal{E}\{\| \bar{\mathbf{y}}^{m-2} \|^2\} + \cdots + \mathcal{E}\{\| \bar{\mathbf{y}}^{1} \|^2\} \\
&= \left(G_{\mathrm{R}}G_{\mathrm{RI}} + {G_{\mathrm{R}}}^2{G_{\mathrm{RI}}}^2 + \cdots + (G_{\mathrm{R}}G_{\mathrm{RI}})^{m-1}\right) \mathcal{E}\left\{\| \bar{\mathbf{y}}^{m} \|^2\right\} \\
&\approx \frac{{G_{\mathrm{R}}}^2 G_{\mathrm{RI}} P_{\mathrm{S}}}{(1-G_{\mathrm{R}}G_{\mathrm{LI}})(1-G_{\mathrm{R}}G_{\mathrm{RI}})}
\end{aligned} \tag{3.48}$$

where $G_{\mathrm{RI}} = \mathcal{E}\{|h_{\mathrm{RI}}(m-k)|^2\}$ for $k \in \{0, 1, \cdots, m-1\}$, denotes the channel gain of the reflected link. Here, we assume the data from different OFDM blocks are independent from each other. Similar to the derivation of (3.44), we can obtain the noise power at the destination as

$$\begin{aligned}\mathcal{E}\left\{|\mathcal{Z}_{\mathrm{D}}(m,n)|^2\right\} =& \mathcal{E}\left\{\| \mathbf{h}^m \|^2 + \| \mathbf{h}^{m-1} \|^2 + \cdots\right\} P_{\mathrm{N}} + P_{\mathrm{N}} \\ \approx& \frac{G_{\mathrm{R}}}{(1 - G_{\mathrm{R}}G_{\mathrm{LI}})(1 - G_{\mathrm{R}}G_{\mathrm{RI}})} P_{\mathrm{N}} + P_{\mathrm{N}} \end{aligned} \tag{3.49}$$

where the first term is the forwarded noise from the IBFD relay, and the second term is the ambient noise at the destination. By substituting (3.38), (3.48), and (3.49) into (3.34), we can obtain the SINR for this case. The SINR degrades due to the existence of self-loop and reflected self-interference, which may lead to severe performance loss.

2) Delay diversity at the destination

In this section, we show that delay diversity can be obtained from the forwarded signal and the reflected self-interference. According to (3.47), the received signals at the destination are shown in Fig. 3.11, in which each received OFDM block is the superposition of the current and previously transmitted OFDM blocks from the source. With interference cancellation, typically we have $G_{\mathrm{RI}} << 1$, then, the interference from the previous OFDM blocks decreases rapidly over time. Thus, we can approximate the received signals at the destination as the superposition of the current OFDM block and a few previously transmitted OFDM blocks.

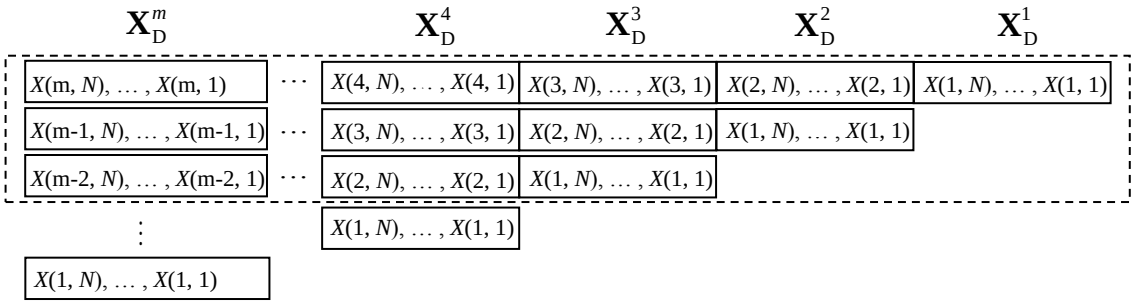

Figure 3.11: Delay diversity sturcture at the destination.

As an example, in Fig. 3.11, we consider the interference from the two previous OFDM blocks, which are highlighted in the dashed-line box. Here, $X(m,k)$ denotes the symbol on the k-th subcarrier in the m-th OFDM block. For simplicity, the channel impulse responses have not been written out explicitly. In this example, the relaying system is equivalent to a system having three streams of transmissions. The delay is the duration of one OFDM block between two neighboring transmissions. Note that the number of streams to be combined depends on the level of the residual reflected self-interference (G_{RI}). If the residual reflected self-interference is not strong, we may only need to consider the superposition of the first several (2 or 3) streams, which is discussed in detail in the simulation section.

3) Detection by Viterbi algorithm

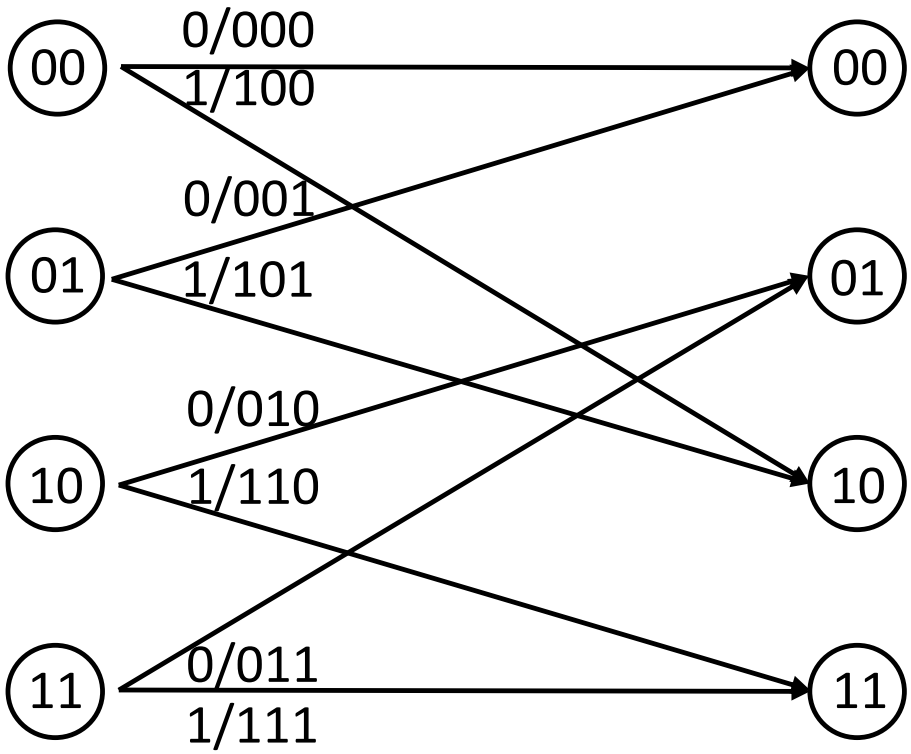

Figure 3.12: Trellis for delay diversity with three paths (desired signal mixed with the first two streams) using BPSK modulation.

At the destination node, a Viterbi detector can be used to detect the superposed streams. We assume M-ary phase shift keying (PSK) modulation is adopted at the source. The number of previous OFDM blocks that are utilized in the delay diversity scheme is $D-1$, and the number of data streams is D in the delay diversity structure. Then, at the destination node, after channel equalization, we can employ a Viterbi detector with M^D states for maximum likelihood (ML) detection of the transmitted symbols at each OFDM subcarrier. In particular, N parallel Viterbi decoders are required, and the k-th Viterbi detector is used to detect the transmitted symbols over the k-th subcarrier; the k-th Viterbi detector generates an estimated sequence $\{X^1(k), X^2(k), X^3(k), \cdots\}$. For example, to decode the signals shown in Fig. 3.11, the associated trellis for the Viterbi detector with binary PSK (BPSK) modulation is shown in Fig. 3.12.

To reduce the detection delay, Viterbi detectors with truncated path memory can be employed [88]. Note that, in OFDM systems (for example, Wi-Fi systems), the signals are usually transmitted in frames, and one frame consists of multiple OFDM blocks. Thus, the truncated length can be the number of OFDM blocks in one frame.

3.3.3.3 Interference from Direct Link: Delay Diversity Structure

As mentioned in [89], the interference from the direct link may cause severe performance degradation. At the destination, the frequency-domain received signals, after CP removal, can be written as

$$\mathbf{X}_{\mathrm{D}}^{m} = \sum_{k=1}^{m-1} \mathbf{X}^{m-k} \cdot \mathbf{H}_{\mathrm{SR}}^{m-k} \cdot \mathbf{H}_{\mathrm{RD}}^{m-k} \cdot \mathbf{H}^{m-k} + \mathbf{X}^{m} \cdot \mathbf{H}_{\mathrm{SD}}^{m} + \mathbf{Z}^{m} \tag{3.50}$$

where $\mathbf{H}_{\mathrm{SD}}^{m}$ represents the frequency response of the source-to-destination link for the m-th OFDM block. In this case, the received signals get additional interference from the direct-link signal, which will further decrease the system performance. However, similar to the analysis in Subsection 3.3.3.2, we can consider the interference from the direct link as an additional stream in the delay diversity scheme, and also employ a parallel Veterbi decoder to detect these delayed signals.

3.3.4 Results

3.3.4.1 Simulation Setup

In this section, we demonstrate the effectiveness of the proposed delay diversity scheme through computer simulations. For the system model shown in Fig. 3.10, we use the BELLOP ray tracing model [90–92] to generate the impulse responses of specific channel realizations, including the source-to-relay, the relay-to-destination, the source-to-destination, and the reflected channels. The self-loop channel has only one tap (no multipath). Also, only time-invariant impulse responses are considered. In generating the impulse response, we assume a flat sea surface and seafloor in a water depth of 300 m, with the sound speed profile shown in Fig. 3.13. The source, relay, and destination nodes are all positioned at 35 m above the seafloor. The distance between the source and the relay nodes is 2 km, and the destination node is also 2 km away from the relay on the other side. The distance between the IBFD relay's transducer and hydrophone is 15 cm.

The source and relay transmit at the same power P_{S}. The ambient non-white noise in the ocean is modeled with the empirical formulation in [53], the mean power of which is denoted as P_N. The system has a center frequency of 15 kHz and a bandwidth of 10 kHz. BSPK mapping and OFDM modulation is employed at the source. The number of OFDM subcarriers is 512 and the CP ratio (the ratio of the CP length to the OFDM block length) is 1/4. The number of OFDM blocks in one frame is $M = 20$. At the destination, the length of the truncated path in the Viterbi detector is the same as the number of OFDM blocks in one frame.

In the following results, we show the system performance as a function of the average received SNR at the destination, which is defined as $\mathrm{SNR} = (P_{\mathrm{S}}\gamma_{\mathrm{SR}}G_{\mathrm{R}}\gamma_{\mathrm{RD}})/P_N$, where $\gamma_{\mathrm{SR}} = \mathcal{E}\{\| \mathbf{h}_{\mathrm{SR}} \|_2^2\}$ and $\gamma_{\mathrm{RD}} = \mathcal{E}\{\| \mathbf{h}_{\mathrm{RD}} \|_2^2\}$. Note that, we assume the relay node also transmits with the same power P_{S}, thus, we have $G_{\mathrm{R}}\gamma_{\mathrm{SR}} = 1$, and $\mathrm{SNR} = P_{\mathrm{S}}\gamma_{\mathrm{RD}}/P_N$. All the following results are averaged over 1000 channel realizations.

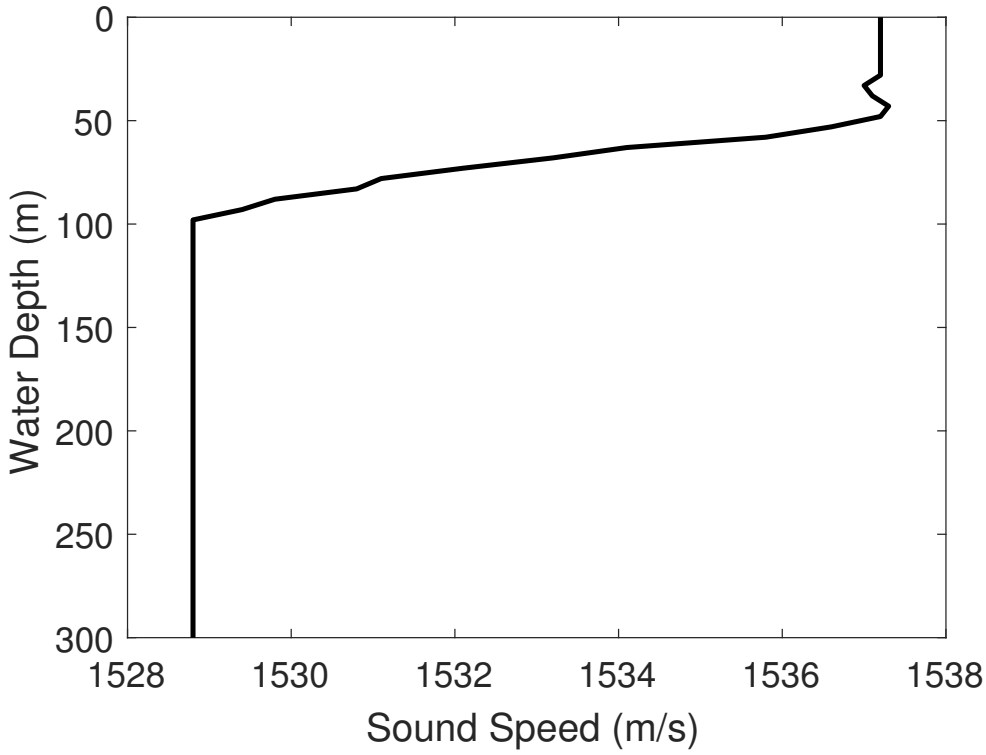

Figure 3.13: Sound speed profile adopted in the simulations.

3.3.4.2 Simulation Results and Discussion

The impact of the residual self-loop interference is shown in Fig. 3.14, in which the error rate performance is plotted as a function of the received SNR at the destination, for different levels of self-loop interference. Here, we assume the system only suffers from self-loop interference, i.e., there is no interference from the reflected link and the direct link. The "ideal" case, in which perfect interference cancellation is assumed, is given as a reference. For the other three cases, different levels of self-loop interference are represented by different $G_{\mathrm{R}}G_{\mathrm{LI}}$. Note that, G_{R} and G_{LI} are the amplifying gain at the IBFD relay and the equivalent channel gain of the residual self-loop interference, respectively. Thus, $G_{\mathrm{R}}G_{\mathrm{LI}}$ denotes the relative power of the self-loop interference compared to the power of the received signal at the relay. In particular, $G_{\mathrm{R}}G_{\mathrm{LI}} = -3$ dB represents the case where, after interference cancellation (using a

directional transducer, analog cancellation, and digital cancellation), the power of the residual self-loop interference is 3 dB lower than that of the received signal at the relay. We can see that, compared to the "ideal" case, both the OFDM block error rate (BLER) and the bit error rate (BER) performance loss are negligible if the self-loop interference can be suppressed to 9 dB lower than the power of the received signal. Thus, OFDM is able to deal with the residual self-loop interference effectively when it is relatively weak.

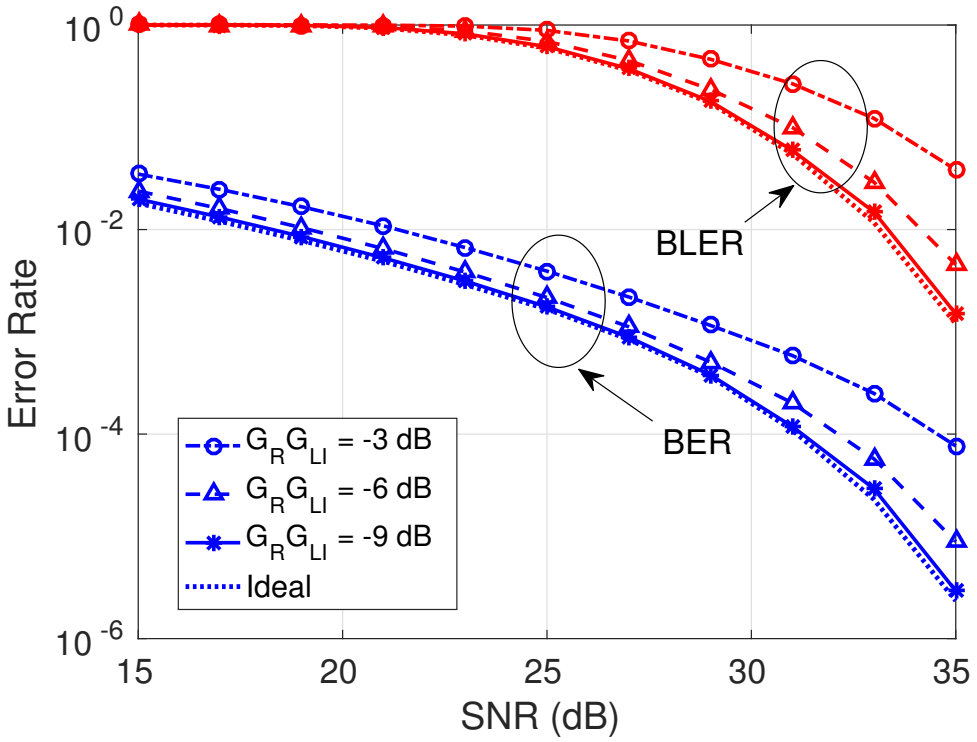

Figure 3.14: Error rate performance for different levels of residual self-loop interference. Only self-loop interference is present.

Next, in Figs. 3.15-3.17, we show the performance of the delay diversity schemes, when the system suffers from both self-loop interference and reflected self-interference but there is no direct link from the source to the destination. The reflected channel is generated with the BELLOP model, and could be a multi-tap channel. Similarly, we use $G_{\mathrm{R}}G_{\mathrm{RI}}$ to denote different levels of reflected self-interference after interference

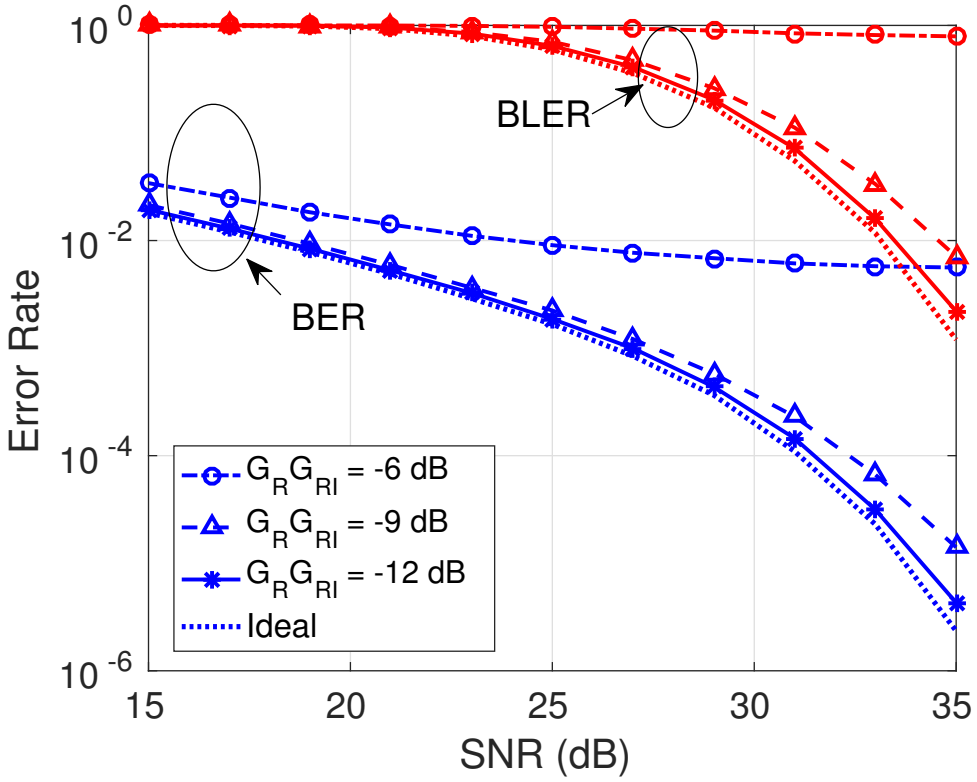

Figure 3.15: Error rate performance with $D = 2$ streams in the delay diversity structure, for different levels of reflected self-interference. There is both self-loop interference and reflected self-interference, and $G_{\mathrm{R}}G_{\mathrm{LI}} = -9$ dB.

cancellation using a directional transducer and digital cancellation), i.e., the relative power of the residual reflected self-interference compared to the power of the received signal at the relay.

In Fig. 3.15, the error rate performance is presented as a function of the received SNR at the destination, for different levels of reflected self-interference, when there are $D = 2$ streams in the delay diversity structure. The "ideal" case is also given as a reference. To focus on the effects of the reflected interference, we assume $G_{\mathrm{R}}G_{\mathrm{LI}} = -9$ dB so that the residual self-loop interference would not play a critical role in the system performance. We can see that the system encounters a very high error floor when $G_{\mathrm{R}}G_{\mathrm{RI}}$ is higher than -6 dB. In contrast, both the BLER and BER performance

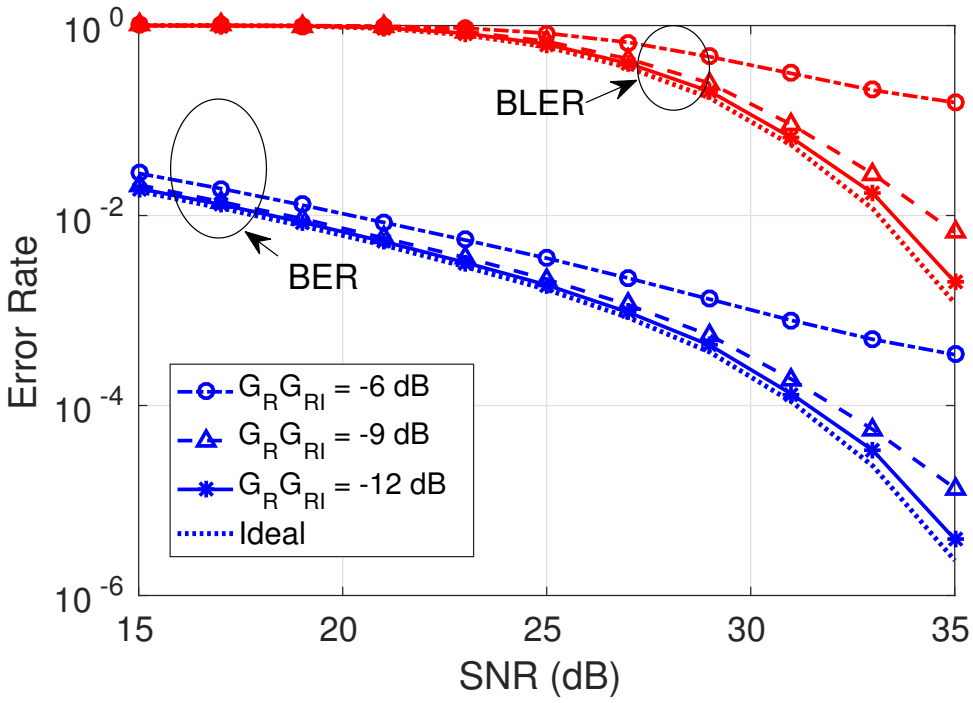

Figure 3.16: Error rate performance with $D = 3$ streams in the delay diversity structure, for different levels of reflected self-interference. There are both self-loop interference and reflected self-interference, and $G_{\mathrm{R}}G_{\mathrm{LI}} = -9$ dB.

are close to that of the ideal case when $G_{\mathrm{R}}G_{\mathrm{RI}} = -9$ dB, and the performance loss is negligible when $G_{\mathrm{R}}G_{\mathrm{RI}} = -12$ dB. Similar conclusions can be drawn from Fig. 3.16, in which $D = 3$ streams are employed in the delay diversity structure; however, with $D = 3$ streams, the system is more robust to the reflected self-interference. For example, with $D = 3$, both the BLER and BER performance are much better than the case of $D = 2$ when $G_{\mathrm{R}}G_{\mathrm{RI}} = -6$ dB. This is because, when we have relatively strong interference, the high-order terms in (3.30) cannot be ignored, i.e., the ISI from previous OFDM blocks is still strong. Thus, we need to include more streams in the Viterbi decoder at the destination to detect this "interference".

To compare the system performance with different numbers of streams employed in the delay diversity scheme, the system error rate performance is plotted as a function

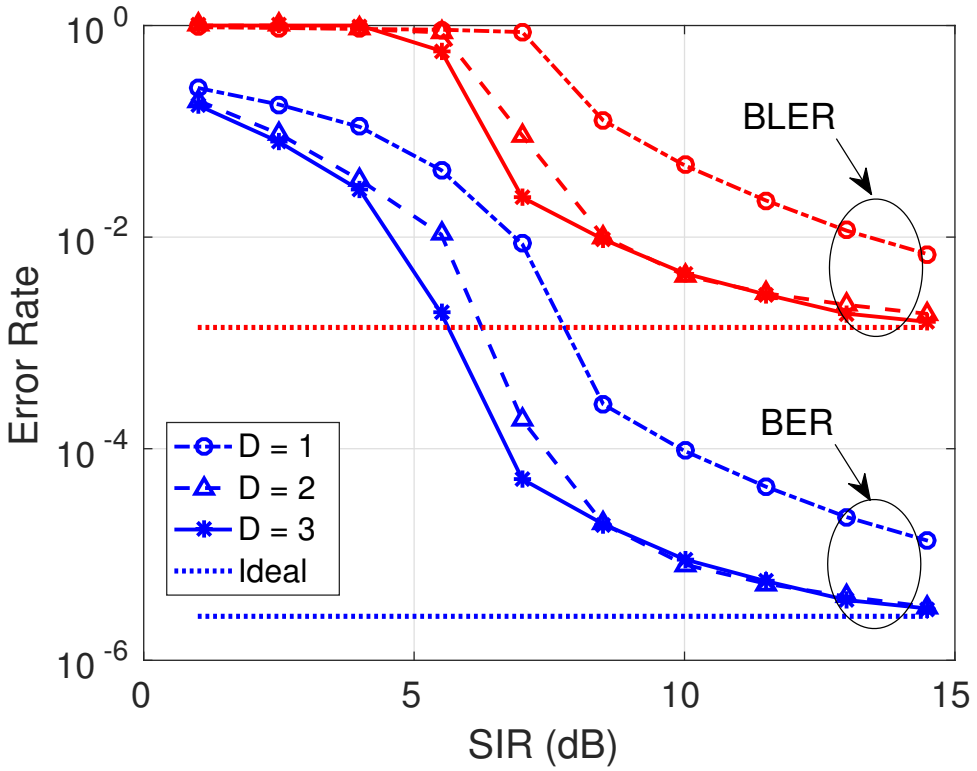

Figure 3.17: Error rate performance as a function of the power of the reflected self-interference, for different number of streams in the delay diversity structure. There is both self-loop interference and reflected self-interference, $G_{\mathrm{R}}G_{\mathrm{LI}} = -9$ dB, and SNR = 35 dB.

of the power of the reflected self-interference in Fig. 3.17, with a received SNR of 35 dB. Also, the residual self-loop interference is such that $G_{\mathrm{R}}G_{\mathrm{LI}} = -9$ dB. Note that $D = 1$ indicates that the system only detects the current OFDM block, i.e., the system does nothing to deal with the reflected self-interference. First of all, due to the existence of reflected self-interference, in the case of $D = 1$, the system suffers from significant performance loss even with weak interference ($G_{\mathrm{R}}G_{\mathrm{RI}} = -15$ dB). Further, with $D = 2$ streams at the Viterbi decoder, the system performance is very close to that of the ideal case when the residual reflected self-interference is not too strong, for example, when $G_{\mathrm{R}}G_{\mathrm{RI}}$ is less than -9 dB. On the other hand, more streams have to be included to guarantee the system performance if the residual interference is strong, and there is

a trade-off between the system performance and decoding complexity.

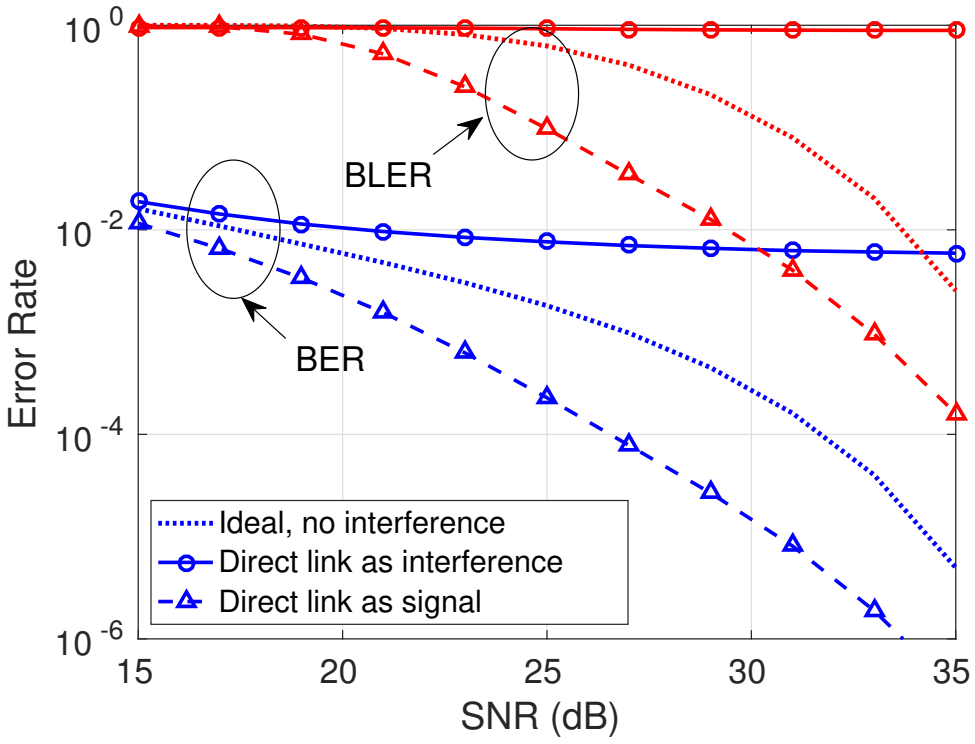

Figure 3.18: Error rate performance with $D = 3$ streams in the delay diversity structure by combining the "interference" from the direct link. We include interference from the self-loop link, the reflected link, and the direct link. ($|\beta h_{\mathrm{LI}}(m)|^2 = -9$ dB and $||\beta \mathbf{h}_f||_2^2 = -12$ dB.)

Finally, in Fig. 3.18, we include all possible interference from the self-loop link, the reflected link and the direct link. To focus on investigating the impact of the direct link, here, we assume we have small residual self-loop interference ($G_{\mathrm{R}}G_{\mathrm{LI}} = -9$ dB) and reflected self-interference ($G_{\mathrm{R}}G_{\mathrm{RI}} = -12$ dB). Note that, by including a larger residual interference, the system performance gets worse, but the relative performance gain or loss is not affected. For the Viterbi decoder at the destination, we have $D = 3$, where the three streams are the "interference" from the direct link, the current OFDM block, and the ISI from the previous OFDM block. On the one hand, we can see that the system error rate performance degrades severely if we do not carefully deal with the direct link (marked as "direct link as interference"). Since the source and

destination nodes are only 4 km away and the relay node has the same power as the source node, the "interference" from the direct link is strong enough to interfere with the reception of the signals from the relay at the destination. On the other hand, the system performance outperforms that of the ideal case when we combine the stream from the direct link at the destination (marked as "direct link as signal"); this gain comes from the utilization of the direct link. Therefore, the delay diversity scheme can work effectively to combat the reflected self-interference and the interference from the direct link.

3.4 Summary

In this chapter, we proposed to develop acoustic IBFD systems, which could potentially double the spectral efficiency in the underwater environment. By analyzing the challenges in implementing IBFD UWA systems, we presented a hybrid design that includes both analog and digital cancellation for the underwater acoustic environment. Further, we analyzed its performance in the presence of imperfect CSI, ambient noise, and ADC quantization noise. In a deep ocean environment, we showed that the combination of directional transmission, analog cancellation, and digital cancellation can be used to suppress the self-loop interference. In shallow water, the self-multipath interference may pose challenges to the IBFD transceiver if it is not carefully treated.

Also, for IBFD UWA relaying, OFDM techniques were employed to overcome the impact of the residual self-loop interference. Simulation results show that there is not significant performance loss when the residual self-loop interference is not very strong. To deal with the reflected interference, a delay diversity scheme was implemented at the destination and Viterbi algorithm was used to detect the transmitted signals. Both analyses and simulation results show that the proposed scheme can effectively combat the reflected interference effectively.

In the future, the following two aspects could be investigated to further evaluate the feasibility of IBFD UWA systems: 1) verify and improve the proposed hybrid cancellation scheme by doing experiments in real sea environments; and 2) propose

other types of space-time coding schemes or more efficient detectors to utilized the reflected interference in IBFD UWA relaying systems

Chapter 4

INTER-SYSTEM INTERFERENCE IN UNLICENSED BAND

4.1 Introduction

As explained in Chapter 1, to alleviate the problem of scarce spectrum resources and keep up with the ever growing traffic demands in cellular systems, the 3GPP standardization group has investigated and standardized LAA in LTE release 13 [2,27,93]. Recently, 3GPP Release 15 has proposed "new radio (NR) based unlicensed access" and "enhancements to LTE operation in unlicensed spectrum," where the evolution of LAA will be standardized to allow 5G to access the unlicensed spectrum [15–17,94–96]. In particular, channels in the unlicensed bands (specifically the 5-GHz band) are used as secondary carrier frequencies which are anchored by licensed primary carrier frequencies within the LTE carrier aggregation framework. The primary licensed carrier frequencies are used to exchange critical control signals to guarantee the quality of service, whereas, the secondary unlicensed carrier frequencies are used opportunistically to boost downlink bandwidth. Compared to the traditional offloading of cellular traffic to Wi-Fi networks, which relies on the connection between the LTE core network and Wi-Fi, LAA can potentially provide better coverage, higher capacity, and lower latency, with seamless data flows, by using the same core radio technology across both licensed and unlicensed spectrum. Further, with a single evolved packet core (EPC) network, LAA could facilitate integrated network management and more efficient resource utilization, and, thus, lower operational costs [97–100].

Wi-Fi, which includes IEEE 802.11 a/n/ac [3], has had tremendous success, becoming the primary incumbent in the 5-GHz unlicensed band. Because LTE was originally designed to operate in licensed bands, it can optimize the physical (frequency and

time) resource allocation based on a centralized Media Access Control (MAC) protocol; this, however, does not provide any coexistence mechanisms when operating in the unlicensed 5-GHz band. Thus, deploying LTE directly in the unlicensed band would lead to significant performance degradation for Wi-Fi systems. In addition, different geographical regions have different regulatory requirements on transmissions in unlicensed spectrum [98]; this makes LTE Unlicensed (LTE-U), which occupies the channel using a static/dynamic muting approach, infeasible in certain regions. Therefore, a major focus of the Release 13 LAA specification is to design mechanisms for LTE to coexist with Wi-Fi so as to contend for access in the unlicensed band.

To provide efficient access to the unlicensed spectrum, IEEE 802.11 networks employ Carrier Sense Multiple Access with Collision Avoidance (CSMA/CA) in the MAC layer [3]. This mechanism, which is also known as the Distributed Coordination Function (DCF), enables Wi-Fi nodes to coexist with one another. To avoid interfering with existing Wi-Fi networks, 3GPP proposes that an LAA network should employ a fair coexistence mechanism so as not to impact Wi-Fi transmissions more than an additional Wi-Fi network would [2]. Thus, a similar Listen-Before-Talk (LBT) procedure was recommended for LAA in Release 13 in order to sense (using energy detection) whether the channel is idle or not before transmission.

There have been several previous studies on the coexistence of Wi-Fi and LAA [101–107]. In [101], a performance evaluation shows that LTE operating in the unlicensed band generally outperforms Wi-Fi in similar scenarios. In addition, a comparison is made in [102] among different coexistence mechanisms, including static muting, LBT, and Request-To-Send/Clear-To-Send (RTS/CTS), and the results show that the RTS/CTS based method provides significant performance gain over the other mechanisms for indoor scenarios. In [104], system-level simulation results are presented for indoor and outdoor scenarios which show that fair coexistence of LAA and Wi-Fi can be achieved, and the deployment of LAA can also provide a gain for Wi-Fi performance. In [103], two LBT-based channel access techniques are evaluated with different

signal and energy detection thresholds, and the simulation results show that the detection thresholds play a critical role in the system performance. However, incorporating RTS/CTS into LAA requires redesigning the LTE protocol, and the 3GPP standard only recommends energy detection for LAA, so that RTS/CTS or signal detection might not be practical. Further, though different detection thresholds are evaluated, no solutions have been proposed to adapt the detection thresholds to further improve the coexistence performance. In [106], the user association and resource allocation are jointly optimized to improve the system throughput and fairness in coexistent Wi-Fi and LTE-U networks.

Also, work has been performed from a theoretical perspective. The authors in [105] analyze the coexistence of LAA and Wi-Fi, and derive the optimum spectrum access for LAA by switching between scheduling-based and random access schemes. Also, a fair LBT algorithm is proposed in [107] to allocate proper idle periods for Wi-Fi nodes by jointly considering the total system throughput and coexistence fairness. In [106], the coexistence of LTE-U and Wi-Fi is improved by optimizing user association and resource allocation using the IEEE 802.11 Point Coordination Function (PCF)[1] access protocol. Although these theoretical analyses provide insights and guidelines to enhance/optimize the coexistence of Wi-Fi and LAA, their solutions either ignore the details of LBT (CSMA/CA) or use a centralized controller.

In addition, to provide ultra high-speed and low-latency communications, IEEE 802.11ac and LTE networks utilize channel bonding and carrier aggregation mechanisms, respectively, to aggregate multiple channels/carriers. For LAA systems, different options for multi-carrier LBT are proposed in [2] so that LAA can access multiple carriers effectively without adversely affecting the performance of the coexistent Wi-Fi systems. Among recent works, a coexistence solution based on carrier selection is proposed in [108], in which UE measurements are used to optimize the network sum capacity. In [109], a new LBT mechanism is proposed to avoid the adverse impact of

[1] In PCF, an optional MAC technique used in IEEE 802.11 networks, the channel access is centralized through access points (APs).

radio RF leakage on multi-carrier operations for LAA. In [110], different carrier aggregation schemes are evaluated to show their effectiveness in improving throughput performance and end-user experience in a dense network with multiple carriers. These techniques improve the coexistence performance, but require additional feedback or significant modifications in the current multi-carrier LBT procedure.

The main goals of the work presented in this chapter are to investigate the impact of energy detection thresholds on the coexistence of Wi-Fi and LAA networks, and to propose an adaptive energy detection algorithm to improve the performance of both networks. We first analyze the coexistence challenges of Wi-Fi and LAA posed by frequent collisions that result from the employment of different sensing/detection methods and the asymmetric setting of energy detection thresholds in CSMA/CA and LBT. To improve the coexistence performance of Wi-Fi and LAA in downlink transmissions, we propose a distributed adaptive algorithm to adjust LAA's Energy Detection (LAA-ED) thresholds per user or per base station. Via simulations, we show that the proposed adaptive energy detection algorithm can achieve significant performance gain compared to using a fixed energy detection threshold for LAA transmitters. Also, the proposed adaptive algorithm can achieve performance comparable to that of the RTS/CTS based method [102], but with a much simpler implementation. In addition, we extend the adaptive energy detection algorithm to the multi-carrier case. To further improve the coexistence performance, based on the adaptive energy detection algorithm, we propose a simple, but efficient, carrier-selection algorithm based on LAA-ED thresholds. In particular, carriers with low energy detection thresholds may suffer from interference and, then, are less likely to be aggregated.

4.2 Coexistence of Wi-Fi and LAA Networks with Adaptive Energy Detection

4.2.1 CSMA/CA in Wi-Fi and Cat 4 LBT in LAA

4.2.1.1 Review of CSMA/CA Adopted in Wi-Fi

IEEE 802.11 employs CSMA/CA for all APs and stations (STAs) to contend for access to the shared medium, and the basic idea of CSMA/CA is to sense the channel idle or not whenever a Wi-Fi node has a pending transmission [3]. Specifically, an AP/STA having data to transmit first performs a Clear Channel Assessment (CCA), which is followed by an exponential backoff mechanism to avoid collisions when more than one node senses the medium idle and transmits at the same time. The sensitivity requirements of CCA depend on two thresholds, CCA Carrier Sense (CCA-CS) and CCA Energy Detection (CCA-ED), which vary according to the transmission bandwidth. CCA-CS refers to the capability of the receiver to detect and decode the preambles of incoming Wi-Fi signals, and CCA-ED is used to detect the energy level of the signals present on the shared channel. In the context of coexistence of Wi-Fi and LAA, Wi-Fi nodes are not able to decode any LAA signals. Thus, Wi-Fi nodes apply CCA-ED to detect potential interference from LAA nodes, and both CCA-ED and CCA-CS to detect and decode signals from other Wi-Fi devices[2].

4.2.1.2 Review of Cat 4 LBT Adopted in LAA in Release 13

In comparison, as specified by 3GPP [2], an LBT procedure plays a critical role in the coexistence of multiple LAA networks (of the same or different operators), and the coexistence of LAA with Wi-Fi in the same unlicensed spectrum.

The Category 4 LBT (Cat 4 LBT) mechanism [2], depicted in Fig. 4.1, has been included in LTE Release 13 for LAA downlink transmissions. The key idea of Cat 4 LBT is similar to CSMA/CA, i.e., an LAA eNB is required to perform CCA to determine whether the channel is idle or not before transmission. Specifically, Cat

[2] For Wi-Fi, CCA-CS is performed to decode possible valid Wi-Fi preambles; if the preamble portion is missed, CCA-ED is performed to detect any possible interference.

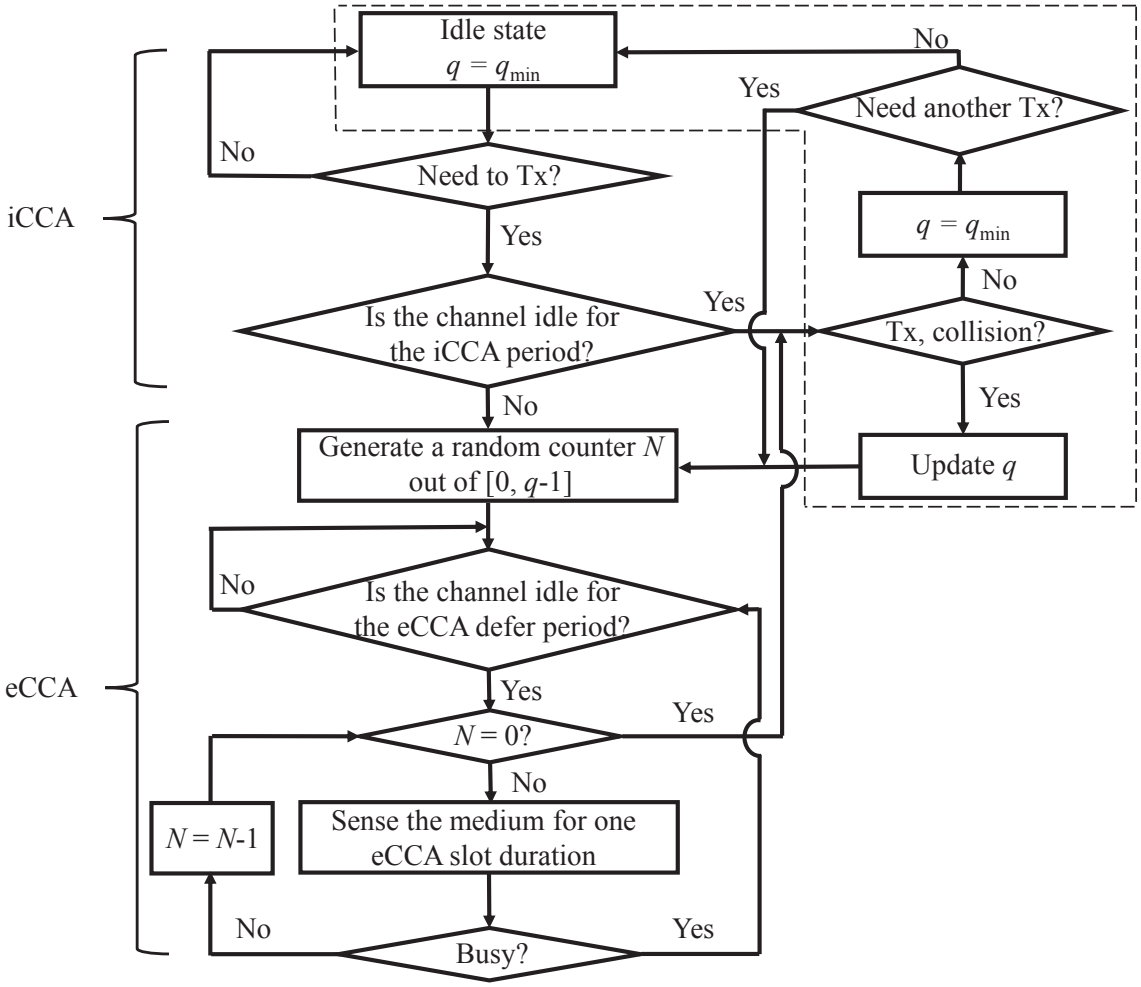

Figure 4.1: Cat 4 LBT procedure, which consists of LBT-iCCA and LBT-eCCA procedures [2].

4 LBT consists of the LBT initial CCA (LBT-iCCA) and the LBT extended CCA (LBT-eCCA) procedures. An LAA eNB begins by executing LBT-iCCA, when there is data to be transmitted, to check whether the channel is idle or not. If the channel is idle for an iCCA period (e.g., 34 μs)[3], data transmission can proceed; otherwise, the LBT-eCCA procedure begins as follows. The LAA eNB starts a backoff process to defer its access to the shared channel. To back off, the LAA eNB first picks a random

[3] In the CSMA/CA procedure, the distributed coordination function interframe space (DIFS) duration is 34 μs for IEEE 802.11a/n/ac (5 GHz).

number N uniformly from the interval $[0, q-1]$, where q is the current contention window size. Then, the channel is checked to see if it is idle or not for an eCCA defer period (e.g., 34 μs). If the channel is sensed busy during the eCCA period, the LAA eNB continues sensing until the channel is free. Once the channel becomes free, it continuously conducts a CCA for another eCCA slot duration (e.g., 9 μs or 10 μs) and decrements N if the channel is sensed idle. This process is repeated until N reaches zero and, at that time, the LAA eNB can begin its transmission. Note that, after a successful transmission, if the LAA eNB still has pending packets to be transmitted, the LBT-eCCA procedure, rather than the LBT-iCCA procedure, is performed. In addition, the contention window size q is updated whenever a collision occurs, or reset to the minimum contention window size ($q_{\min}$) with a successful transmission. Note that the dashed box in Fig. 1 highlights the procedures of Cat 4 LBT that we will modify and extend to include the proposed adaptive energy detection, which is described in Section IV.

4.2.2 Coexistence Challenges: Collisions in Wi-Fi/LAA Networks

Although the Cat 4 LBT procedure enables LAA to coexist with Wi-Fi, the fundamental differences between LAA and Wi-Fi may still degrade the performance. The three key differences between the two technologies are as follows:

- In CSMA/CA, there exist two different mechanisms to sense/detect the idle or busy condition of a medium: CCA-CS and CCA-ED. For instance, for operations on a 20-MHz channel, the threshold for CCA-CS (η_{CCACS}) is -82 dBm to decode the Wi-Fi preambles, and the threshold for CCA-ED (η_{CCAED}) is set to -62 dBm for detecting any signal, both Wi-Fi, if the Wi-Fi preamble portion was missed, and non-Wi-Fi signals. In contrast, in Cat 4 LBT, energy detection is the only recommended sensing method for all signals.
- For Wi-Fi, an AP serves only one STA in a single transmit time interval[4], and the contention window size q is updated if the AP does not receive associated ACKs. In contrast, an LAA eNB can schedule multiple UEs in a single transmit

[4] Multi-user multi-input multi-output (MU-MIMO) technology can enable one Wi-Fi AP to transmit data to different STAs simultaneously; this is not considered in this thesis.

time interval and their respective ACKs may be received at different times or even not received by the anchored LTE eNB. In that case, a criterion is required for LAA eNB to update q when the LTE eNB does not receive all ACKs from the involved UEs within a certain time interval.

- CSMA/CA employs an exponential backoff procedure, where q is doubled when a collision occurs, until reaching its maximum value. In contrast, for Cat 4 LBT, there exist multiple candidate backoff procedures, including exponential backoff as in Wi-Fi.

In this section, we focus on analyzing the potential collisions caused by the different sensing schemes adopted in Wi-Fi and LAA.

4.2.2.1 Hidden Node Problem in Wi-Fi Networks

In Wi-Fi networks, the hidden node problem occurs when two (or more) transmitter nodes, not detectable by each other, transmit data simultaneously to the same receiver node [111,112]. Hidden nodes may cause collisions in both the uplink (multiple STAs transmit data to an AP) and the downlink (multiple APs transmit data to their associated STAs) transmissions. In this paper, we focus on the downlink transmissions, and an example is shown in Fig. 4.2, with two APs (A_1 and A_2) and two associated STAs (S_1 and S_2). When A_1 is transmitting data to S_1, the hidden node A_2 would not be silenced, i.e., A_2 can also transmit data to S_2. Thus, a collision occurs at S_1 in this case.

Usually, such collisions occur to STAs located close to the edge of an AP's transmission area, which may not happen very often. However, in a coexistent network of Wi-Fi and LAA, due to the different energy detection thresholds adopted for APs and eNBs, such collisions may occur more frequently during downlink data transmissions.

4.2.3 Collisions in Coexistent Networks of Wi-Fi and LAA

In the network scenario studied in 3GPP [2], as shown in Fig. 4.3, two operators (Operator A using IEEE 802.11ac and Operator B using LAA) share a single 20-MHz channel, and each operator deploys four small cells in a one-floor building (Wi-Fi APs and LAA eNBs are marked as circles and diamonds, respectively). Considering

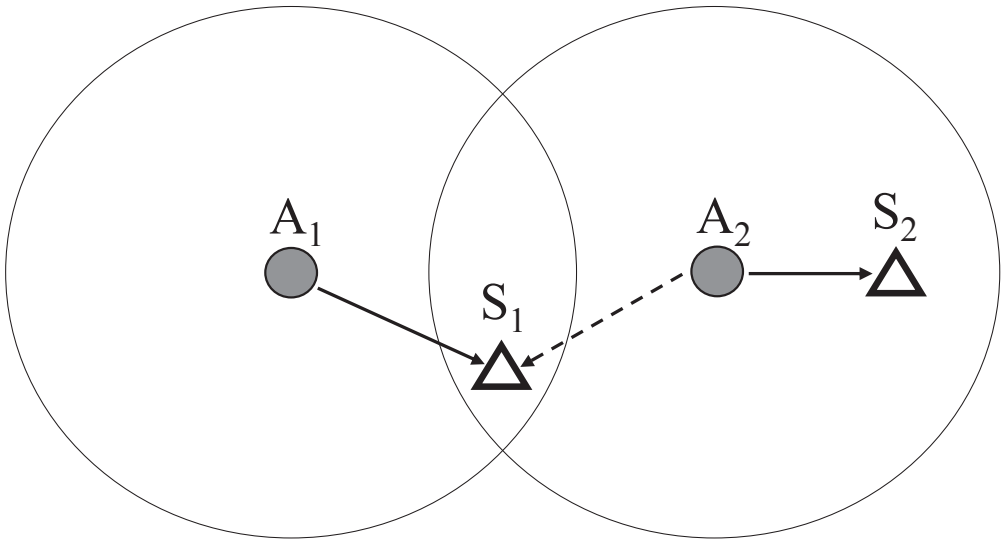

Figure 4.2: An example of hidden nodes in a pure Wi-Fi network, where A_1 and A_2 are two APs, and S_1 and S_2 are the associated STAs.

the leftmost three transmitters (Wi-Fi #1, LAA #2 and Wi-Fi #3) under the 3GPP fading model [2], since both Wi-Fi #1 and #3 adopt the same η_{CCACS} (-82 dBm) to sense the channel, a transmission from one AP will block a transmission from the other AP[5]. The resulting two sequential transmission scenarios are shown in Fig. 4.4(a): if Wi-Fi #1 transmits first, Wi-Fi #3 would back off to wait until the channel becomes idle, and *vice versa*.

In contrast, in Fig. 4.4(b), both LAA #2 and WiFi #3 use energy detection to detect each other's transmissions. For example, the threshold of CCA-ED for Wi-Fi is -62 dBm, and we assume the LAA-ED threshold is -70 dBm. Then, if Wi-Fi #3 transmits first, LAA #2 might back off due to its lower LAA-ED threshold. On the other hand, if LAA #2 transmits first and the received power at Wi-Fi #3 is lower than -62 dBm, Wi-Fi #3 may sense the channel idle and begin its data transmission, which could result in collisions at both the UEs of LAA #2 and the STAs of Wi-Fi

[5] Collisions may still occur in this case if Wi-Fi #1 and #3 both have data to transmit and happen to choose the same countdown counter. The collision probability, which depends on the current contention window size, is usually not very large.

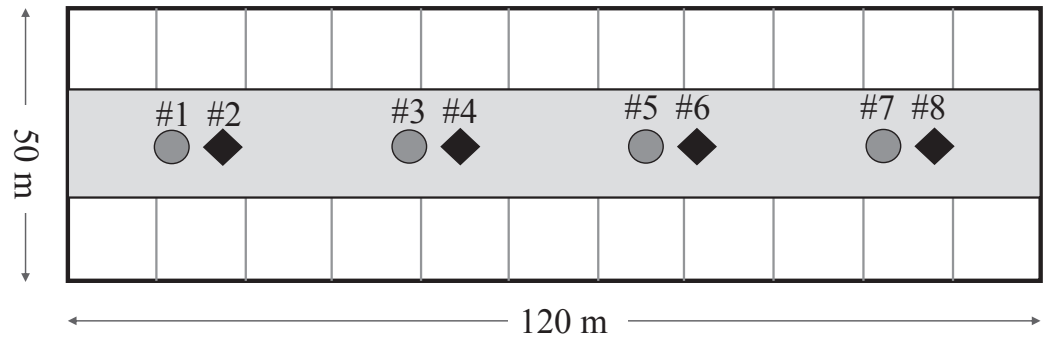

Figure 4.3: 3GPP indoor topology with 4 Wi-Fi APs (circles, labeled as #1, #3, #5, and #7) and 4 LAA eNBs (diamonds, labeled as #2, #4, #6, and #8).

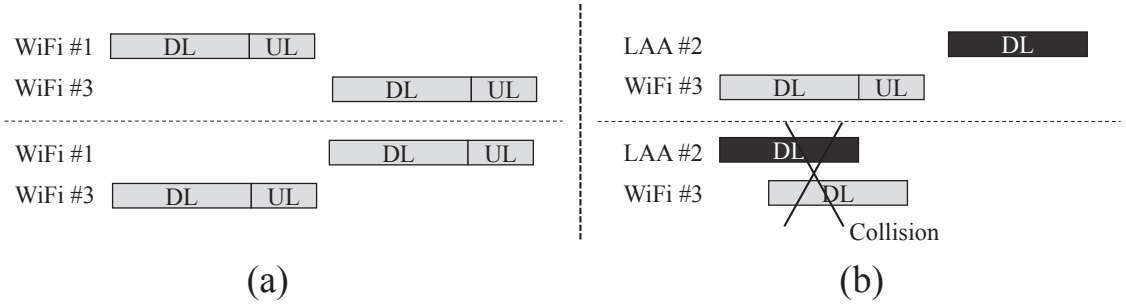

Figure 4.4: Hidden node problems in a coexistent network of Wi-Fi and LAA: the light colored blocks are Wi-Fi's downlink or uplink transmissions, and the dark colored blocks are LAA's downlink transmissions (LAA's uplink transmissions are fulfilled over the licensed band).

#3. Such asymmetric threshold settings cause Wi-Fi/LAA networks to suffer from "hidden" node problems (in this case, Wi-Fi #3 is visible from LAA #2, but LAA #2 is not visible from Wi-Fi #3). Note that, this hidden node problem is different from the conventional hidden node problem in a (pure) Wi-Fi network (in which two or multiple nodes are not detectable from each other), and frequent collisions may occur due to the asymmetric energy detection thresholds. To avoid such collisions, one could consider setting the LAA-ED threshold to be -62 dBm. However, this would introduce unfairness when Wi-Fi signals below -62 dBm, but above -82 dBm, are detected by other Wi-Fi nodes using carrier sensing (which will then back off) but not by other

LAA nodes.

In addition to the hidden node problem, Wi-Fi networks also suffer from an *exposed node* problem. Such a problem occurs when a node is unnecessarily silenced because of a neighboring transmitter, which might result in decreased overall throughput, especially in dense networks. The exposed node problem also exists in coexistent networks of Wi-Fi and LAA.

IEEE 802.11 employs the RTS/CTS mechanism to (partially) address both hidden and exposed node problems [111], and a similar scheme has been applied to LAA networks in [102], which protects the destination node from the "hidden" nodes. However, such RTS/CTS based methods are not mandated by the 3GPP LAA specifications, and thus require proprietary modifications to the LTE frame structures, which would be impractical in the near future.

4.2.4 Adaptive Energy Detection Algorithm

To manage the impact of "hidden"/exposed nodes, as well as to improve the coexistence performance of Wi-Fi and LAA, we study adaptive energy detection schemes for LAA eNBs. We first discuss the impact of LAA-ED thresholds on system performance, and then propose a distributed adaptive energy detection algorithm.

In a coexistent network of Wi-Fi and LAA, we assume all the APs and eNBs transmit at the same power P_t. Let $\mathcal{T}$ and $\mathcal{R}$ denote the set of transmitters (APs and eNBs) and receivers (STAs and UEs)[6], respectively. Also, let $\mathcal{T}_{\mathcal{L}}$ and $\mathcal{T}_{\mathcal{W}}$ denote the set of LAA eNBs and the set of Wi-Fi APs, respectively, i.e., $\mathcal{T}_{\mathcal{L}} \cup \mathcal{T}_{\mathcal{W}} = \mathcal{T}$. The channel gain from transmitter i to receiver j is denoted as $h_{tr}(i,j)$ ($i \in \mathcal{T}$ and $j \in \mathcal{R}$).

[6] This paper focuses on increasing LAA downlink data rates. Here, the APs and eNBs are the transmitters, and the STAs and UEs are the receivers. Note that uplink transmissions still exist for control signals (e.g., data requests and ACKs), and UEs/STAs are transmitters in this case.

Therefore, the received SINR at receiver j from transmitter i is

$$\gamma_i(j) = \frac{P_t|h_{tr}(i,j)|^2\mathcal{S}(i)}{\sum\limits_{k\in\{\mathcal{T}\setminus i\}} P_t|h_{tr}(k,j)|^2\mathcal{S}(k) + P_N} \tag{4.1}$$

where $\mathcal{T} \setminus i$ denotes the set of transmitters excluding transmitter i, P_N denotes noise power, and $\mathcal{S}(i)$ denotes the transmission status of transmitter i. Specifically, $\mathcal{S}(i) = 1$, if the channel is occupied by transmitter i; $\mathcal{S}(i) = 0$, otherwise.

At the receiver side, a larger $\gamma_i(j)$ typically results in higher throughput. Also, if $\gamma_i(j)$ is less than a predefined SINR threshold, the incoming packets cannot be decoded successfully, and hence there will be no ACK returned to the corresponding transmitter. In this case, receiver j experiences either a collision or a deep fade, and the system suffers a performance loss.

We define the throughput achieved for the link from transmitter i to receiver j as $C(i,j) = f(\gamma_i(j))$, where function $f(\cdot)$ can be determined by the Shannon Capacity [113] or by the specific modulation-coding schemes in IEEE 802.11ac [3] and the LTE [2] specifications. Let $\mathcal{R}_i$ denote the set of receivers involved in individual transmissions with transmitter i ($\mathcal{R}_i \subset \mathcal{R}$). Note that a Wi-Fi AP transmits data to one STA at each time instance, i.e., $|\mathcal{R}_i| = 1$ for Wi-Fi APs, where $|\cdot|$ denotes the cardinality. In contrast, an LAA eNB can transmit data to multiple UEs simultaneously, i.e., $|\mathcal{R}_i| \geq 1$ for LAA eNBs. Therefore, to maximize the system throughput,

$$\max_{\mathcal{S}} \sum_{i\in\mathcal{T}} \sum_{j\in\mathcal{R}_i} C(i,j) \tag{4.2}$$

we need to find the "optimal" transmission vector $\mathcal{S}$ so that the number of effective concurrent transmissions is maximized, while not resulting in performance losses caused by SINR degradation or collisions, especially for neighboring transmissions. For the two extreme cases, when $\mathcal{S}(i) = 0$ for all $i \in \mathcal{T}$, there is zero throughput for the network; when $\mathcal{S}(i) = 1$ for all $i \in \mathcal{T}$, there exists severe interference, leading to small $\gamma_i(j)$ and low data rates.

As explained in Section 4.2.1, Wi-Fi employs both CCA-CS and CCA-ED to detect signals present on the shared channel, and LAA only uses energy detection. Let $h_{tt}(k,i)$ denote the channel gain from transmitter k to transmitter i. Given a transmitter i, if it is a Wi-Fi AP (i.e., $i \in \mathcal{T}_{\mathcal{W}}$) and has data to transmit to one of its associated STA, with the CSMA/CA procedure, we have

$$\mathcal{S}(i) = \begin{cases} 0, \ 10\log_{10}\left(\mathcal{I}(k,i)\right) > \eta_{\text{CCACS}}, \ \text{for } k \in \{\mathcal{T}_{\mathcal{W}} \setminus i\} \\ 0, \ 10\log_{10}\left(\sum\limits_{k\in\{\mathcal{T}\setminus i\}} \mathcal{I}(k,i)\right) > \eta_{\text{CCAED}} \\ 1, \ \text{otherwise} \end{cases} \tag{4.3}$$

where $\mathcal{I}(k,i) = P_t|h_{tt}(k,i)|^2\mathcal{S}(k)/P_N$ denotes the normalized sensed energy at transmitter i from transmitter k, and $\mathcal{T}_{\mathcal{W}} \setminus i$ denotes the set of Wi-Fi APs excluding the transmitter AP i.

Eq. (4.3) indicates that Wi-Fi AP i cannot transmit (i.e., will back off) in two cases: 1) when any other Wi-Fi transmission exists for which the sensed energy at AP i is greater than η_{CCACS} (i.e., the preamble portion can be decoded), and 2) when the aggregated interference level from the ongoing Wi-Fi/LAA transmissions is larger than η_{CCAED}. In particular, in the second case, the aggregated interference also includes Wi-Fi signals because the preamble decoding could be unsuccessful if there are multiple concurrent Wi-Fi transmissions. Note that $\mathcal{I}(k,i)$ is the sensed energy (interference) at transmitter i from transmitter k, which determines whether transmitter i should back off or not. In contrast, the SINR defined in (4.1) is the received SINR, which determines the achievable throughput at receiver j.

On the other hand, if transmitter i is an LAA eNB (i.e., $i \in \mathcal{T}_{\mathcal{L}}$) and has data to transmit to its associated UEs, with the Cat 4 LBT procedure, we have

$$\mathcal{S}(i) = \begin{cases} 0, \ 10\log_{10}\left(\sum\limits_{k\in\{\mathcal{T}\setminus i\}} \mathcal{I}(k,i)\right) > \eta_{\text{LAAED}}(i,j), \ \text{for any } j \in \mathcal{R}_i \\ 1, \ \text{otherwise} \end{cases} \tag{4.4}$$

where $\eta_{\text{LAAED}}(i,j)$ is the LAA-ED threshold for UE j, which is involved in the data transmission from eNB i ($j \in \mathcal{R}_i$). Eq. (4) indicates that eNB i will not transmit

if the normalized sensed energy is higher than any of the energy detection thresholds assigned to its intended UEs.

Given (4.3) and (4.4), because η_{CCAED} and η_{CCACS} are fixed values defined by the IEEE 802.11 standard, the issue of finding the optimal transmission vector $\mathcal{S}$ becomes one of choosing a configuration of $\eta_{\text{LAAED}}(i,j)$ so that the system throughput is maximized. To model the coexistence performance of downlink traffic in 3GPP, both procedures, CSMA/CA and Cat 4 LBT, must be incorporated. However, it is nontrivial to formulate the CSMA/CA and Cat 4 LBT procedures as constraints into the optimization problem defined in (4.2). In addition, to avoid the signaling overhead associated with any centralized solution, here, we focus on distributed Adaptive Energy Detection (AED) solutions.

The basic idea of the proposed distributed AED algorithm is that an eNB's LAA-ED threshold is decreased if this eNB encounters frequent collisions; otherwise, a high LAA-ED threshold is maintained to encourage concurrent transmissions.

The extended Cat 4 LBT with the proposed AED algorithm is shown in Fig. 4.5, where the LAA-ED threshold is adaptively updated due to collisions. The differences between the two procedures are highlighted by the dashed boxes in Figs. 4.1 and 4.5. Specifically, let $\eta_{\min}$ and $\eta_{\max}$ denote the predefined minimum and maximum LAA-ED thresholds, respectively. In our study, we set $\eta_{\min} = \eta_{\text{CCACS}} = -82$ dBm, and $\eta_{\max} = \eta_{\text{CCAED}} = -62$ dBm for a 20-MHz channel. Variable n_r denotes the number of retransmissions for a specific packet, which is initialized to zero. Also, the contention window size q is set to its minimum value $q_{\min}$. The LAA-ED threshold $\eta_{\text{LAAED}}(i,j)$ is initialized to $\eta_{\max}$, which makes the LAA eNBs aggressive at the beginning of the data transmission. In a network with weak interference and light traffic, having a high LAA-ED threshold is beneficial to LAA while not hurting Wi-Fi. However, in a dense network with heavy traffic, keeping a high LAA-ED threshold will result in frequent collisions for both LAA and Wi-Fi. Therefore, if a packet cannot be successfully transmitted from eNB i to UE j within N_r trials, it is reasonable to decrease $\eta_{\text{LAAED}}(i,j)$ until either the packet is transmitted successfully, or $\eta_{\text{LAAED}}(i,j)$ reaches or falls below

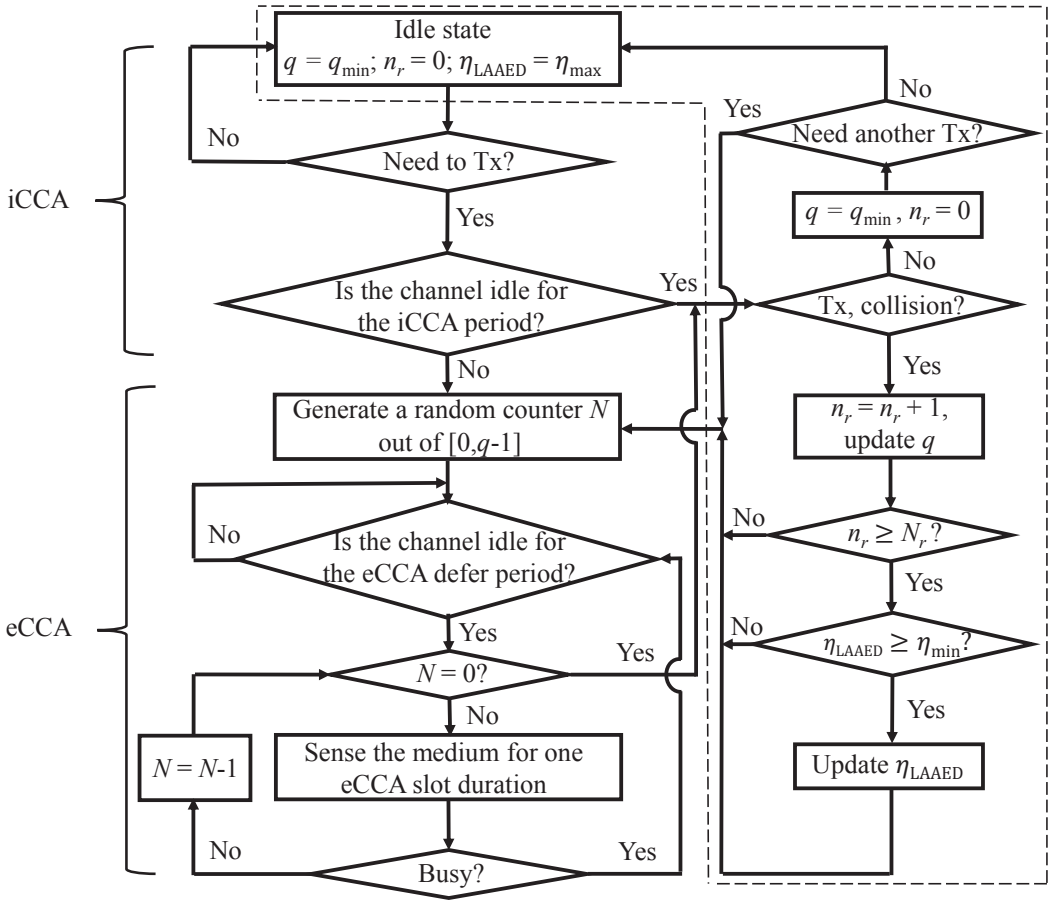

Figure 4.5: The extended Cat 4 LBT with the proposed AED algorithm, where the LAA-ED threshold is adaptively updated due to collisions.

its minimum value. This decreases the transmission opportunities from eNB i to UE j, but is beneficial to the entire network since the probability of collisions is reduced.

To adjust the LAA-ED threshold, we propose two methods as follows:

I: Update $\eta_{\text{LAAED}}(i,j)$ **per UE**: each LAA eNB can set different thresholds for its associated UEs.

II: Update $\eta_{\text{LAAED}}(i,j)$ **per eNB**: each LAA eNB sets the same threshold for all of its associated UEs, but the thresholds can be different for different eNBs.

For Method I, the proposed AED algorithm adaptively changes the LAA-ED threshold per UE. Specifically, if a packet fails to be transmitted in N_r trials, $\eta_{\text{LAAED}}(i,j)$ is decremented by 1, i.e., $\eta_{\text{LAAED}}(i,j) = \eta_{\text{LAAED}}(i,j) - 1$. With the AED algorithm, a

UE that is close to its associated eNB will have a higher LAA-ED threshold because the received signal power will still be strong enough compared to the interference from other ongoing transmissions. eNBs refrain from transmission by setting lower LAA-ED thresholds to the UEs who are far away from their associated eNBs. By having different LAA-ED thresholds for different UEs, the system can handle more concurrent transmissions without causing too many collisions. Due to this flexibility, the AED algorithm using Method I has the potential to achieve better performance.

For Method II, the LAA-ED thresholds are adaptively adjusted per eNB, which may be more practical for LAA networks. The updating rule for LAA-ED thresholds is $\eta_{\text{LAAED}}(i,k) = \eta_{\text{LAAED}}(i,k) - 1/N_i$ for all UE k ($k \in \mathcal{R}_i$), which is derived from

$$\begin{aligned}\eta_{\text{LAAED}}(i,k) &= \frac{1}{N_i}\left[\eta_{\text{LAAED}}(i,k) - 1\right] + \frac{N_i - 1}{N_i}\eta_{\text{LAAED}}(i,k) \\ &= \eta_{\text{LAAED}}(i,k) - \frac{1}{N_i} \end{aligned} \tag{4.5}$$

where N_i denotes the number of UEs associated with eNB i. The updating rule shares the same idea as that of Method I. The rationale is that one of the LAA-ED threshold values is decremented by 1 due to collisions ($\eta_{\text{LAAED}}(i,k) - 1$), and all the others maintain the same threshold as before ($\eta_{\text{LAAED}}(i,k)$). Then, the new LAA-ED threshold at eNB i is the average of all these threshold values.

In addition to the two updating methods used in Fig. 4.5, all the eNBs can employ the same $\eta_{\text{LAA-ED}}$ for all the UEs, an approach termed **Method III**. Since we assume eNBs cannot communicate with each other, it is difficult to update the LAA-ED threshold to be the same for all the different transmitters during transmissions. For evaluation, we choose a common value of η_{LAAED} for all the eNBs, and, in the next section, present the coexistence performance of Wi-Fi and LAA with different values of η_{LAAED}.

4.2.5 Evaluation of Coexistence Performance

4.2.5.1 Simulation Setup

To evaluate the coexistence performance of Wi-Fi and LAA with the AED algorithm, we adopt the indoor scenario specified by 3GPP [2], and consider a congested case with a single unlicensed 20-MHz channel shared between LAA and Wi-Fi (IEEE 802.11ac) [3] networks. As shown in Fig. 4.3, each operator (Operator A for IEEE 802.11ac, or Operator B for LAA) deploys four cells in a one-floor building. The four eNBs or four APs are equally spaced (30 meters apart) and centered along the shorter dimension of the building. The distance between each neighbouring pair of eNB and AP is 5 meters. Each eNB/AP serves five UEs/STAs, and all UEs/STAs are randomly located within the coverage area of their associated eNBs/APs.

The transmit power of LAA eNBs, Wi-Fi APs, and STAs in the unlicensed spectrum is set to 23 dBm, 23 dBm, and 18 dBm, respectively[7]. The two detection thresholds for Wi-Fi nodes are $\eta_{\mathrm{CCAED}} = -62$ dBm and $\eta_{\mathrm{CCACS}} = -82$ dBm, and the energy detection threshold for LAA (η_{LAAED}) varies from -82 dBm to -62 dBm. The indoor hotspot path loss and shadowing models from [9] are used. The transmission opportunity length (TxOP, referring to a bounded time interval during which one transmitter is permitted to send multiple packets after gaining access to the channel) of the LAA eNBs is fixed as 4 ms, which is the same for Wi-Fi. To focus on studying the impact of LAA-ED thresholds, we assume Cat 4 LBT employs exponential backoff as used in Wi-Fi. For each LAA eNB, the contention window size q is doubled (until it reaches the predefined maximum value) if there is no ACK received from any involved UE. For LAA and IEEE 802.11ac, the minimum and maximum values for q are 16 and 64, respectively.

In addition, we assume all eNBs/APs/UEs/STAs are equipped with only one antenna. The adaptive modulation-coding schemes (MCS), which are given in Table

[7] For LAA networks, the transmit power of the UEs is 18 dBm in the anchored LTE licensed band.

4.1, are implemented for both IEEE 802.11ac [3] and LTE [114] systems[8]. In particular, the modulation type can be Quadrature Phase Shift Keying (QPSK), 16 Quadrature Amplitude Modulation (16-QAM) and 64-QAM, and the code rate r is 1/2 or 3/4. The SINR threshold denotes the minimum required SINR to transmit with a specific MCS over the associated radio link[9]. We assume LAA systems employ the same types of MCS, SINR thresholds, and physical rates as those in LTE systems. Further, traffic is modeled as an FTP download of a 0.5 MB file with different Poisson request rates (λ) [2]. Each simulation is executed for 500 seconds with a random deployment of UEs/STAs, and results are averaged over 50 runs.

Table 4.1: Different types of MCS, the associated SINR thresholds and the absolute physical rates adopted in IEEE 802.11ac and 3GPP LTE specifications.

	SINR Threshold (dB)		Physical Rate (Mbps)	
MCS	802.11ac	LTE (LAA)	802.11ac	LTE (LAA)
QPSK, r = 1/2	5.0	2.0	14.4	16.8
QPSK, r = 3/4	9.0	5.5	21.7	25.2
16-QAM, r = 1/2	11.0	7.9	28.9	33.6
16-QAM, r = 3/4	15.0	12.2	43.3	50.4
64-QAM, r = 1/2	18.0	15.3	57.8	67.2
64-QAM, r = 3/4	20.0	17.5	65.0	75.6

4.2.5.2 Simulation Results and Discussion

In Fig. 4.6, the aggregate throughputs of Wi-Fi and LAA networks for different LAA-ED thresholds are shown, respectively, with a Poisson request rate of $\lambda = 2.5$ for

[8] There are 12 and 15 different types of MCS in IEEE 802.11ac and 3GPP LTE specifications, respectively. For simplicity, we choose 6 common MCS (adopted in both IEEE 802.11ac and 3GPP specifications) in the simulations.

[9] Compared to IEEE 802.11ac, LTE has a lower SINR threshold as well as a higher absolute physical rate due to the adoption of different physical layer techniques and hybrid automatic repeat request schemes.

Method III, where all eNBs have the same LAA-ED threshold. Here, the throughput is measured by the number of successfully transmitted bits over the total transmission period, and the aggregate throughput is the sum of the individual throughputs of eNBs/APs for one operator. It is observed that Wi-Fi outperforms LAA when the LAA-ED threshold is -82 dBm. As the LAA-ED threshold increases, Wi-Fi's performance degrades while LAA's improves. This is because, with a higher LAA-ED threshold, Wi-Fi APs back off more frequently since CCA-CS is employed for Wi-Fi's transmissions. With a lower LAA-ED threshold, LAA becomes less aggressive, which yields more transmission opportunities to Wi-Fi.

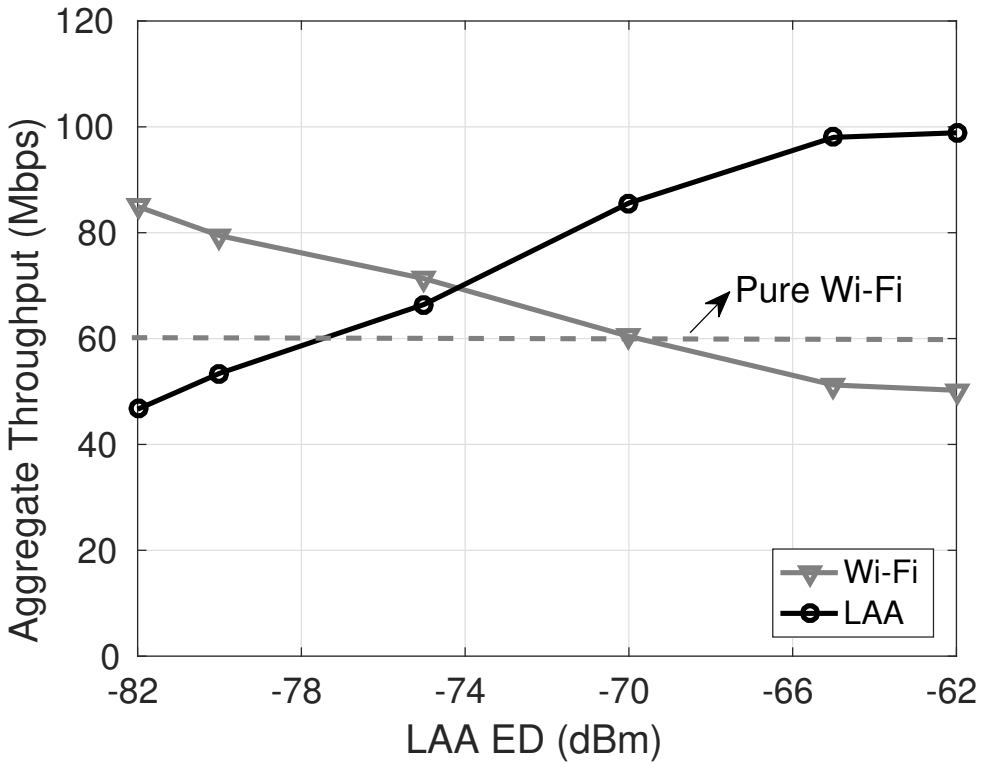

Figure 4.6: Performance of Wi-Fi and LAA systems with $\lambda = 2.5$ as a function of the LAA-ED threshold, which is the same across all eNBs (Method III).

The performance of a pure Wi-Fi network is also shown in Fig. 4.6 (dashed lines), where both Operator A and Operator B deploy Wi-Fi APs. The aggregate

throughputs of Operator A and Operator B are 59.88 Mbps and 60.20 Mbps, respectively, where the two corresponding dashed lines overlap with each other in the figure. In comparison, for the performance of a coexistent network of Wi-Fi and LAA with $\eta_{\text{LAAED}} = -75$ dBm, as shown in Fig. 4.6, the aggregate throughputs of Operator A (Wi-Fi) and Operator B (LAA) are 71.32 Mbps and 66.44 Mbps, respectively. In terms of the sum of the aggregated throughputs of Operator A and B, the percentage improvement of a coexistent Wi-Fi and LAA deployment is about 15% over a pure Wi-Fi deployment. This demonstrates that introducing an LAA network to an existing Wi-Fi network can improve the performance of both networks compared to introducing an additional Wi-Fi network. The reasons are two fold: 1) LTE provides a higher absolute physical rate than IEEE 802.11ac for the same SINR, and the same physical rates are employed by LAA as in LTE; and 2) compared to a pure Wi-Fi network, there are more concurrent transmissions in a coexistent Wi-Fi and LAA network. In this deployment, a Wi-Fi AP detects the transmissions from other LAA eNBs using CCA-ED, and an LAA eNB senses other signals using LAA-ED with threshold η_{LAAED}. In contrast, in a pure Wi-Fi network, the CCA-CS mechanism is used to decode the Wi-Fi preambles, and CCA-ED is employed only when the preamble portion is missed or corrupted. Since η_{CCACS} is much lower than η_{CCAED} (and even η_{LAAED}), the transmitters in a pure Wi-Fi network will back off more often than those in a coexistent LAA and Wi-Fi network. Note that having a higher sensing threshold encourages more concurrent transmissions, but it could also lead to more collisions.

The results in Fig. 4.6 also show that, around $\eta_{\text{LAAED}} = -75$ dBm, LAA and Wi-Fi can achieve similar performance (or fair coexistence). In the following simulations, we will generally use $\eta_{\text{LAAED}} = -75$ dBm as a reference to evaluate the performance of the proposed AED algorithm.

In Fig. 4.7, we plot the aggregate throughput of the coexistent Wi-Fi and LAA network with four different methods. From left to right, the first method is for Method III with a fixed LAA-ED threshold of -75 dBm, the second scheme uses the RTS/CTS method [102] with an LAA-ED threshold of -75 dBm, the third scheme is

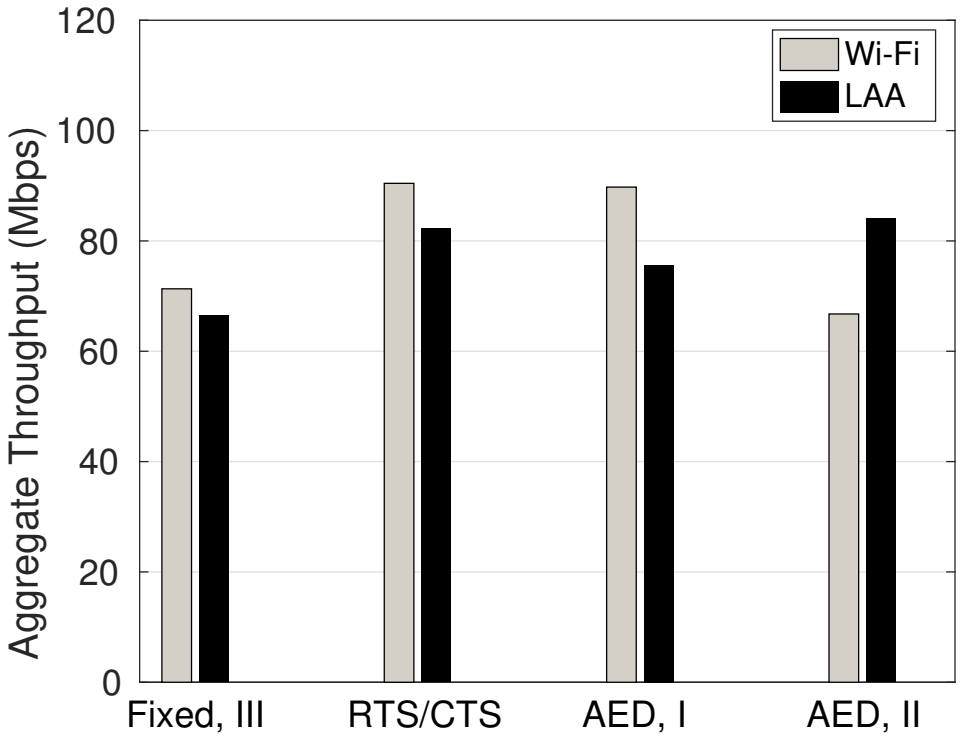

Figure 4.7: Performance of Wi-Fi and LAA with $\lambda = 2.5$ for four methods: Method III with $\eta_{\text{LAAED}} = -75$ dBm, RTS/CTS with $\eta_{\text{LAAED}} = -75$ dBm, AED with Method I using $N_r = 1$, and AED with Method II using $N_r = 1$.

the AED algorithm with Method I using $N_r = 1$, and the fourth scheme is the AED algorithm with Method II using $N_r = 1$. First of all, we see that RTS/CTS and the proposed AED algorithm can achieve visible performance gains compared to Method III with a fixed-threshold $\eta_{\text{LAAED}} = -75$ dBm: the percentage improvements over Method III for RTS/CTS, AED with Method I, and AED with Method II are about 25%, 20% and 10%, respectively. This indicates that both RTS/CTS and adaptive energy detection can improve the system performance by avoiding collisions. Also, RTS/CTS provides the best overall performance, and the proposed AED algorithm with Method I can achieve similar performance as RTS/CTS. Considering that the introduction of RTS/CTS control messages requires a significant change to the LTE protocol, it might not be feasible. Therefore, the adaptive LAA-ED threshold algorithm

is a better alternative since it only requires updating a specific parameter (the LAA-ED threshold). Further, we observe that the proposed AED algorithm with Method II can also improve the network's overall performance compared to Method III with a fixed LAA-ED threshold for all the LAA eNBs. Since the LAA eNBs do not need to update the LAA-ED thresholds individually for their associated UEs, this scheme provides a tradeoff between implementation complexity and performance, at the expense of some degradation to Wi-Fi.

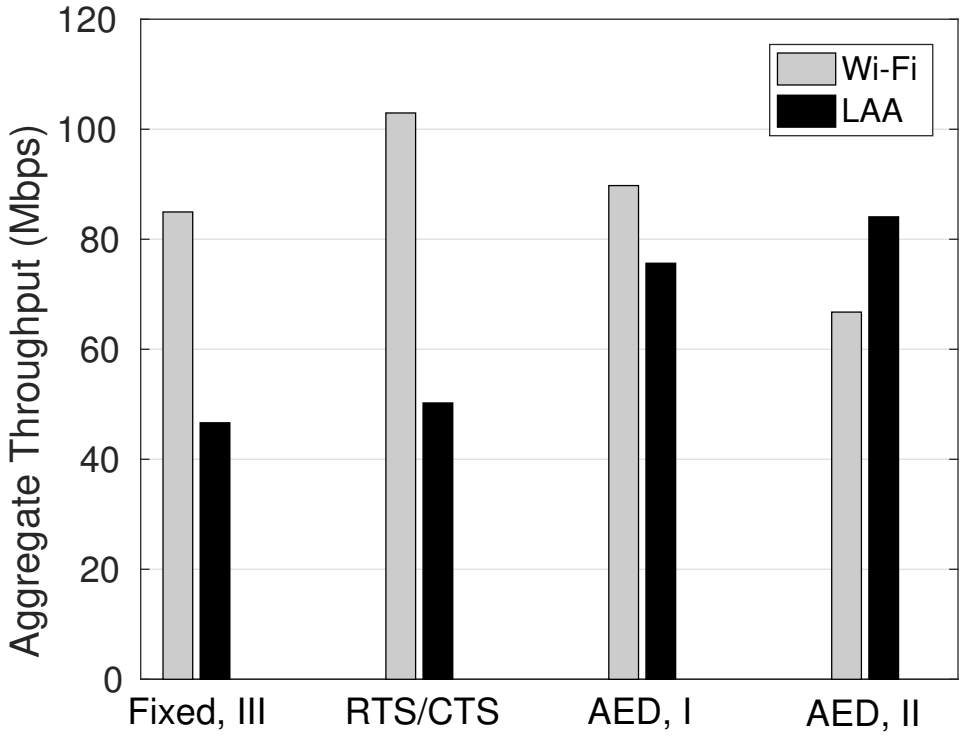

Figure 4.8: Performance of Wi-Fi and LAA with $\lambda = 2.5$ for the four methods ($\eta_{\text{LAAED}} = -82$ dBm and $N_r = 1$).

For comparison purposes, the performance of Wi-Fi and LAA for Method III and the RTS/CTS method with a fixed LAA-ED threshold of $\eta_{\text{LAAED}} = -82$ dBm are shown in Fig. 4.8. As expected, LAA suffers a lot with a low LAA-ED threshold. For the AED algorithm, it does not have such an issue, since the LAA-ED thresholds are

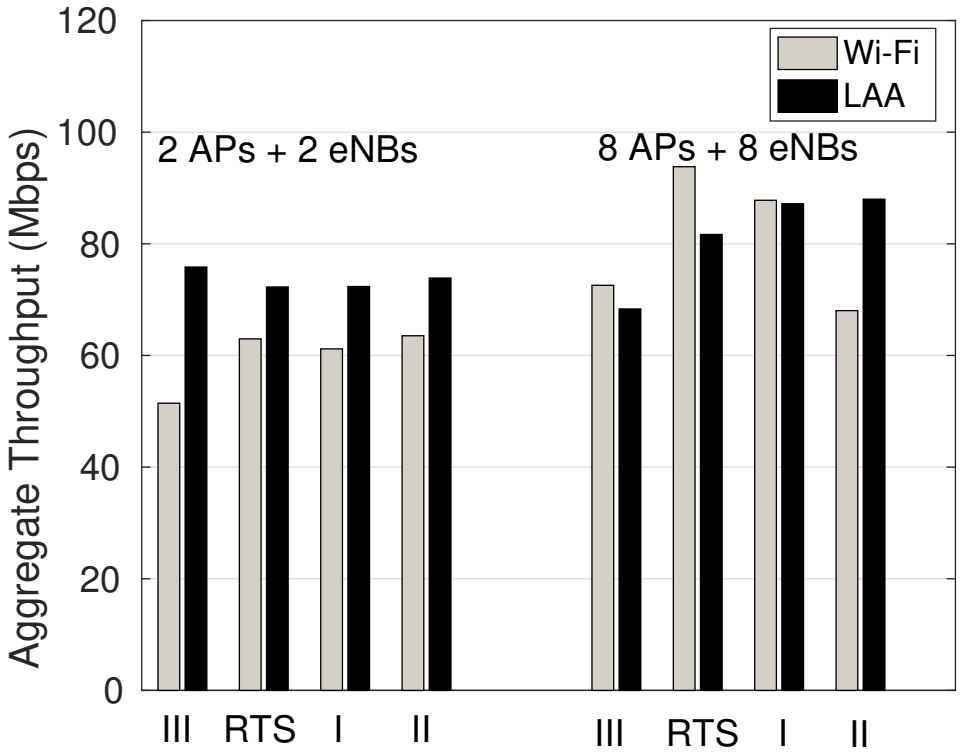

Figure 4.9: Performance of Wi-Fi and LAA with $\lambda = 2.5$ for the four methods ($\eta_{\text{LAAED}} = -75$ dBm and $N_r = 1$), under two different deployments: 2 APs coexist with 2 eNBs, and 8 APs coexist with 8 eNBs.

adaptively changed based on collisions. In other words, we need to "specify" a good LAA-ED threshold for the RTS/CTS method to achieve fair coexistence, which might depend on architectures, traffic models, traffic loads, and other factors.

As shown in Fig. 4.9, the coexistence performance of Wi-Fi and LAA has also been studied for two other deployments with the four methods. Different from the 3GPP indoor scenario, in the first deployment of "2 APs +2 eNBs", each operator deploys two small cells (APs or eNBs) in the one-floor building, and the two small cells are 60 meters apart. In the deployment of "8 APs +8 eNBs", each operator deploys eight small cells, which are equally spaced, 15 meters apart. Note that all the simulation settings in Fig. 4.9 are the same as those in Fig. 4.7, except for the numbers of APs

and eNBs deployed. First of all, it can be observed that, as the number of small cells is doubled, although the aggregated throughput increases, it is much less than double. The reasons are two-fold: 1) the coexistence performance has been evaluated with heavy traffic that almost saturates the channel; 2) the size of the building is the same for all three deployments, which would lead to more interference as the number of small cells increases. Also, due to fewer collisions occurring for LAA with a smaller number of cells, using Method III and RTS/CTS, LAA outperforms Wi-Fi in the deployment of "2 APs + 2 eNBs", while Wi-Fi outperforms LAA in the deployment of "8 APs + 8 eNBs". In contrast, the proposed AED algorithm adaptively updates the thresholds to improve the performance of both networks and to achieve fairer coexistence.

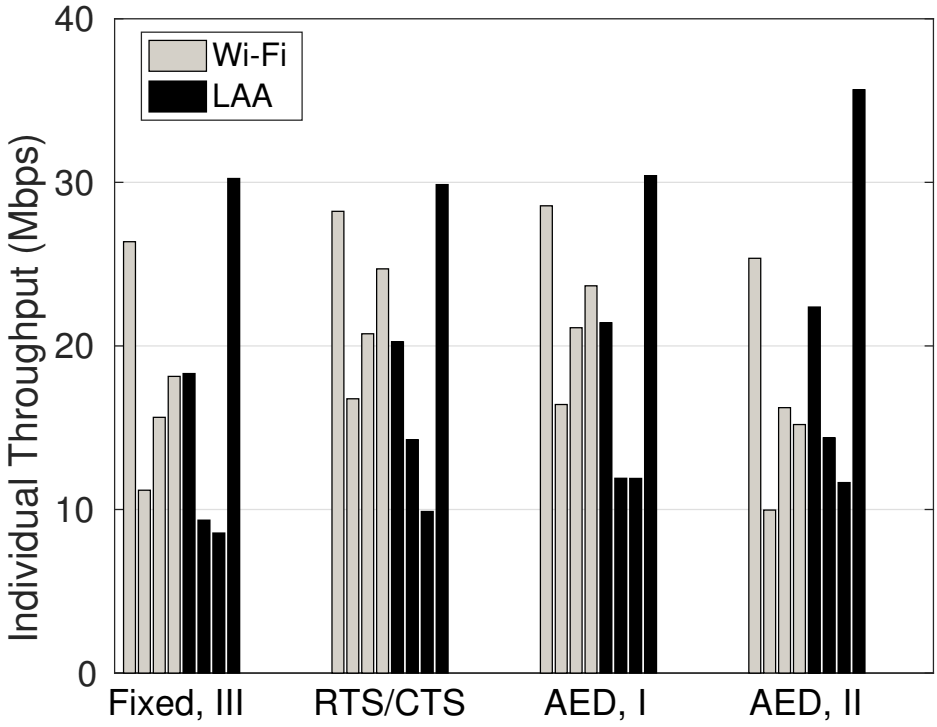

Figure 4.10: Performance for individual APs and eNBs with $\lambda = 2.5$ for the four methods ($\eta_{\text{LAAED}} = -75$ dBm and $N_r = 1$). In each method, the transmitters are, from left to right, Wi-Fi #1, Wi-Fi #3, Wi-Fi #5, Wi-Fi #7, LAA #2, LAA #4, LAA #6 and LAA #8.

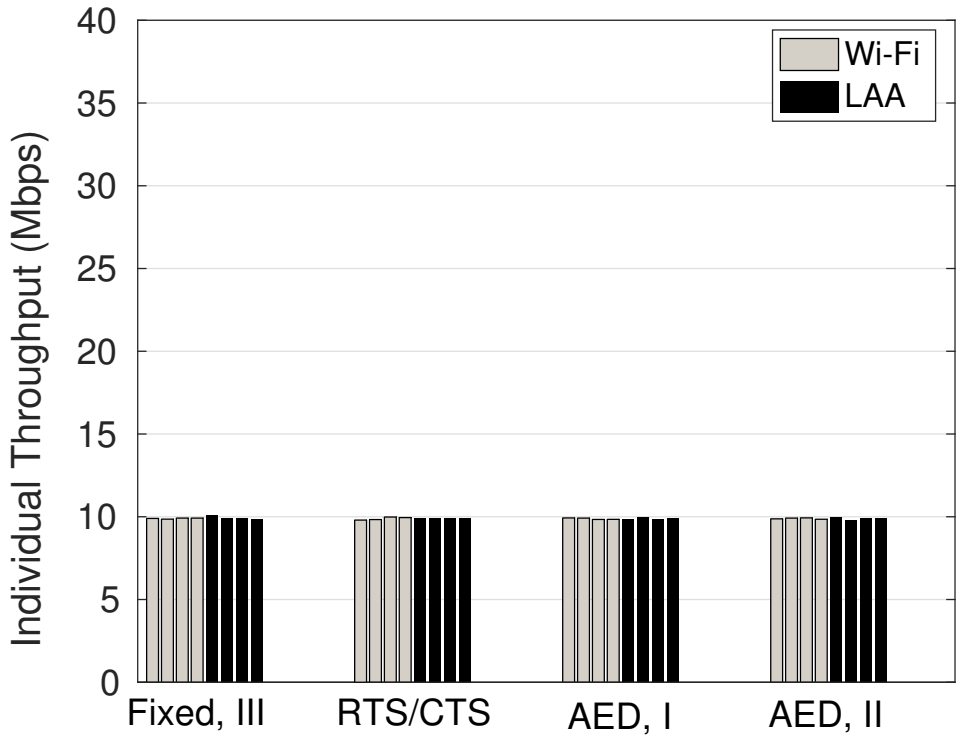

Figure 4.11: Performance for individual APs and eNBs with $\lambda = 0.5$ for the four methods ($\eta_{\text{LAAED}} = -75$ dBm and $N_r = 1$). In each method, the transmitters are, from left to right, Wi-Fi #1, Wi-Fi #3, Wi-Fi #5, Wi-Fi #7, LAA #2, LAA #4, LAA #6 and LAA #8.

In Fig. 4.10, the throughputs of individual APs and eNBs are shown, for a Poisson request rate of $\lambda = 2.5$, using the previously described four methods. The light colored bars for each scheme represent the individual throughput of WiFi #1, WiFi #3, WiFi #5, and WiFi #7 (APs in Fig. 4.3). Similarly, the dark colored bars for each scheme denote the individual throughput of LAA #2, LAA #4, LAA #6, and LAA #8, respectively. Due to this specific 3GPP layout, the transmitters in the middle will be disadvantaged since they need to contend for access to the shared channel with transmitters from both sides, while the transmitters at the edge only need to compete with the transmitters on one side. Therefore, in a congested scenario, the performance of the receivers associated with the transmitters in the middle is significantly worse

than that of the receivers associated with the transmitters at the edge, which is also true for a pure Wi-Fi network. In Fig. 4.11, we decrease the Poisson request rate to $\lambda = 0.5$. In this case, we have light-traffic conditions, every transmitter can finish their data transmissions, and they achieve similar throughputs.

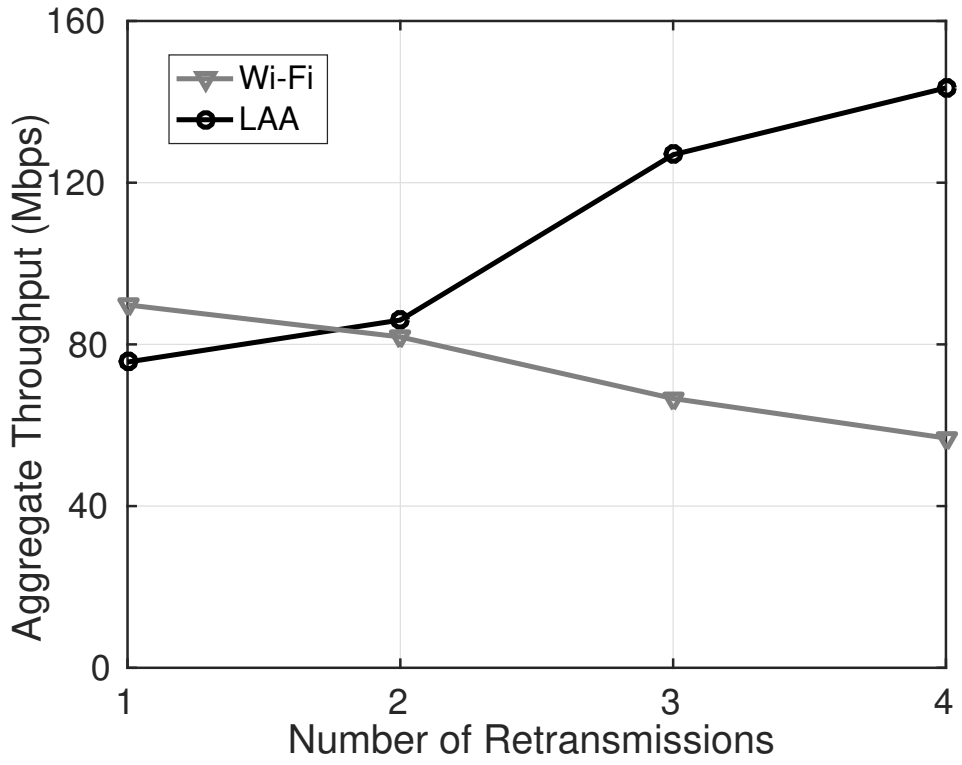

Figure 4.12: Performance of Wi-Fi and LAA as a function of the number of retransmissions N_r for AED with Method I. ($\lambda = 2.5$).

From Fig. 4.7, we notice that, for Method I, Wi-Fi outperforms LAA by using the proposed AED algorithm with $N_r = 1$. Since the LAA-ED threshold will decrease if collisions still occur after N_r retransmissions, we can choose a larger N_r to make the LAA-ED threshold decrease at a slower rate so as to provide LAA with more transmitting opportunities. As shown in Fig. 4.12, LAA has similar performance as Wi-Fi (coexist well with each other) for $N_r = 2$ (Wi-Fi: 81.84 Mbps, LAA: 86.04 Mbps). If we continue to increase N_r, LAA's performance keeps improving while Wi-Fi's degrades. Therefore, we need to choose the proper N_r based on the system

requirements. Also, for the AED algorithm with Method II using $N_r = 1$, Wi-Fi's performance is worse than LAA's since the LAA-ED threshold decreases at an even slower rate compared to that of Method I. One simple way to equalize the performance of Wi-Fi and LAA is to decrease LAA's initial LAA-ED thresholds. For example, when $\eta_{\max} = -70$ dBm is used in AED with Method II, the aggregate throughputs of Wi-Fi and LAA are 74.88 Mbps and 64.56 Mbps, respectively.

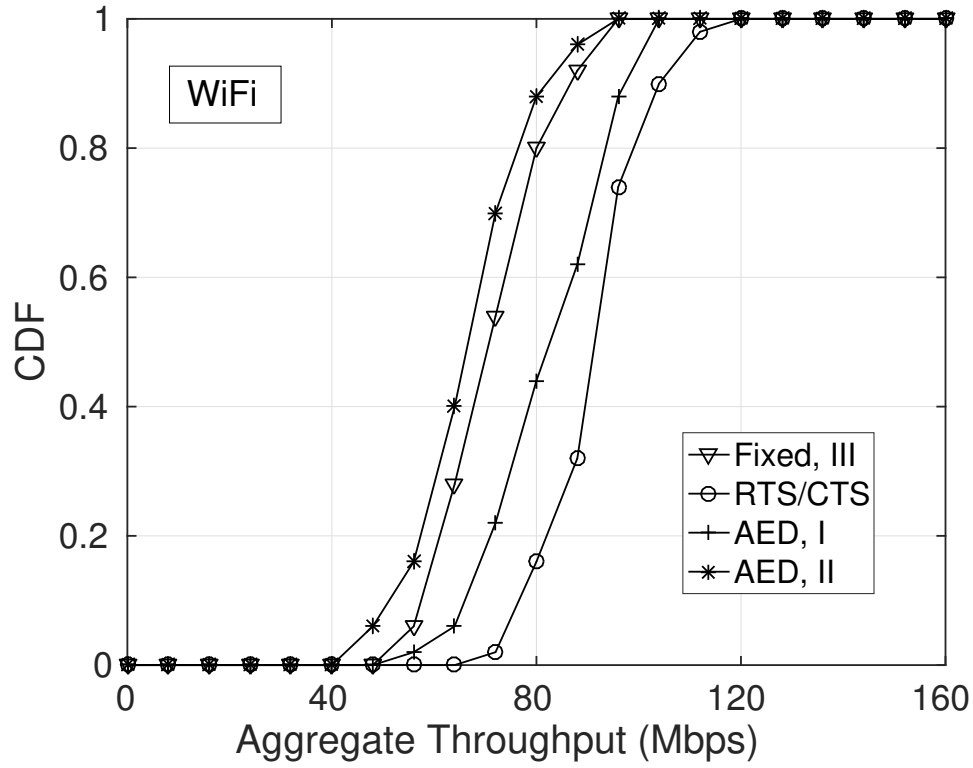

Figure 4.13: The CDF of the aggregate throughput for Wi-Fi APs over 50 runs, with four different schemes: Method III with $\eta_{\text{LAAED}} = -75$ dBm, RTS/CTS with $\eta_{\text{LAAED}} = -75$ dB, AED with Method I using $N_r = 2$, and AED with Method II using $N_r = 1$. ($\lambda = 2.5$).

Finally, the aggregate throughputs shown in Figs. 4.6-4.12 are averages over 50 trials. To better understand the performance, cumulative distribution functions (CDF) of the aggregate throughputs for both Wi-Fi and LAA systems using the four different methods are shown in Figs. 4.13 and 4.14, respectively. It is observed that the AED

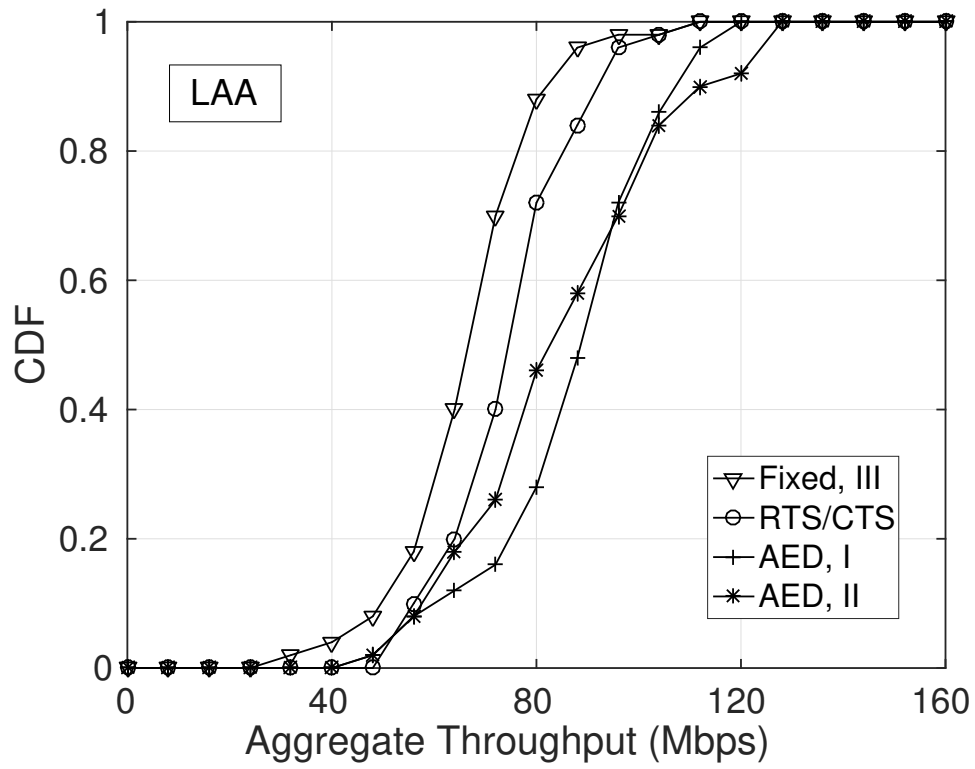

Figure 4.14: The CDF of the aggregate throughput for LAA eNBs, with four different schemes: Method III with $\eta_{\text{LAAED}} = -75$ dBm, RTS/CTS with $\eta_{\text{LAAED}} = -75$ dB, AED with Method I using $N_r = 2$, and AED with Method II using $N_r = 1$. ($\lambda = 2.5$).

algorithm with Method I can always achieve significant performance gain compared to Method III with a fixed LAA-ED threshold, while the AED algorithm using Method II can maintain similar performance for LAA as that of Method I at the expense of a slight performance loss to Wi-Fi.

In summary, LAA can fairly coexist with Wi-Fi: (1) Introducing an LAA network to an existing Wi-Fi network can improve the overall performance of both networks as compared to introducing an additional Wi-Fi network. (2) The AED algorithm can further improve the system performance compared to the use of a fixed LAA-ED (Method III), especially when an eNB can set different LAA-ED thresholds for its UEs (Method I). (3) The AED algorithm can achieve similar performance to

RTS/CTS, but with simpler implementations than incorporating RTS/CTS into LAA.

4.3 Multi-Carrier LBT Operation for LAA with Adaptive Energy Detection and Carrier Selection

4.3.1 Multi-Carrier Transmissions for IEEE 802.11ac and LAA Networks

In this section, we discuss the CSMA/CA and LBT operations at the APs and eNBs, respectively, when there are multiple carriers available.

4.3.1.1 Multi-carrier access in IEEE 802.11ac

CSMA/CA is employed in IEEE 802.11 for Wi-Fi nodes, i.e., APs and STAs, to contend for access to the shared unlicensed medium. In the IEEE 802.11ac standard, channel bonding is employed for a node to switch transmission bandwidth dynamically on a frame-by-frame basis (i.e., 20 MHz, 40 MHz, 80 MHz, or 160 MHz). Also, *primary* and *secondary* channels[10] are introduced to facilitate transmissions over multiple channels.

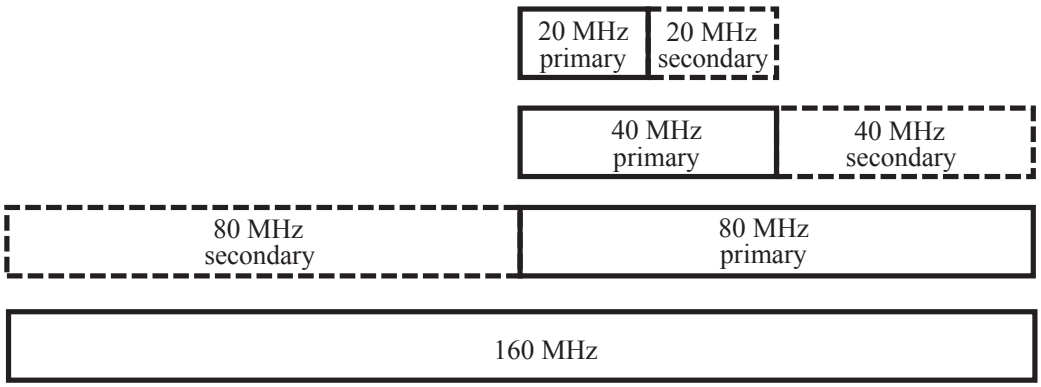

Figure 4.15: Specific patterns for channel bonding in IEEE 802.11ac [3].

[10] To follow the terminology used by IEEE 802.11 standard, "channel" is used here, which has the same meaning as "carrier" in the LTE standard.

The relationship between the channels composing the wider channel is illustrated in Fig. 4.15. In particular, channel bonding requires that: 1) a primary channel should always be included in each channel bandwidth; and 2) only adjacent channels in specific patterns can be combined to obtain a wider channel [3]. In addition, the whole CSMA procedure is only performed on the primary channel; on the associated secondary channel, only a quick clear channel access (CCA) check, i.e., the duration of a point coordination function interframe space (PIFS), is performed before transmitting data.

4.3.1.2 Multi-carrier LBT operation for LAA

As described in the beginning of this section, 3GPP introduces an LBT procedure to facilitate the coexistence of LAA and Wi-Fi, as well as multiple LAA networks, in the same unlicensed spectrum [2]. The basic idea of Cat 4 LBT is similar to CSMA/CA: an LAA eNB is required to perform a CCA to check whether the carrier is idle or not before transmission [3]. To access a wider carrier in an LAA system, 3GPP proposes two main options:

- Option 1: Similar to Wi-Fi, only one full Cat 4 LBT procedure is completed on one selected carrier (primary carrier), and quick CCA checks (PIFS) are performed on other carriers (secondary carriers) before data transmission.
- Option 2: Multiple Cat 4 LBT procedures are independently performed on different carriers, and the data transmissions over multiple carriers are aligned by introducing a self-deferral period.

Figs. 4.16 and 4.17 present an example of the two options with four candidate carriers (each carrier has a bandwidth of 20 MHz). In Option 1, as shown in Fig. 4.16, the LAA eNB performs a full Cat 4 LBT procedure on the "primary" carrier (which is the first carrier in this example), and performs sensing for the duration of PIFS before transmitting data on all the "secondary" carriers. Different from the channel bonding approach adopted in a Wi-Fi system, LAA can aggregate any idle carriers. In Option 2, as shown in Fig. 4.17, four LBT procedures are performed independently on all four carriers. Different carriers will finish their individual LBT procedures at different times. To synchronize transmissions across multiple carriers, a self-deferral

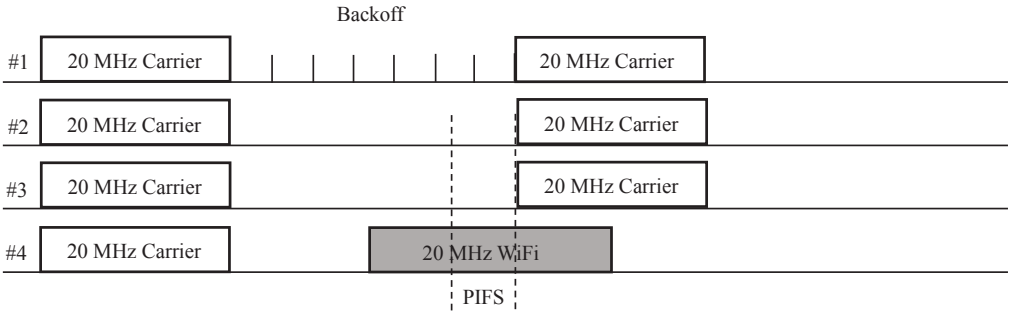

Figure 4.16: Multi-carrier LBT Option 1: a single Cat 4 LBT procedure is performed on the "primary" carrier.

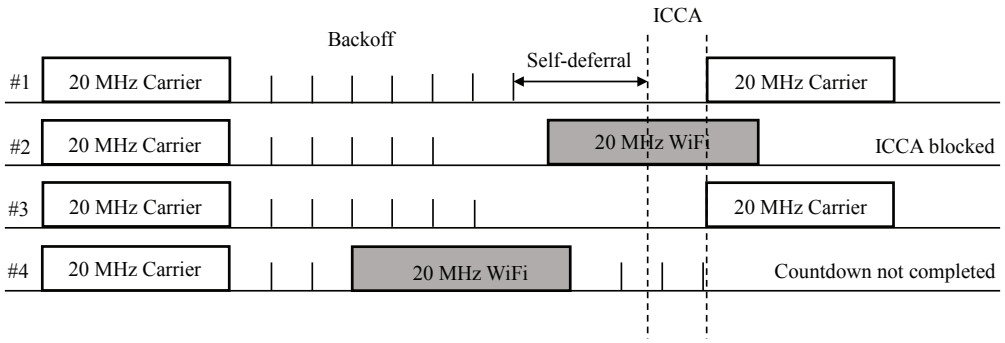

Figure 4.17: Multi-carrier LBT Option 2: Cat 4 LBT procedures are independently performed on all four carriers.

period is added to the carrier that finishes its LBT procedure first. After the the self-deferral period, the carriers who finish their Cat 4 LBT procedures will be selected for data transmission after a quick iCCA check[11]. Between the two options, Option 1 is generally more aggressive and might be unfair to Wi-Fi, while Option 2 is an extension of the Cat 4 LBT for the single carrier case, and the performance depends on the self-deferral period. With a large self-deferral period, the idle carriers might be occupied by other systems; with a small self-deferral period, the system would only be able to transmit data on a few carriers, since the Cat 4 LBT procedures on other carriers might not be finished yet.

4.3.2 Multi-carrier LBT with Adaptive Energy Detection and Carrier Selection

In a coexistent network of Wi-Fi and LAA, due to the asymmetric detection thresholds adopted for APs and eNBs, frequent collisions may occur during data transmissions.

4.3.2.1 Multi-carrier Cat 4 LBT with the AED algorithm

In this subsection, Cat 4 LBT with AED, as described in Section 4.2, is extended to the case of multiple carriers. We also assume that each LAA eNB i can have different thresholds $\eta_{\text{LAAED}}(i,j)$ for its associated UE j.

Let $\mathcal{C}$ denote the set of available carriers in the coexistent LAA and Wi-Fi systems. We define $\mathcal{C}(i,j)$ to denote the candidate carriers for data transmission from eNB i to UE j, i.e., the carriers considered to be idle after performing the multi-carrier LBT procedure (Option 1 or Option 2). Let $\mathcal{K}(i,j)$ denote the actual aggregated carriers for the data transmissions from eNB i to UE j. Since there might be a limit

[11] In a real LAA system, multiple candidate carriers could exist; the maximum number of carriers that can be aggregated depends on the system configuration and requirements.

N on the maximum number of carriers that can aggregated for each transmission, let $|\mathcal{K}(i,j)| \leq N$, where $|\cdot|$ denotes the cardinality. We then have

$$\mathcal{K}(i,j) \subseteq \mathcal{C}(i,j) \subseteq \mathcal{C} \tag{4.6}$$

In addition, we define $\eta_{\text{LAAED}}(i,j,k)$ as the energy detection threshold from eNB i to UE j on carrier k, and $\eta_{\text{LAAED}}(i,j,k)$ is initialized to the maximum threshold $\eta_{\max}$ for $k \in \mathcal{C}(i,j)$. After multi-carrier LBT procedures, if collisions happen during data transmissions, we decrease $\eta_{\text{LAAED}}(i,j,k)$, $k \in \mathcal{K}(i,j)$, to avoid frequent collisions until either the packet is transmitted successfully, or $\eta_{\text{LAAED}}(i,j,k)$ reaches or falls below its minimum value ($\eta_{\min}$). Specifically, the updating rule for the LAA-ED threshold (η_{LAAED}) in Fig. 4.5 is

$$\eta_{\text{LAAED}}(i,j,k) = \eta_{\text{LAAED}}(i,j,k) - 1, \quad \text{for } k \in \mathcal{K}(i,j) \tag{4.7}$$

The updating rule for the AED algorithm is the same for both Option 1 and Option 2, i.e., even though Cat 4 LBT procedures are applied to one carrier (Option 1) or multiple carriers (Option 2), the LAA-ED thresholds are updated on all aggregated carriers if collisions occur (leading to unsuccessful transmissions).

Here, we decrease the energy detection thresholds on all aggregated carriers k ($k \in \mathcal{K}(i,j)$) after collisions for two reasons: 1) for an unsuccessful data transmission over multiple carriers, we may have no information about which carrier suffers from severe interference; and 2) by decreasing the energy detection thresholds of all aggregated carriers rather than only specific carriers, the probability of aggregating multiple carriers is decreased, which could be beneficial to both LAA and Wi-Fi systems due to the power limitation in the unlicensed band. By aggregating fewer carriers, the LAA eNB can transmit with a relatively high power, which makes the system more robust to interference in a dense network.

Note that, because different carriers may be aggregated during different transmissions, the LAA-ED thresholds of $\eta_{\text{LAAED}}(i,j,k)$ can be different from each other for $k \in \mathcal{C}(i,j)$. Also, if there is no more data to be transmitted from eNB i to UE j, the system will reset $\eta_{\text{LAAED}}(i,j,k)$ to $\eta_{\max}$ for all $k \in \mathcal{C}(i,j)$.

4.3.2.2 Multi-carrier Cat 4 LBT with carrier selection

With multiple carriers available, carrier selection can significantly improve the performance of coexistent Wi-Fi and LAA systems [108], in which carrier selection is fulfilled based on UE measurements. In this paper, we propose a carrier selection algorithm based on the current LAA-ED thresholds of different carriers per UE, which requires no additional feedback from UEs.

To avoid potential collisions with Wi-Fi or other LAA networks, we follow two general rules in the carrier selection procedure:

1. Choose "clean" carriers to transmit data.
2. Choose carriers that are less likely to break the channel bonding patterns adopted in Wi-Fi systems.

For example, we assume that we have four carriers: #1, #2, #3 and #4, and Wi-Fi's primary channel is #1. In this case, LAA would prefer to choose Carrier #3 or #4 rather than #2 or #1, which could be relatively "clean" and give Wi-Fi more opportunities to transmit data with a higher bandwidth.

The key idea of the proposed carrier selection algorithm is that, for data transmissions from eNB i to UE j, eNB i will first aggregate the carriers with high LAA-ED thresholds. This is because a certain carrier k, shared by multiple systems, is more likely to have a low $\eta_{\text{LAAED}}(i, j, k)$ to avoid too many collisions according to the AED algorithm. Thus, aggregating carriers with high LAA-ED thresholds would lead the LAA system to choose relatively "clean" carriers. In addition, we add another preference for the carrier aggregation in LAA systems: LAA eNBs follow the channel bonding patterns as adopted in the Wi-Fi system if there are multiple candidate carriers. With this preference, LAA can transmit with a large bandwidth as well as reduce the negative impact on the channel bonding scheme used by the Wi-Fi networks.

In summary, for Option 1, the "primary" carrier is predefined, and the aggregated "secondary" carriers are chosen to satisfy

$$\eta_{\text{LAAED}}(i,j,k) \geq \eta_{\text{LAAED}}(i,j,\bar{k}), \text{for } k \in \mathcal{K}(i,j), \\ \bar{k} \in \mathcal{C}(i,j) \backslash \mathcal{K}(i,j) \tag{4.8}$$

For Option 2, there are no "primary" or "secondary" carriers, so all aggregated carriers should satisfy (4.8). Moreover, for both Option 1 and Option 2, to fairly coexist with Wi-Fi, the carrier aggregation scheme will try to follow the channel bonding approach in Wi-Fi systems, if possible.

4.3.3 Simulation Results

Similar to the simulation setup in Section 4.2.5.1, to evaluate the coexistence performance of Wi-Fi and LAA with adaptive energy detection and carrier selection, we adopt the indoor scenario specified by 3GPP [2]. Each operator (Operator A for IEEE 802.11ac, or Operator B for LAA) deploys four cells in a one-floor building. Each eNB/AP serves five UEs/STAs, and all UEs/STAs are randomly located within the coverage area of their associated eNBs/APs. The total transmit power of LAA eNBs, Wi-Fi APs, and STAs in the unlicensed spectrum is set to 23 dBm, 23 dBm, and 18 dBm, respectively. Traffic is modeled as an FTP download of a 0.5 MB file with a Poisson request rate of $\lambda = 2.5$. The self-deferral period of Option 2 is 10 ms. LAA/Wi-Fi can aggregate/bond at most 4 carriers, and there are 8 unlicensed 20-MHz carriers in total to be shared by LAA and Wi-Fi (IEEE 802.11ac) networks. The energy detection thresholds scale up with increasing channel bandwidth due to the power limitation in the unlicensed 5-GHz band. Each simulation is executed for 500 seconds with a random deployment of UEs/STAs, and results are averaged over 50 runs. The remaining simulation setting and parameters are the same as those in Section 4.2.5.1.

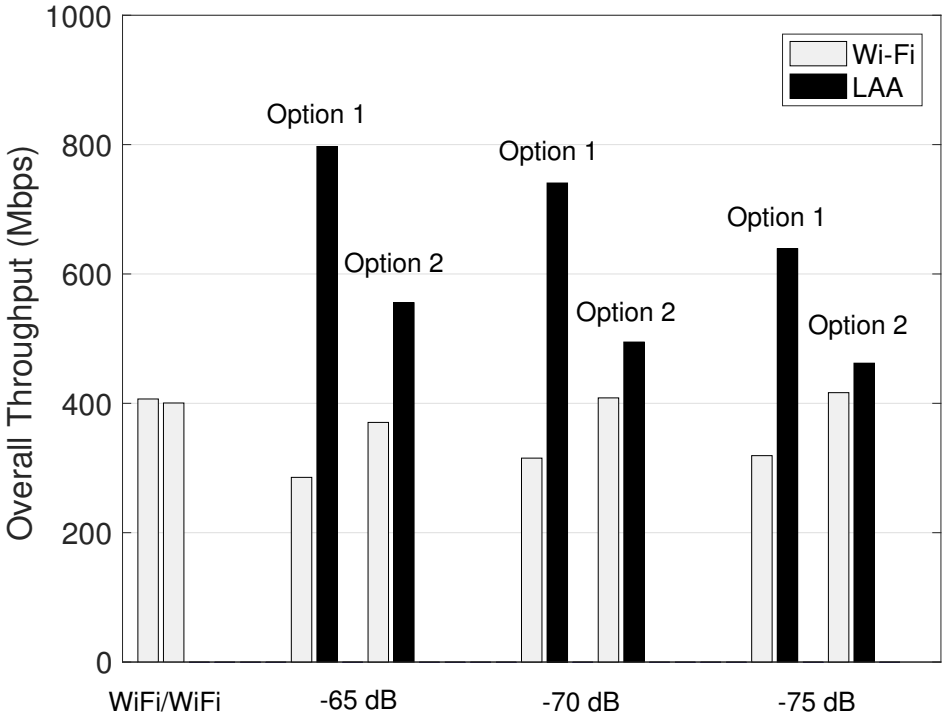

Figure 4.18: Overall throughput performance of Wi-Fi and LAA systems with different LAA-ED thresholds for multi-carrier LBT Option 1 and Option 2.

In Fig. 4.18, the aggregate throughputs of the Wi-Fi and LAA networks are shown for different LAA-ED thresholds, where all eNBs have the same LAA-ED threshold for all UEs (-65 dBm, -70 dBm, and -75 dBm). Here, after multi-carrier LBT procedures, we assume that the actual aggregated carriers $\mathcal{K}(i,j)$ are randomly selected from the idle carriers $\mathcal{C}(i,j)$ for eNB i and UE j. For comparison purposes, the performance of a pure Wi-Fi network is also shown in Fig. 4.18, where both Operator A and Operator B deploy Wi-Fi APs. Note that the throughput is measured by the number of successfully transmitted bits over the total transmission period, and the aggregate throughput is the sum of the individual throughputs of the eNBs/APs for one operator. It is observed that: 1) introducing an LAA operator can improve the overall

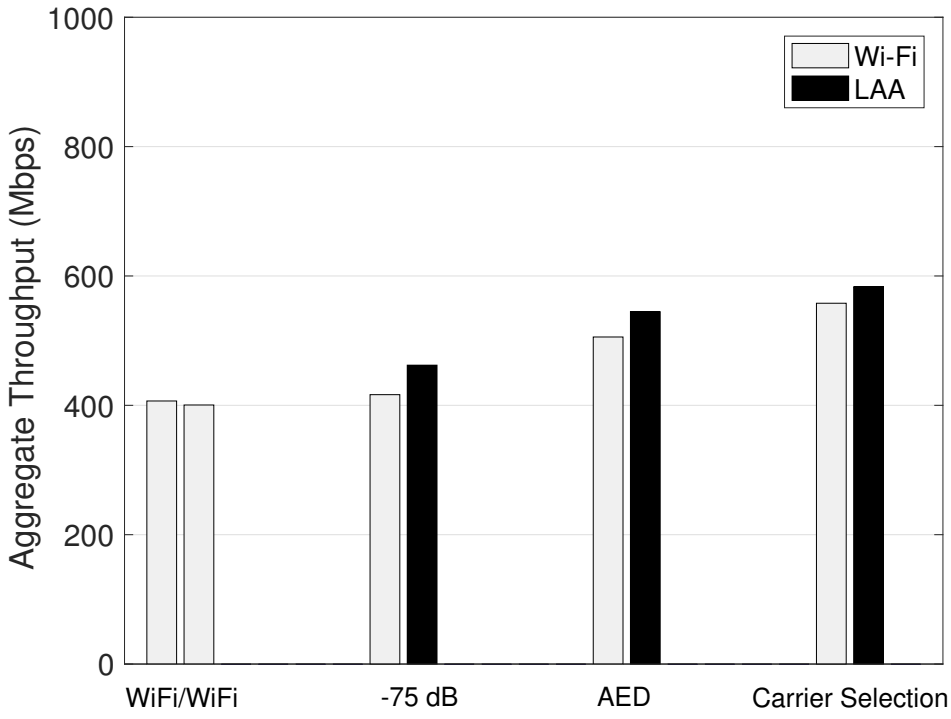

Figure 4.19: Aggregate throughput performance of Wi-Fi and LAA for four cases: pure Wi-Fi, LAA with a fixed LAA-ED threshold of −75 dBm, LAA with adaptive energy detection, and LAA with adaptive energy detection and carrier selection.

throughput (the sum throughput of both Operator A and Operator B); 2) Wi-Fi systems may suffer from severe performance loss, especially for Option 1; 3) by setting a low LAA-ED threshold, LAA becomes less aggressive, which yields more transmission opportunities for Wi-Fi. In the following simulations, we focus on the simulation of multi-carrier LBT Option 2 since this option coexists better with Wi-Fi networks.

Fig. 4.19 illustrates the aggregate throughput of the coexistent Wi-Fi and LAA network for four different cases. From left to right, 1) a pure Wi-Fi network that acts as our reference; 2) a Wi-Fi/LAA coexistent network, in which the LAA operator employs multi-carrier LBT Option 2, with a fixed LAA-ED threshold of −75 dBm and random carrier selection; 3) a Wi-Fi/LAA coexistent network, in which the

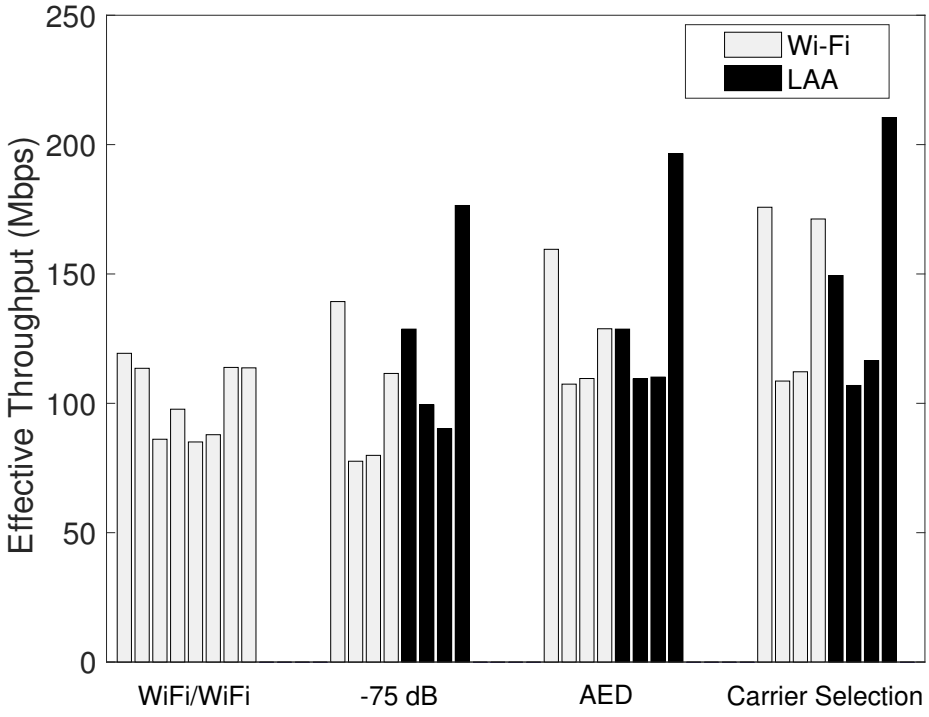

Figure 4.20: Effective throughput performance for individual APs and eNBs for four cases: pure Wi-Fi, LAA with a fixed LAA-ED threshold of −75 dBm, LAA with AED, and LAA with AED and carrier selection.

LAA operator employs multi-carrier LBT Option 2 with the AED algorithm; and 4) a Wi-Fi/LAA coexistent network, in which the LAA operator employs multi-carrier LBT Option 2 with the AED algorithm and the proposed carrier selection algorithm. The sum throughputs of Operator A and Operator B are 807.24 Mbps, 878.56 Mbps, 1050.38 Mbps and 1141.11 Mbps for the four cases, respectively. Particularly, for the last two cases, i.e., multi-carrier LBT with AED, multi-carrier LBT with AED and carrier selection, the aggregated throughput gains are 19.56% and 29.88%, respectively, compared to the case of multi-carrier LBT with a fixed LAA-ED threshold. Moreover, we can see that, by extending the AED algorithm in [115] to multi-carrier LBT and including carrier selection, not only does the system performance improve more, but LAA can also coexist better with Wi-Fi networks in terms of fairness.

In Fig. 4.20, the throughputs of individual APs and eNBs are shown for the previously described four cases. The light colored bars for each case represent the individual throughputs of WiFi #1, WiFi #3, WiFi #5, and WiFi #7, respectively. Similarly, the dark colored bars for each scheme denote the individual throughputs of LAA #2, LAA #4, LAA #6, and LAA #8, respectively. Due to the specific linear 3GPP layout, the transmitters in the middle will be disadvantaged since they need to contend for access to the shared carrier with transmitters from both sides, while the transmitters at the edge only need to compete with the transmitters on one side.

4.4 Summary

In this chapter, we discussed the hidden and exposed node problems in a mixed Wi-Fi and LAA network, due to different energy detection strategies adopted for Wi-Fi APs and LAA eNBs. We showed that the LAA-ED plays a critical role in the system's performance. With a high LAA-ED, the system supports more concurrent transmissions but collisions also happen very often, which limits the system's overall performance; with a low LAA-ED threshold, the system would also suffer from performance loss due to needless backoff. Therefore, the Dis-AEDU algorithm has been proposed to adaptively change LAA-ED per user to encourage concurrent transmissions as well as avoid collisions. Further, considering practical implementation issues, the Dis-AEDB algorithm has also been provided to update LAA-ED per base station, which can improve the system performance but not as much as that of the Dis-AEDU algorithm.

In addition, in a coexistent network of Wi-Fi and LAA with multiple carriers available, we studied and evaluated two different schemes for multi-carrier LBT. We showed LAA with multi-carrier LBT Option 2 coexists better with Wi-Fi because it performs LBT procedures on all carriers and introduces a self-deferral period, which can give Wi-Fi more opportunities to transmit data. Then, the previously proposed adaptive energy detection algorithm was extended to the multi-carrier case, to achieve a better coexistence performance. In addition, a new carrier selection algorithm was

proposed, in which the carriers with high LAA energy detection thresholds would be aggregated first; this was demonstrated to further improve the coexistence performance.

In the future, the following two aspects should be investigated to further evaluate the coexistence challenges of Wi-Fi and LAA systems: (i) analyze the impact of LAA-ED on the system performance from a theoretical viewpoint by simplifying channel sensing procedures and using probability traffic models; and (ii) evaluate the proposed adaptive energy detection and carrier selection algorithms using a network simulator (like ns-3).

Chapter 5

CONTRIBUTIONS AND FUTURE WORK

This chapter summarizes the main contributions of the dissertation and discusses potential future research. Section 5.1 summarizes our work and gives some concluding remarks. Section 5.2 discusses a variety of directions for future research relating to our viewpoint on interference management in wireless networks.

5.1 Contributions

Today, and in the future, wireless networks will continue to face one of their greatest limiting factors: interference. This is due to the limited spectrum available and the increased temporal and spectral reuse of these resources. As we introduced in Chapter 1, new types of intra- and inter-system interference are created by some recently proposed advanced technologies. In this dissertation, we provided both theoretical analyses and practical insights on interference management in wireless communications systems.

Performance Analysis of IBFD Relaying with Residual Interference

Cooperative relaying techniques can significantly increase system throughput and extend coverage of wireless networks by introducing spatial diversity to combat fading on wireless channels, and there are two main relaying protocols: HD and FD (IBFD). In HD relaying, the transmission is usually organized in two time slots. During the first slot, the source broadcasts its message and all cooperating nodes listen, and during the second slot, some relays are selected to forward the source information to the destination. In IBFD relaying, the relays transmit and receive at the same time on the same frequency, which can ideally double the spectral efficiency achieved with HD.

However, the main problem with IBFD operation is that the system performance might decrease rapidly because of strong interference, which could be difficult to completely suppress. In Chapter 2, we analyzed the spectral efficiency of cooperative IBFD systems with self-loop and cross-talk interference, and also studied the impact of the direct link on the system's performance. These studies show that the IBFD relaying's performance is strongly dependent on the residual interference.

Interference Cancellation and Utilization for UWA Transmissions

For IBFD UWA systems, the interference cancellation in the dynamic ocean is even more challenging than that of IBFD radios. These challenges include 1) strong self-loop interference from its own transmission; 2) interference due to reflections from the sea surface and sea floor with huge delays (caused by the slow speed of sound waves); and 3) some cancellation schemes adopted in IBFD radios, like analog cancellation and antenna cancellation, will be much more difficult to implement and might not even work in IBFD UWA systems. In Chapter 3, we proposed a hybrid cancellation strategy for IBFD UWA systems. With some simplifications, the simulations results show that IBFD UWA systems are feasible and can provide performance gain for UWA communications. Then, OFDM with a sufficient length of CP, and delay diversity coding were employed to deal with the residual self-loop interference and the reflected interference.

Efficient and Effective Coexistence of Wi-Fi and LAA systems

To achieve higher data rates, LAA expands operation of the LTE standard into the unlicensed bands. However, LTE was originally designed to operate in licensed bands, and LAA could lead to significant performance degradation for Wi-Fi systems. In Chapter 4, we first evaluated the coexistence challenges, and proposed adaptive energy detection algorithms to achieve fair and effective coexistence between Wi-Fi and LAA in a single 20-MHz channel. Due to the large amount of spectrum available in the 5-GHz unlicensed band, 3GPP LAA and IEEE 802.11ac can both operate on channels wider than 20 MHz. Thus, we extended our adaptive energy detection algorithm to the

multi-carrier case for two different options of multi-carrier LBT. To further improve the coexistence performance, an efficient carrier selection was proposed, in which the carriers with high LAA energy detection thresholds are aggregated first.

5.2 Future Research Opportunities

For RF IBFD cooperative communications, one potential topic of interests is to analyze the spectral efficiency of IBFD relaying with all kinds of interference, i.e., the interference from one relay's own transmission, from other relays' transmissions, and also from the source's transmission. Also, to reduce the throughput loss of HD relaying and avoid introducing the severe interference of IBFD relaying, several hybrid schemes (between HD and FD) have been proposed in the literature [47–50]. The basic idea of these techniques is to adopt a two-relay network where the two relays alternately forward messages from a source terminal to a destination terminal, i.e., during the first (second) time slot, the source and the first (second) relay transmit to the second (first) relay and the destination, respectively. Thus, the messages are transmitted at the same time in the same frequency band; we call this approach FD-like relaying. In [51], the authors employ HD relays with buffers to mimic FD relays, and the relay with the largest SNR among multiple relays is always chosen to forward messages to the destination. Intuitively, the FD-like schemes can avoid the factor of 1/2 in HD relaying without introducing strong self-loop interference as in IBFD relaying. Thus, it is valuable to study whether an FD-like scheme can achieve similar performance as in ideal IBFD relaying.

For UWA transmissions, it is very important to do experiments in real sea environments to verify and improve the proposed cancellation schemes. Acoustic interference cancellation for high frequencies, 120-140 kHz, should also be studied. At these frequencies, attenuation is significant for the reflected interferences. For example, in the 30-m deep ocean, surface interference will experience 30 dB of attenuation, in addition to the scattering and reflection loss from the dynamic surface. To characterize the multipath interference, an acoustic system could be deployed to collect interference

measurements for 1) multiple transducer-hydrophone separation distances and different transducer orientations, and 2) different sensor depths, water column conditions, and sea states. With the data from these real experiments, the previously proposed cancellation scheme can be improved and made adaptive to different practical environments. In addition, for IBFD UWA relaying, the current proposed delay diversity scheme works well for IBFD relays with reflected interference from the sea surface. In shallow water, the interference utilization will be much more difficult to implement due to reflections from both the sea surface and sea floor. One straightforward solution is to view those reflections as additional "antennas" in the delay diversity scheme; however, the decoding complexity of the Viterbi detector will increase exponentially. Thus, it is important to investigate other STC schemes or more efficient detectors to utilize the reflected interference in IBFD UWA relaying systems.

For LAA networks, one potential useful future activity is to verify the proposed algorithm with a network simulator, such as ns-3. Based on the results from ns-3, the adaptive energy detection and carrier selection could be further optimized. Also, other schemes can be developed to ensure fair and efficient scheduling/interference management for heterogeneous Wi-Fi/LAA networks. In particular, multi-user (MU) MIMO beamforming can support multiple streams sharing the same frequency without detrimentally interfering with each other. However, ideal channel state information is required for MU beamforming, which may be impractical when LAA and Wi-Fi are not allowed to coordinate with each other. Thus, the exploration of the use of long-term channel statistics can be one option to avoid interference and devise new MU beamforming schemes, which can achieve enhanced overall throughput while maintaining fair coexistence between Wi-Fi and LAA.

BIBLIOGRAPHY

[1] M. B. Porter and H. P. Bucker, "Cisco visual networking index: global mobile data traffic forecast update, 2017-2022 white paper," 2017. Available at https://www.cisco.com/c/en/us/solutions/collateral/service-provider/visual-networking-index-vni/mobile-white-paper-c11-520862.pdf.

[2] 3GPP TR 36.889 V13.0.0, "Study on licensed-assisted access to unlicensed spectrum," June 2015.

[3] IEEE Std. 802.11ac

[4] E. Hossain, M. Rasti, H. Tabassum, and A. Abdelnasser, "Evolution toward 5G multi-tier cellular wireless networks: An interference management perspective," *IEEE Wireless Communications*, vol. 21, pp. 118–127, June 2014.

[5] A. Sendonaris, E. Erkip, and B. Aazhang, "User cooperation diversity. part I. system description," *IEEE Transactions on Communications*, vol. 51, pp. 1927–1938, Nov. 2003.

[6] A. Sendonaris, E. Erkip, and B. Aazhang, "User cooperation diversity. part II. implementation aspects and performance analysis," *IEEE Transactions on Communications*, vol. 51, pp. 1939–1948, Nov. 2003.

[7] V. R. Cadambe and S. A. Jafar, "Interference alignment and degrees of freedom of the k-user interference channel," *IEEE Transactions on Information Theory*, vol. 54, pp. 3425–3441, Aug. 2008.

[8] D. P. Palomar, J. M. Cioffi, and M. A. Lagunas, "Joint Tx-Rx beamforming design for multicarrier MIMO channels: a unified framework for convex optimization," *IEEE Transactions on Signal Processing*, vol. 51, pp. 2381–2401, Sept. 2003.

[9] 3GPP TR 36.814 v9.0.0, "Technical specification group radio access network," Mar. 2010.

[10] J. Choi, M. Jain, K. Srinivasan, P. Levis, and S. Katti, "Achieving single channel, full duplex wireless communication," in *Proceedings of the Sixteenth Annual International Conference on Mobile Computing and Networking*, MobiCom '10, pp. 1–12, 2010.

[11] M. Duarte, C. Dick, and A. Sabharwal, "Experiment-driven characterization of full-duplex wireless systems," *IEEE Transactions on Wireless Communications*, vol. 11, pp. 4296–4307, Dec. 2012.

[12] E. Aryafar, M. A. Khojastepour, K. Sundaresan, S. Rangarajan, and M. Chiang, "MIDU: Enabling MIMO full duplex," in *Proceedings of the 18th Annual International Conference on Mobile Computing and Networking*, Mobicom '12, pp. 257–268, 2012.

[13] D. Bharadia, E. McMilin, and S. Katti, "Full duplex radios," in *Proceedings of the ACM SIGCOMM 2013 Conference on SIGCOMM*, SIGCOMM '13, pp. 375–386, 2013.

[14] I. Krikidis, H. A. Suraweera, P. J. Smith, and C. Yuen, "Full-duplex relay selection for amplify-and-forward cooperative networks," *IEEE Transactions on Wireless Communications*, vol. 11, pp. 4381–4393, Dec. 2012.

[15] 3GPP TSG RAN Meeting 75, "New WID: enhancements to LTE operation in unlicensed spectrum," Mar. 2017.

[16] Q. Cui, Y. Gu, W. Ni, and R. P. Liu, "Effective capacity of licensed-assisted access in unlicensed spectrum for 5G: From theory to application," *IEEE Journal on Selected Areas in Communications*, vol. 35, pp. 1754–1767, Aug. 2017.

[17] A. Mukherjee, J. F. Cheng, S. Falahati, H. Koorapaty, D. H. Kang, R. Karaki, L. Falconetti, and D. Larsson, "Licensed-assisted access LTE: coexistence with IEEE 802.11 and the evolution toward 5G," *IEEE Communications Magazine*, vol. 54, pp. 50–57, June 2016.

[18] M. Feng, S. Mao, and T. Jiang, "Base station on-off switching in 5g wireless networks: Approaches and challenges," *IEEE Wireless Communications*, vol. 24, pp. 46–54, Aug 2017.

[19] Y. Liu, X. G. Xia, and H. Zhang, "Distributed space-time coding for full-duplex asynchronous cooperative communications," *IEEE Transactions on Wireless Communications*, vol. 11, pp. 2680–2688, July 2012.

[20] Y. Liu, X. G. Xia, and H. Zhang, "Distributed linear convolutional space-time coding for two-relay full-duplex asynchronous cooperative networks," *IEEE Transactions on Wireless Communications*, vol. 12, pp. 6406–6417, Dec. 2013.

[21] X. Lurton, *An Introduction to Underwater Acoustics*. New York: Springer, 2002.

[22] G. Qiao, S. Z. Liu, Z. X. Sun, and F. Zhou, "Full-duplex, multi-user and parameter reconfigurable underwater acoustic communication modem," in *Proceedings of 2013 MTS/IEEE OCEANS*, pp. 1–8, Sept. 2013.

[23] M. Stojanovic and J. Preisig, "Underwater acoustic communication channels: Propagation models and statistical characterization," *IEEE Communications Magazine*, vol. 47, pp. 84–89, Jan. 2009.

[24] D. B. Kilfoyle and A. B. Baggeroer, "The state of the art in underwater acoustic telemetry," *IEEE Journal of Oceanic Engineering*, vol. 25, pp. 4–27, Jan. 2000.

[25] X. Wang, L. Pollock, and K. Vijay-Shanker, "Developing a model of loop actions by mining loop characteristics from a large code corpus," in *Proceedings of 31st International Conference on Software Maintenance and Evolution (ICSME)*, pp. 35–44, IEEE, 2015.

[26] 3GPP Study Item - RP-141397, "Study on licensed-assisted access using LTE," Sept. 2014.

[27] Qualcomm, "On LTE-U/WiFi coexistence," 2015. Available at http://www.wi-fi.org/file/wi-fi-lte-u-coexistence-test-workshop-presentations-november-2015.

[28] Ericsson, "LTE licensed assisted access," 2015. Available at http://www.ericsson.com/res/thecompany/docs/press/media kits/ ericsson-license-assisted-access-laa-january-2015.pdf.

[29] L. Li, D. Qu, and T. Jiang, "Partition optimization in LDPC-coded OFDM systems with PTS PAPR reduction," *IEEE Transactions on Vehicular Technology*, vol. 63, pp. 4108–4113, Oct 2014.

[30] D. Qu, L. Li, and T. Jiang, "Invertible subset LDPC code for PAPR reduction in OFDM systems with low complexity," *IEEE Transactions on Wireless Communications*, vol. 13, pp. 2204–2213, April 2014.

[31] L. Li and D. Qu, "Joint decoding of LDPC code and phase factors for OFDM systems with PTS PAPR reduction," *IEEE Transactions on Vehicular Technology*, vol. 62, pp. 444–449, Jan 2013.

[32] T. Kwon, S. Lim, S. Choi, and D. Hong, "Optimal duplex mode for DF relay in terms of the outage probability," *IEEE Transactions on Vehicular Technology*, vol. 59, pp. 3628–3634, Sept. 2010.

[33] B. Yu, L. Yang, X. Cheng, and R. Cao, "Transmit power optimization for full duplex decode-and-forward relaying," in *2013 IEEE Global Communications Conference*, pp. 3347–3352, Dec. 2013.

[34] G. Kramer, M. Gastpar, and P. Gupta, "Cooperative strategies and capacity theorems for relay networks," *IEEE Transactions on Information Theory*, vol. 51, pp. 3037–3063, Sept. 2005.

[35] H. Alves, D. B. da Costa, R. D. Souza, and M. Latva-aho, "Performance of block-Markov full duplex relaying with self interference in Nakagami-m fading," *IEEE Wireless Communications Letters*, vol. 2, pp. 311–314, June 2013.

[36] I. Krikidis and H. A. Suraweera, "Full-duplex cooperative diversity with Alamouti space-time code," *IEEE Wireless Communications Letters*, vol. 2, pp. 311–314, June 2013.

[37] A. Bletsas, A. Khisti, D. P. Reed, and A. Lippman, "A simple cooperative diversity method based on network path selection," *IEEE Journal on Selected Areas in Communications*, vol. 24, pp. 659–672, Mar. 2006.

[38] J. N. Laneman and G. W. Wornell, "Distributed space-time-coded protocols for exploiting cooperative diversity in wireless networks," *IEEE Transactions on Information Theory*, vol. 49, pp. 2415–2425, Oct. 2003.

[39] Y. Xiao and L. J. Cimini, "Impact of overhead on spectral efficiency of cooperative relaying," *IEEE Transactions on Wireless Communications*, vol. 12, pp. 2228–2239, May 2013.

[40] Y. Jing and H. Jafarkhani, "Single and multiple relay selection schemes and their achievable diversity orders," *IEEE Transactions on Wireless Communications*, vol. 8, pp. 1414–1423, Mar. 2009.

[41] J. Luo, R. S. Blum, L. J. Cimini, L. J. Greenstein, and A. M. Haimovich, "Link-failure probabilities for practical cooperative relay networks," in *2005 IEEE 61st Vehicular Technology Conference*, vol. 3, pp. 1489–1493, May 2005.

[42] B. Sirkeci-Mergen and A. Scaglione, "Randomized space-time coding for distributed cooperative communication," *IEEE Transactions on Signal Processing*, vol. 55, pp. 5003–5017, Oct. 2007.

[43] M. Haenggi, J. G. Andrews, F. Baccelli, O. Dousse, and M. Franceschetti, "Stochastic geometry and random graphs for the analysis and design of wireless networks," *IEEE Journal on Selected Areas in Communications*, vol. 27, pp. 1029–1046, Sept. 2009.

[44] L. Zhang and L. J. Cimini, "Efficient power allocation for decentralized distributed space-time block coding," *IEEE Transactions on Wireless Communications*, vol. 8, pp. 1102–1106, Mar. 2009.

[45] X.-B. Liang, "Orthogonal designs with maximal rates," *IEEE Transactions on Information Theory*, vol. 49, pp. 2468–2503, Oct. 2003.

[46] W. E. Ryan and S. Lin, *Fundamentals of Statistical Signal Processing: Estimation Theory*. Englewood Cliffs, NJ: Prentice-Hall, 1993.

[47] B. Rankov and A. Wittneben, "Spectral efficient protocols for half-duplex fading relay channels," *IEEE Journal on Selected Areas in Communications*, vol. 25, pp. 379–389, Feb. 2007.

[48] F. Xue and S. Sandhu, "Cooperation in a half-duplex Gaussian diamond relay channel," *IEEE Transactions on Information Theory*, vol. 53, pp. 3806–3814, Oct. 2007.

[49] Y. Fan, C. Wang, J. Thompson, and H. V. Poor, "Recovering multiplexing loss through successive relaying using repetition coding," *IEEE Transactions on Wireless Communications*, vol. 6, pp. 4484–4493, Dec. 2007.

[50] D. S. Michalopoulos and G. K. Karagiannidis, "Bypassing orthogonal relaying transmissions via spatial signal separation," *IEEE Transactions on Communications*, vol. 58, pp. 3028–3038, Oct. 2010.

[51] A. Ikhlef, J. Kim, and R. Schober, "Mimicking full-duplex relaying using half-duplex relays with buffers," *IEEE Transactions on Vehicular Technology*, vol. 61, pp. 3025–3037, Sept. 2012.

[52] M. Rahmati and T. M. Duman, "Achieving delay diversity in asynchronous underwater acoustic (UWA) cooperative communication systems," *IEEE Transactions on Wireless Communications*, vol. 13, pp. 1367–1379, Mar. 2014.

[53] M. Stojanovic and J. Preisig, "Underwater acoustic communication channels: Propagation models and statistical characterization," *IEEE Communications Magazine*, vol. 47, pp. 84–89, Jan. 2009.

[54] A. Song, M. Badiey, V. K. McDonald, and T. C. Yang, "Time reversal receivers for high data rate acoustic multiple-input multiple-output communication," *IEEE Journal of Oceanic Engineering*, vol. 36, pp. 525–538, Oct. 2011.

[55] C. R. Berger, S. Zhou, J. C. Preisig, and P. Willett, "Sparse channel estimation for multicarrier underwater acoustic communication: From subspace methods to compressed sensing," *IEEE Transactions on Signal Processing*, vol. 58, pp. 1708–1721, Mar. 2010.

[56] M. Stojanovic, "Low complexity OFDM detector for underwater acoustic channels," in *Proceedings of 2006 MTS/IEEE OCEANS*, pp. 1–6, Sept. 2006.

[57] B. Li, S. Zhou, M. Stojanovic, L. Freitag, and P. Willett, "Multicarrier communication over underwater acoustic channels with nonuniform doppler shifts," *IEEE Journal of Oceanic Engineering*, vol. 33, pp. 198–209, Apr. 2008.

[58] A. Song, M. Badiey, and V. K. McDonald, "Multichannel combining and equalization for underwater acoustic MIMO channels," in *Proceedings of 2008 MTS/IEEE OCEANS*, pp. 1–6, Sept. 2008.

[59] B. Li, J. Huang, S. Zhou, K. Ball, M. Stojanovic, L. Freitag, and P. Willett, "MIMO-OFDM for high-rate underwater acoustic communications," *IEEE Journal of Oceanic Engineering*, vol. 34, pp. 634–644, Oct. 2009.

[60] Z. Yang and Y. R. Zheng, "Iterative channel estimation and turbo equalization for multiple-input multiple-output underwater acoustic communications," *IEEE Journal of Oceanic Engineering*, vol. 41, pp. 232–242, Jan. 2016.

[61] J. Zhang, X. Ma, G. Qiao, and C. Wang, "A full-duplex based protocol for underwater acoustic communication networks," in *Proceedings of 2013 MTS/IEEE OCEANS*, pp. 1–6, Sept. 2013.

[62] G. Xie, J. Gibson, and K. Bektas, "Evaluating the feasibility of establishing full-duplex underwater acoustic channels," in *Proceedings of 2014 MED-HOC-Net Workshop*, pp. 1–5, June 2014.

[63] S. Al-Dharrab, M. Uysal, and T. M. Duman, "Cooperative underwater acoustic communications," *IEEE Communications Magazine*, vol. 51, pp. 146–153, July 2013.

[64] R. Cao, F. Z. Qu, and L. Q. Yang, "Asynchronous amplify-and-forward relay communications for underwater acoustic networks," *IET Communications*, vol. 10, pp. 677–864, Apr. 2016.

[65] X. Cheng, L. Yang, and X. Zhang, *Cooperative OFDM Underwater Acoustic Communications*. Springer International Publishing, 2016.

[66] M. Vajapeyam, S. Vedantam, U. Mitra, J. C. Preisig, and M. Stojanovic, "Distributed space-time cooperative schemes for underwater acoustic communications," *IEEE Journal of Oceanic Engineering*, vol. 33, pp. 489–501, Oct. 2008.

[67] Z. Han, Y. L. Sun, and H. Shi, "Cooperative transmission for underwater acoustic communications," in *Proceedings of 2008 IEEE International Conference on Communications*, pp. 2028–2032, May 2008.

[68] A. Salim and T. M. Duman, "A delay-tolerant asynchronous two-way-relay system over doubly-selective fading channels," *IEEE Transactions on Wireless Communications*, vol. 14, pp. 3850–3865, July 2015.

[69] E. Panayirci, H. Senol, M. Uysal, and H. V. Poor, "Sparse channel estimation and equalization for OFDM-based underwater cooperative systems with amplify-and-forward relaying," *IEEE Transactions on Signal Processing*, vol. 64, pp. 214–228, Jan. 2016.

[70] R. Cao, L. Yang, and F. Qu, "On the capacity and system design of relay-aided underwater acoustic communications," in *Proceedings of 2010 IEEE Wireless Communication and Networking Conference*, pp. 1–6, Apr. 2010.

[71] H. Nouri, M. Uysal, and E. Panayirci, "Information theoretical performance analysis and optimisation of cooperative underwater acoustic communication systems," *IET Communications*, vol. 10, pp. 812–823, May 2016.

[72] N. Seshadri and J. H. Winters, "Two signaling schemes for improving the error performance of frequency-division-duplex (FDD) transmission systems using transmitter antenna diversity," in *Proceedings of IEEE 43rd Vehicular Technology Conference*, pp. 508–511, May 1993.

[73] V. Tarokh, N. Seshadri, and A. R. Calderbank, "Space-time codes for high data rate wireless communication: performance criterion and code construction," *IEEE Transactions on Information Theory*, vol. 44, pp. 744–765, Mar. 1998.

[74] D. Gore, S. Sandhu, and A. Paulraj, "Delay diversity codes for frequency selective channels," in *Proceedings of 2002 IEEE International Conference on Communications*, pp. 1949–1953, May 2002.

[75] L. Li, L. J. Cimini, and Y. Xiao, "Spectral efficiency of cooperative full-duplex relaying with imperfect channel estimation," in *Proceedings of 2014 IEEE Global Communications Conference*, pp. 4203–4208, Dec. 2014.

[76] J. I. Choi, M. Jain, K. Srinivasan, P. Levis, and S. Katti, "Achieving single channel, full duplex wireless communication," in *Proceedings of the Sixteenth Annual International Conference on Mobile Computing and Networking (MobiCom)*, pp. 1–12, Sept. 2010.

[77] M. Duarte, C. Dick, and A. Sabharwal, "Experiment-driven characterization of full-duplex wireless systems," *IEEE Transactions on Wireless Communications*, vol. 11, pp. 4296–4307, Dec. 2012.

[78] D. Bharadia, E. McMilin, and S. Katti, "Full duplex radios," in *Proceedings of the ACM SIGCOMM 2013 Conference on SIGCOMM*.

[79] T. Riihonen, S. Werner, and R. Wichman, "Optimized gain control for single-frequency relaying with loop interference," *IEEE Transactions on Wireless Communications*, vol. 8, pp. 2801–2806, June 2009.

[80] Y. Jin, X. G. Xia, Y. Chen, and R. Li, "Full-duplex delay diversity relay transmission using bit-interleaved coded OFDM," *IEEE Transactions on Communications*, vol. 65, pp. 3250–3258, Aug. 2017.

[81] L. Li, A. Song, L. J. Cimini, X.-G. Xia, and C.-C. Shen, "Interference cancellation in in-band full-duplex underwater acoustic systems," in *Proceedings of 2015 MTS/IEEE OCEANS*, pp. 1–6, Oct. 2015.

[82] L. L. Zhang, J. G. Huang, C. K. Tang, and H. B. Song, "Time reversal aided bidirectional OFDM underwater cooperative communication algorithm with the same frequency transmission," *Journal of Sensors*, pp. 1–8, 2017.

[83] CTG, "Model ITC-3001 high power directional transducer," Available at http://www.channeltechgroup.com/publication/model-itc-3001-high-power-directional-transducer.

[84] E. Ahmed, A. M. Eltawil, and A. Sabharwal, "Rate gain region and design tradeoffs for full-duplex wireless communications," *IEEE Transactions on Wireless Communications*, vol. 12, pp. 3556–3565, July 2013.

[85] H. Steendam and M. Moeneclaey, "Analysis and optimization of the performance of OFDM on frequency-selective time-selective fading channels," *IEEE Transactions on Communications*, vol. 47, pp. 1811–1819, Dec. 1999.

[86] T. Riihonen, K. Haneda, S. Werner, and R. Wichman, "SINR analysis of full-duplex OFDM repeaters," in *Proceedings of 2009 IEEE 20th International Symposium on Personal, Indoor and Mobile Radio Communications*, pp. 3169–3173, Sept. 2009.

[87] M. Batariere, K. Baum, and T. P. Krauss, "Cyclic prefix length analysis for 4G OFDM systems," in *Proceedings of 2004 IEEE 60th Vehicular Technology Conference Fall.*, pp. 543–547, Sept. 2004.

[88] W. E. Ryan and S. Lin, *Channel Codes: Classical and Modern*. Cambridge University Press, 2009.

[89] L. Li, L. J. Cimini, and X. G. Xia, "Impact of direct link on outage of cooperative full-duplex relaying," in *Proceedings of 2015 49th Annual Conference on Information Sciences and Systems (CISS)*, pp. 1–6, Mar. 2015.

[90] M. B. Porter and H. P. Bucker, "Gaussian beam tracing for computing ocean acoustic fields," *The Journal of the Acoustical Society of America*, vol. 82, pp. 1349–1359, June 1987.

[91] M. B. Porter and H. P. Bucker, "Modeling broadband ocean acoustic transmissions with time-varying sea surfaces," *The Journal of the Acoustical Society of America*, vol. 124, pp. 137–150, July 2008.

[92] M. B. Porter and H. P. Bucker, "The BELLHOP manual and users guide: preliminary draft," 2011. Available at http://esme.bu.edu/data/papers/HLS-2010-1.pdf.

[93] B. Chen, J. Chen, Y. Gao, and J. Zhang, "Coexistence of LTE-LAA and Wi-Fi on 5 GHz with corresponding deployment scenarios: A survey," *IEEE Communications Surveys Tutorials*, vol. 19, pp. 7–32, Firstquarter 2017.

[94] X. Wang, L. Pollock, and K. Vijay-Shanker, "Automatic segmentation of method code into meaningful blocks: Design and evaluation," *Journal of Software: Evolution and Process*, 2013.

[95] M. Feng and S. Mao, "Interference management and user association for nested array-based massive mimo hetnets," *IEEE Transactions on Vehicular Technology*, vol. 67, pp. 454–466, Jan 2018.

[96] M. Feng, S. Mao, and T. Jiang, "Joint frame design, resource allocation and user association for massive mimo heterogeneous networks with wireless backhaul," *IEEE Transactions on Wireless Communications*, vol. 17, pp. 1937–1950, March 2018.

[97] F. M. Abinader, E. P. L. Almeida, F. S. Chaves, A. M. Cavalcante, R. D. Vieira, R. C. D. Paiva, A. M. Sobrinho, S. Choudhury, E. Tuomaala, K. Doppler, and V. A. Sousa, "Enabling the coexistence of LTE and Wi-Fi in unlicensed bands," *IEEE Communications Magazine*, vol. 52, pp. 54–61, Nov. 2014.

[98] A. Al-Dulaimi, S. Al-Rubaye, Q. Ni, and E. Sousa, "5G communications race: Pursuit of more capacity triggers LTE in unlicensed band," *IEEE Vehicular Technology Magazine*, vol. 10, pp. 43–51, Mar. 2015.

[99] R. Zhang, M. Wang, L. X. Cai, Z. Zheng, X. Shen, and L. L. Xie, "LTE-unlicensed: the future of spectrum aggregation for cellular networks," *IEEE Wireless Communications*, vol. 22, pp. 150–159, June 2015.

[100] X. Wang, L. Pollock, and K. Vijay-Shanker, "Automatically generating natural language descriptions for object-related statement sequences," in *Proceedings of the 24th International Conference on Software Analysis, Evolution and Reengineering (SANER)*, pp. 205–216, Feb 2017.

[101] A. M. Cavalcante, E. Almeida, R. D. Vieira, S. Choudhury, E. Tuomaala, K. Doppler, F. Chaves, R. C. D. Paiva, and F. Abinader, "Performance evaluation of LTE and Wi-Fi coexistence in unlicensed bands," in *Proceedings of 2013 IEEE 77th Vehicular Technology Conference (VTC Spring)*, pp. 1–6, June 2013.

[102] J. Jeon, H. Niu, Q. C. Li, A. Papathanassiou, and G. Wu, "LTE in the unlicensed spectrum: Evaluating coexistence mechanisms," in *Proceedings of 2014 IEEE Globecom Workshops*, pp. 740–745, Dec. 2014.

[103] Y. Gao, X. Chu, and J. Zhang, "Performance analysis of LAA and WiFi coexistence in unlicensed spectrum based on Markov chain," in *2016 IEEE Global Communications Conference (GLOBECOM)*, pp. 1–6, Dec. 2016.

[104] A. Mukherjee, J. F. Cheng, S. Falahati, L. Falconetti, A. Furuskär, B. Godana, D. H. Kang, H. Koorapaty, D. Larsson, and Y. Yang, "System architecture and coexistence evaluation of licensed-assisted access LTE with IEEE 802.11," in *Proceedings of 2015 IEEE International Conference on Communication Workshop*, pp. 2350–2355, June 2015.

[105] S. Y. Lien, J. Lee, and Y. C. Liang, "Random access or scheduling: Optimum LTE licensed-assisted access to unlicensed spectrum," *IEEE Communications Letters*, vol. 20, pp. 590–593, Mar. 2016.

[106] Q. Chen, G. Yu, and Z. Ding, "Optimizing unlicensed spectrum sharing for LTE-U and WiFi network coexistence," *IEEE Journal on Selected Areas in Communications*, vol. 34, pp. 2562–2574, Oct. 2016.

[107] H. Ko, J. Lee, and S. Pack, "A fair listen-before-talk algorithm for coexistence of LTE-U and WLAN," *IEEE Transactions on Vehicular Technology*, vol. 65, pp. 10116–10120, Dec. 2016.

[108] C. Ibars, A. Bhorkar, A. Papathanassiou, and P. Zong, "Channel selection for licensed assisted access in LTE based on UE measurements," in *2015 IEEE 82nd Vehicular Technology Conference (VTC2015-Fall)*, pp. 1–5, Sept. 2015.

[109] J. Liu and G. Shen, "Performance of multi-carrier LBT mechanism for LTE-LAA," in *2016 IEEE 83rd Vehicular Technology Conference (VTC Spring)*, pp. 1–5, May 2016.

[110] J. Liu and W. Xiao, "Advanced carrier aggregation techniques for multi-carrier ultra-dense networks," *IEEE Communications Magazine*, vol. 54, pp. 61–67, July 2016.

[111] M. S. Afaqui, E. Garcia-Villegas, E. Lopez-Aguilera, G. Smith, and D. Camps, "Evaluation of dynamic sensitivity control algorithm for IEEE 802.11ax," in *Proceedings of 2015 IEEE Wireless Communications and Networking Conference*, pp. 1060–1065, Mar. 2015.

[112] L. B. Jiang and S. C. Liew, "Hidden-node removal and its application in cellular WiFi networks," *IEEE Transactions on Vehicular Technology*, vol. 56, pp. 2641–2654, Sept. 2007.

[113] T. M. Cover and J. A. Thomas, *Elements of Information Theory*. New York: Wiley, 1991.

[114] C. Johnson, *Long Term Evolution in Bullets*. 2010.

[115] L. Li, J. P. Seymour, L. J. Cimini, and C. C. Shen, "Coexistence of Wi-Fi and LAA networks with adaptive energy detection," *IEEE Transactions on Vehicular Technology*, vol. 66, pp. 10384–10393, Nov. 2017.

Appendix

IBFD UWA RELAYING WITH RESIDUAL INTERFERENCE

The power of the desired signal is

$$\begin{aligned}\mathcal{E}\{|\mathcal{S}_{\mathrm{D}}(m,n)|^2\} =& \sum_{i=1}^{\infty} c(i)^2 G_{\mathrm{R}}(G_{\mathrm{R}}G_{\mathrm{LI}})^{i-1} \\ =& \sum_{i=1}^{N_{\mathrm{CP}}} G_{\mathrm{R}}(G_{\mathrm{R}}G_{\mathrm{LI}})^{i-1} + \sum_{i=N_{\mathrm{CP}}+1}^{N+N_{\mathrm{CP}}} (\frac{N_{\mathrm{tot}}-i}{N})^2 G_{\mathrm{R}}(G_{\mathrm{R}}G_{\mathrm{LI}})^{i-1} \\ =& \frac{G_{\mathrm{R}}(1-(G_{\mathrm{R}}G_{\mathrm{LI}})^{N_{\mathrm{CP}}})}{1-G_{\mathrm{R}}G_{\mathrm{LI}}} + \sum_{i=1}^{N_{\mathrm{tot}}} (\frac{N_{\mathrm{tot}}-i}{N})^2 G_{\mathrm{R}}(G_{\mathrm{R}}G_{\mathrm{LI}})^{i-1} \\ & - \sum_{i=1}^{N_{\mathrm{CP}}} (\frac{N_{\mathrm{tot}}-i}{N})^2 G_{\mathrm{R}}(G_{\mathrm{R}}G_{\mathrm{LI}})^{i-1} \end{aligned} \tag{A.1}$$

Define $\mathcal{E}_1 = \sum_{i=1}^{N_{\mathrm{tot}}} (\frac{N_{\mathrm{tot}}-i}{N})^2 G_{\mathrm{R}}(G_{\mathrm{R}}G_{\mathrm{LI}})^{i-1}$ and $\mathcal{E}_2 = \sum_{i=1}^{N_{\mathrm{CP}}} (\frac{N_{\mathrm{CP}}-i}{N})^2 G_{\mathrm{R}}(G_{\mathrm{R}}G_{\mathrm{LI}})^{i-1}$ for the second and third terms in (A.1), respectively. Then,

$$\begin{aligned}\mathcal{E}_1 =& \sum_{i=1}^{N_{\mathrm{tot}}} (\frac{N_{\mathrm{tot}}-i}{N})^2 G_{\mathrm{R}}(G_{\mathrm{R}}G_{\mathrm{LI}})^{i-1} \\ =& (\frac{N_{\mathrm{tot}}}{N})^2 \sum_{i=1}^{N_{\mathrm{tot}}} G_{\mathrm{R}}(G_{\mathrm{R}}G_{\mathrm{LI}})^{i-1} - \frac{2N_{\mathrm{tot}}}{N} \sum_{i=1}^{N_{\mathrm{tot}}} i \cdot G_{\mathrm{R}}(G_{\mathrm{R}}G_{\mathrm{LI}})^{i-1} \\ & + \frac{1}{N^2} \sum_{i=1}^{N_{\mathrm{tot}}} i^2 \cdot G_{\mathrm{R}}(G_{\mathrm{R}}G_{\mathrm{LI}})^{i-1} \end{aligned} \tag{A.2}$$

It can be shown that

$$\sum_{i=1}^{N} i \cdot a_0 q^{i-1} = \frac{a_0(1-q^N)}{(1-q)^2} - \frac{N a_0 q^N}{1-q} \tag{A.3}$$

and

$$\begin{aligned}\sum_{i=1}^{N} i^2 \cdot a_0 q^{i-1} =& \frac{a_0(1-q^N)}{(1-q)^2} + \frac{2a_0(q-q^N)}{(1-q)^3} \\ & - \frac{2(N-1)a_0 q^N}{(1-q)^2} - \frac{N^2 a_0 q^N}{1-q} \end{aligned} \tag{A.4}$$

where a_0 is a constant, and $|q| < 1$.

Using (A.3) and (A.4), we can obtain a closed-form expression for (A.2); however, it is fairly complicated and provides little insight. Here, we assume the size of an OFDM block is quite large, so that $(G_{\mathrm{R}}G_{\mathrm{LI}})^N \approx 0$. Then, we consider two extreme cases: (i) the CP is sufficient (i.e., $(G_{\mathrm{R}}G_{\mathrm{LI}})^{N_{\mathrm{CP}}} \approx 0$); and (ii) there is no CP added to the OFDM block (i.e., $N_{\mathrm{CP}} = 0$).

For (i), $\mathcal{E}_1 \approx \mathcal{E}_2$, and the power of the desired signal is

$$\mathcal{E}\{|\mathcal{S}_{\mathrm{D}}(m,n)|^2\} \approx \frac{G_{\mathrm{R}}}{1 - G_{\mathrm{R}}G_{\mathrm{LI}}} \tag{A.5}$$

For (ii), (A.2) can be approximated as

$$\begin{aligned}\mathcal{E}_1 \approx & \frac{G_{\mathrm{R}}}{1 - G_{\mathrm{R}}G_{\mathrm{LI}}} - \frac{2G_{\mathrm{R}}}{N(1 - G_{\mathrm{R}}G_{\mathrm{LI}})^2} \\ & + \frac{G_{\mathrm{R}}}{N^2(1 - G_{\mathrm{R}}G_{\mathrm{LI}})^2} + \frac{2{G_{\mathrm{R}}}^2 G_{\mathrm{LI}}}{N^2(1 - G_{\mathrm{R}}G_{\mathrm{LI}})^3}\end{aligned} \tag{A.6}$$

For large N, we can further ignore the third and fourth terms in (A.6), and the power of the desired signal can be approximated as

$$\mathcal{E}\{|\mathcal{S}_{\mathrm{D}}(m,n)|^2\} \approx \frac{G_{\mathrm{R}}}{1 - G_{\mathrm{R}}G_{\mathrm{LI}}} - \frac{2G_{\mathrm{R}}}{N(1 - G_{\mathrm{R}}G_{\mathrm{LI}})^2} \tag{A.7}$$